

**DEVELOPMENT OF NANOSTRUCTURED ZINC OXIDE-  
COPPER CATALYSTS FOR ENHANCED CATHODIC OXYGEN  
REDUCTION REACTION IN MICROBIAL FUEL CELLS**

by

Nawagamuwage Sujani Perera.

A Thesis Submitted in Partial Fulfillment of the Requirements for the Degree of  
Master of Engineering in Bio-Nano Material Science and Engineering

Examination Committee: Dr. Tanujjal Bora (Chairperson)  
Dr. Raffaele Ricco  
Dr. Wenchao Xue  
Dr. Chamath Yahampath (External Expert)

Nationality: Sri Lankan  
Previous Degree: Bachelor of Engineering and Technology  
University of Kelaniya,  
Sri Lanka

Scholarship Donor: Mr. Jaime & Mrs. Elisa Del Rosario  
Scholarship


Asian Institute of Technology  
School of Engineering and Technology  
Thailand  
May 2024

## **AUTHOUR'S DECLARATIONS**

I, Nawagamuwage Sujani Perera declare that the research work carried out for this thesis was in accordance with the regulations of the Asian Institute of Technology. The work presented in it is my own and has been generated by me as the result of my own original research, and if external sources were used, such sources have been cited. It is original and has not been submitted to any other institution to obtain another degree or qualification. This is a true copy of the thesis, including final revisions.

Date: 04.05.2024

Name (in printed letters): NAWAGAMUWAGE SUJANI PERERA

Signature: 

## ACKNOWLEDGEMENTS

I would like to express my sincere gratitude to my research advisor and chairperson, Dr. Tanujjal Bora, for his invaluable guidance, support, and encouragement throughout my research journey. His advice and guidance have been instrumental in shaping my research questions, methodology, and analysis. I would also like to extend my gratitude to Dr. Raffaele Ricco, who served as the committee member for my thesis. His useful advice and feedback have greatly improved the quality of my work. I am also grateful to Dr. Wenchao Xue for providing me with the necessary equipment and lab facilities that were necessary for my experiment. I would like to thank Dr. Chamath Yahampath for his valuable support and mentoring given during the research. Their support has been crucial to the success of my research. My sincere thanks go to Mr. Jaime and Mrs. Elisa Del Rosario scholarship for providing me with the necessary funding to carry out my studies at AIT. Without financial support, my studies would not have been possible. Finally, I would like to express my heartfelt thanks to my family and AIT friends for their support and encouragement throughout this journey.

## ABSTRACT

Zinc oxide nanorods (ZnO NRs) coated with copper and platinum metal were prepared and tested for different metal loadings on the ZnO NRs as the catalyst to enhance the oxygen reduction reaction (ORR) and apply in the microbial fuel cell (MFC) to improve the performances. The ORR kinetics of developed catalysts were monitored using three-electrode electrochemical cell. The cyclic voltammetry (CV) results showed the best redox current peak at different catalysts. Among them, the Cu (3) coated electrode has a negative onset potential at -0.103 V with the highest area (1.252  $\mu\text{W}$ ) under the reduction peak. This has proved the best results under MCF generating a high power density of 7.846  $\text{mW}/\text{m}^2$ . This was the best power density among the other metal catalysts. The platinum metal coating catalyst electrode showed the best power density of 7.039  $\text{mW}/\text{m}^2$  which has the 0.930  $\mu\text{W}$  area under the reduction peak. The developed nanostructured ZnO NRs-Cu metal catalyst showed high catalytic activity towards the ORR with less charge transfer resistance and high redox current that was harvesting more power in MFCs. The MFC was operated with Cu (3) metal-coated electrode was showed the best coulombic efficiency of 4.9% which was higher than bare graphite coulombic efficiency of 3.9%.

**Keywords:** Oxygen reduction reaction, cyclic voltammetry, maximum power generation

# CONTENTS

	<b>Pages</b>
<b>AUTHOR'S DECLARATION</b>	<b>ii</b>
<b>ACKNOWLEDGMENTS</b>	<b>iii</b>
<b>ABSTRACT</b>	<b>iv</b>
<b>LIST OF TABLES</b>	<b>vii</b>
<b>LIST OF FIGURES</b>	<b>viii</b>
<b>LIST OF ABBREVIATIONS</b>	<b>x</b>
<b>CHAPTER 1 INTRODUCTION</b>	<b>1</b>
1.1 Background of the Study	1
1.2 Statement of the Problem	3
1.3 Objectives of the Study	4
1.4 Scope of the Study	4
1.5 Sustainability Impact	5
<b>CHAPTER 2 LITERATURE REVIEW</b>	<b>6</b>
2.1 Mechanism of Functioning of the Microbial Fuel Cell	6
2.2 Components of the Microbial Fuel Cell	11
2.2.1 Cathode	11
2.2.2 Anode	13
2.2.3 Proton Exchange Membrane	19
2.3 Properties of the Electrode Materials	19
2.3.1 Electrical Conductivity	19
2.3.2 Surface Area and Porosity	20
2.3.3 Stability and Durability	20
2.3.4 Cost and Accessibility	20
2.4 The Catalyst for the Oxygen Reduction Reaction	20
<b>CHAPTER 3 METHODOLOGY</b>	<b>26</b>
3.1 Cathode Electrode Modification	27
3.1.1 Chemicals	28
3.1.2 ZnO Seed Growth on the Graphite	28
3.1.3 ZnO Nanorods Growth on the ZnO Seeds	29
3.1.4 Metal Nanoparticles Deposition on the ZnO Nanorods	30
3.1.5 Sample Characterization	31

3.1.6	Electrode Performances Testing	32
3.1.7	Stability Test of the Modified Cathode Electrode	33
3.2	MFC Fabrication	33
3.2.1	MFC Design	33
3.2.2	MFC Configuration and Assembly	33
3.2.3	The Anode Electrode Acclimatization	35
3.2.4	MFC Operation	35
3.3	Data Acquisition and Chemical Analysis	36
3.3.1	Voltage and Polarization Curve	36
3.3.2	Electrical Characterization of the MFC	36
3.3.3	Chemical Oxygen Demand and Coulombic Efficiency Calculations	37
	<b>CHAPTER 4 RESULTS AND DISCUSSION</b>	<b>39</b>
4.1	Electrode's Morphological & Elemental Analysis	39
4.2	Surface Wettability of the Electrodes	41
4.3	Electrochemical Analysis for ORR Evaluation	42
4.4	Electrode Electrochemical Stability	50
4.5	Electrode Performances When Applied in the MFC	52
4.5.1	Voltage vs Time Response of the Electrode During 72hrs	52
4.5.2	Power Curves of MFC	53
4.5.3	Polarization Curves of MFC	57
4.5.4	COD Concentration, COD Removal Efficiency, and CE of the Electrodes at an Operation Time of 72hrs	60
4.6	Discussion	61
	<b>CHAPTER 5 CONCLUSION</b>	<b>65</b>
5.1	Conclusion	65
5.2	Future Recommendations	66
	<b>REFERENCES</b>	<b>67</b>

## LIST OF TABLES

<b>Tables</b>	<b>Page</b>
Table 2.1 Different Cathode Materials Used in MFC and the Performances	15
Table 2.2 Different Anode Materials Used in MFC and the Performances	17
Table 2.3 Different Catalyst Materials are Applied in MFC	23
Table 4.1 Names of the Electrodes Used in the MFC	39
Table 4.2 MPD, MCD at MPD and $R_{in}$ Changes Over the Electrodes at Operation Time of 72hrs	60

## LIST OF FIGURES

<b>Figures</b>	<b>Page</b>
Figure 1.1 Schematic Representation of a Microbial Fuel Cell (MFC) Showing the Charge Transfer Process Involved to Generate Electricity and Treat Wastewater	2
Figure 2.1 Single Chamber MFC	7
Figure 2.2 Components of the Dual Chamber MFC	8
Figure 2.3 TEM Images of a <i>G. Sulferreducens</i> (Left) and Purified Protein Nanowires (Right) Scale Bars, 1 $\mu\text{m}$ (Left) and 100 nm (Right)	10
Figure 2.4 Different Cathode Materials Used in the MFC, a) Graphite, b) Graphite Felt, c) Carbon Paper, d) Carbon Cloth, e) Reticulated Vitreous Carbon and f) Platinum	12
Figure 2.5 Anode Electrode Modifications	14
Figure 3.1 Overall Methodology of the Research	26
Figure 3.2 Cathode Electrode Modification Steps	27
Figure 3.3 Preparation of ZnO Seed Thin Film Layer on Graphite Surface	28
Figure 3.4 ZnO NRs Growth on the Seed Layer	30
Figure 3.5 Metal NPs Deposition on ZnO NRs	31
Figure 3.6 Electrochemical Cell Using Three Electrodes System	32
Figure 3.7 MFC Drawing From the Solid Works	34
Figure 3.8 Microbial Fuel Cell - Order of the Component Attachment	35
Figure 3.9 The External Hardware Attachment Diagram of the MFC	36
Figure 4.1 FESEM Micrographs of the (a) G, (b) GZ, (c) GZC(up), EDX (bottom), (d) GZP(up), EDX	40
Figure 4.2 Images Showing Water Droplet Interaction With the Electrode Surface, (a) G, (b) GZ, (c) GZC(1), (d) GZC(3), (e) GZC(10), (f) GZP(1), (g) GZP(3) and, (g) GZP(10)	41
Figure 4.3 Summary of the WCA From Various Electrode Surface	42
Figure 4.4 Cyclic Voltammetry of the Electrodes at 20 mV/s in Oxygen-Saturated 50 mM PBS Solution, a) G, b) GZ, and, c) Area Under the Reduction Peak in $\mu\text{W}$	43



Figure 4.5	Cyclic Voltammetry of the Electrodes of GZC at 20 mV/s in Oxygen-Saturated 50 mM PBS Solution, CV Plot of a) GZC(1), b) GZC(3), and c) GZC(10)	46
Figure 4.6	Cyclic Voltammetry of the Electrodes of GZP at 20 mV/s in Oxygen-Saturated 50 mM PBS Solution, CV Plot of a) GZP(1), b) GZP(3), and c) GZP(10)	47
Figure 4.7	Area Under the Reduction Peak in $\mu\text{W}$ of the Electrodes. a) GZC(3) and, b) GZP(10)	49
Figure 4.8	Cyclic Voltammetry Test of the Electrodes at 1st Cycle and 1000th Cycle. a) G, b) GZ, c) GZC(3), and, d) GZP(10)	50
Figure 4.9	Voltage vs Time Response of the MFC Under Different Electrode	53
Figure 4.10	Power Curves of the Electrode Operated in MFC at a) 24 hrs, b) 48 hrs, and c) 72 hrs	54
Figure 4.11	MPD of the MFC with Modified Electrodes at the Operation Time of 24hrs, 48hrs and, 72hrs	56
Figure 4.12	Polarization Curves of the Electrode Operated in MFC at, a)24 hrs, b) 48 hrs, and 72 hrs	57
Figure 4.13	Rin of the MFC Under Modified Electrodes at the Operation Time of 24hrs, 48hrs and, 72 hrs	59
Figure 4.14	(a) COD Concentration (Influent, Effluent) and, (b) COD Removal Efficiency and CE of the G and GZC Electrodes at an Operation Time of 72hrs	61

## LIST OF ABBREVIATIONS

CB	= Carbon Black
CE	= Coulombic Efficiency
COD	= Chemical Oxygen Demand
CNTs/CNFs	= Carbon Nanotubes/Carbon Nanofibers
CV	= Cyclic Voltammograms
DBFC	= Direct Borohydride Fuel Cell
DMFC	= Direct Methanol Fuel Cell
EDX	= Energy Dispersive x-ray spectroscopy
FESEM	= Field Emission Scanning Electron Microscope
G	= Graphite
GB/NPC	= Graphite Fiber Brush Nitrogen and Phosphorous Co-Doped Carbon
GZ	= Graphite/Zinc Oxide Nanorods
GZC	= Graphite/Zinc Oxide Nanorods/Copper
GZP	= Graphite/Zinc Oxide Nanorods/Platinum
HMT	= Hexamethylenetetramine
HSM	= Hydrothermally Synthesized MnO <sub>2</sub>
LCV	= Linear Cyclic Voltammograms
MCD	= Maximum Current Density
MFC	= Microbial Fuel Cell
MPD	= Maximum Power Density
ORR	= Oxygen Reduction Reaction
PBS	= Phosphate Buffer Solution
PEM	= Proton Exchange Membrane
ROS	= Reactive Oxygen Species
RVC	= Reticulated Vitreous Carbon
SHE	= Standard Hydrogen Electrode
SSFFs	= Stainless-Steel Fiber Felts
WCA	= Water Contact Angle
ZnO NRs	= Zinc Oxide Nanorods

# CHAPTER 1

## INTRODUCTION

### 1.1 Background of the Study

The energy requirements for wastewater treatment can vary significantly depending on several factors, including the type and size of the treatment facility, the treatment processes used, the volume and composition of the wastewater, and the environmental regulations in place. The conventional methods of wastewater treatment are expensive, chemically and energetically intensive, and fail to generate a revenue stream. The standard municipal wastewater treatment with nutrient removal has an annual mean primary power requirement that ranges from 0.003-0.015 kW/inhabitant (Svardal & Kroiss, 2011). Therefore innovative, eco-friendly, and sustainable technologies have been developed today to treat wastewater.

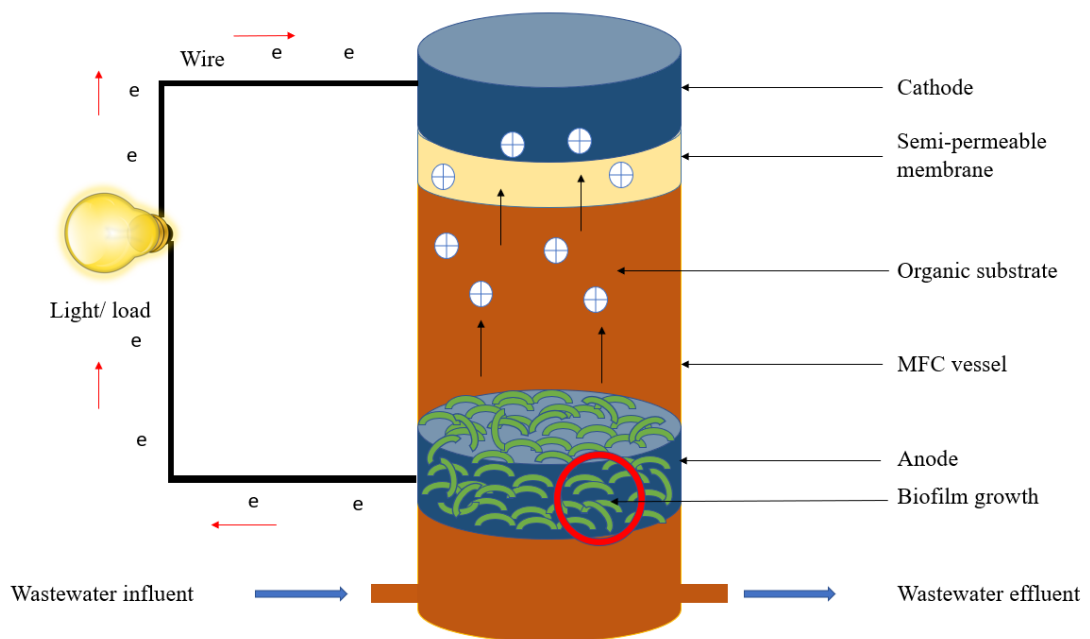
Microbial Fuel Cell (MFC) is one of the innovative technologies that oxidize organic substances in wastewater and produce electricity by using microorganisms as catalysts (Rabaey & Verstraete, 2005). MFCs have recently get a great deal of attention in scientific studies because of their exceptional characteristics of universality in various organic fuels, capability to clean wastewater, gentle reaction conditions, and inexpensive. MFC is fundamentally a fuel cell providing green energy as well as treating wastewater simultaneously. It uses a bio-electrochemical technique that uses respiring bacteria and oxidation-reduction reactions to convert chemical energy from organic substrates into electrical energy. The primary distinction is evident in the name, in contrast to conventional fuel cells, which use chemical catalysts to oxidize fuel at the anode chamber and reduce fuel at the cathode chamber, MFCs use living biocatalysts (bacteria) to transfer electrons throughout their systems, where a semi-permeable membrane that is immersed in an electrolyte solution divides the anode and cathode to create an operational MFC (Figure 1.1).

The working mechanism of MFC is as follows: it converts the chemical energy contain in the organic residues by electrochemically active bacteria which acts as a biocatalyst with hydrogen or hydrocarbon. Oxygen is the cathodic electron acceptor and water is the product after the cathodic reduction reaction. During the substrate oxidation by the bacteria, electrons and protons (hydrogen ions) are released to the anode compartment.

An outside circuit is used to move the electrons to the cathode compartment. Protons flow across a proton exchange membrane that separates the anode and cathode chambers while they diffuse through the electrolyte. An oxygen reduction reaction (ORR) occurs in the cathode chamber when protons and electrons join to convert oxygen into water. The quantity of metabolic energy that bacteria may acquire is affected directly by the difference between the anode potential and the substrate redox potential. (Silva-Palacios et al., 2023).

**Figure 1.1**

*Diagrammatic Illustration of a MFC Showing the Charge Transfer Process Involved in Generating Electricity and Treating Wastewater.*



The biocatalyst (bacteria), organic material (substrate), internal resistance, electrode material qualities, membrane properties, and ion concentration all have an impact on the MFC's performance and efficiency. (Yaqoob et al., 2021). The cost of electrode materials, the low buffering capacity of domestic waste water, high overpotentials and slow reaction kinetics of the ORR are the most arise issues when comes to the practical application of the MFC (Rismani-Yazdi et al., 2008).

## 1.2 Statement of the Problem

For effective energy conversion in MFCs, the ORR is crucial because it involves the transfer of electrons, which results in the production of electrical energy. However, it is also a challenging reaction, as the O<sub>2</sub> molecule is inherently stable and wants a catalyst to reduce the energy barrier for the reaction to proceed at a reasonable rate. ORR is a multistep process (section 2.2.1) and reacts slowly under acidic electrolytes (Ashmath et al., 2022). Therefore, it is a must to eliminate these limitations and speed up the ORR by using catalysts.

In many energy conversion devices, the ORR reaction is very important, as it provides the means for the cell to produce electrical energy by converting chemical energy from a fuel source. To increase the electricity generation and efficiency of the MFC, the electron transfer and ORR rate should be increased. For that, MFC requires electrode materials with high performance. In most cases, the cathode electrode is the limiting factor of MFC due to its high over-potential limiting ORR. The high over-potential typically occurs due to the limited presence of protons and hydroxyl ions (OH<sup>-</sup>) under neutral media which limits the ORR in the cathode chamber. (Chandrasekhar, 2018).

Therefore, to promote ORR active catalysts are required. Different types of catalyst substances have been applied in MFC, such as carbon-based catalysts (carbon black, graphene, carbon nanofibers), metal-based catalysts (platinum, iron, cobalt, manganese, vanadium), metal-carbon hybrids, M-N-C (metal-carbon-nitrogen) complexes and biocatalyst (Chandrasekhar, 2018). Out of these, platinum is the best catalyst used for the ORR which is supported by carbon (Pt/C) (Ben Liew et al., 2014). The properties of the Pt are excellent electrical conductors with great electrical energy density, high active surface area, and low resistance. However, the extreme price and toxicity of the microorganisms utilized in the MFC limit its applicability (T. Zhang et al., 2020). Also, Pt is a rare metal and a less durable material in fuel cells (Ashmath et al., 2022). Moreover, in the presence of Sulfur or Sulfur-compounds in wastewater, Pt active sites are deactivated by catalyst poisoning due to strong Pt-Sulfur covalent bonding (Santoro et al., 2013).

Manganese oxides are used as cathode catalysts for long-term ORR activity (Majidi et al., 2019). However, the powerful bonds between the electrons surrounding the atoms

in the crystal, manganese oxide exhibits poor electrical conductivity under normal circumstances.

. Iron is used as a catalyst but it is prone to rusting and will eventually be ruined by repeated rusting. Sometimes, Iron catalysts can be toxic to microorganisms and can cause biofouling (H. Yuan et al., 2016).

Therefore, fabricating an alternative catalyst that is easily accessible and capable of enhancing the ORR is very important to increase the efficiency of MFC. As different materials have different electrical and physical properties, combining them can increase the catalytic activity.

### **1.3 Objectives of the Study**

The main objective of this research is to improve the ORR in MFC by developing a high surface area graphite-based cathode decorated with nanostructured metal catalysts. During the study period, the following three particular objectives are specified in order to accomplish this overall objective.

1. To enhance the surface area of a graphite-based electrode by growing a dense array of vertically aligned zinc oxide nanorods (ZnO NRs) directly on it.
2. To deposit metal nanoparticles as catalysts on the modified graphite cathode and electrochemically evaluate their ORR performances. We explored Platinum (Pt) and Copper (Cu) metals as potential catalysts in this study.
3. To fabricate an MFC using the modified graphite-based cathodes containing ZnO and metal nanoparticles and evaluate its performance in terms of the power density, current density, and coulombic efficiency.

### **1.4 Scope of the Study**

The research aims to develop a graphite-based cathode containing ZnO and a nanostructured metal catalyst to increase the ORR in MFC. The material and cathode morphologies are studied using the Scanning Electron Microscope (SEM), their elemental analysis is investigated by using energy dispersive X-ray (EDX) technique, and water contact angle measurements are considered to measure the surface wetting behavior of the electrodes.

The cathodic catalyst for oxygen reduction is tested under aqueous conditions with oxygen in its dissolved form. To evaluate its applications, a two-chamber MFC is employed as representative of similar types of fuel cells. The catalyst is only examined for its suitability in carbonaceous cathodes. A cation exchange membrane served as the separator in the MFCs. The cathode catalyst was assessed within a laboratory-scale reactor, with each chamber having a volume of 116 mL.

### **1.5 Sustainability Impact**

This research provides a new avenue for renewable energy generation utilizing wastewater thus helping towards achieving targets in SDG 7, especially 7. a, 7. b which focuses on enhancing renewable energy generation capacities in developing countries, small islands, and landlocked countries by financial and technological means. The MFC oxidizes organic waste by using microorganisms to generate energy and in the process reduces the organic waste matter that would have been discharged to the environment otherwise. This, therefore, further helps towards attaining SDG 12.5 which intends to decrease waste production by means of reuse, recycling, prevention, and reduction. As the amount of research conducted in this area is relatively low, this research will provide a limelight that can kickstart a whole new arena. This will help towards SDG 9.5 which is to increase scientific research conducted in the industrial sector.

## CHAPTER 2

### LITERATURE REVIEW

#### **2.1 Mechanism of Functioning of the Microbial Fuel Cell**

MFC is advantageous for treating wastewater because it can effectively treat various types of compounds found in domestic, industrial, and agricultural wastewater. In contrast, many other fuel cell types are designed for specific fuels and specialized applications. For example, the proton exchange membrane fuel cell (PEMFC) relies on pure hydrogen as fuel (Murugan & Brown, 2015), the direct methanol fuel cell (DMFC) operates using methanol (Gwak et al., 2015), and the direct borohydride fuel cell (DBFC) functions under sodium borohydride (Celik et al., 2010). Therefore, the MFC does not require costly fuel to operate. The MFC is a distinctive technology that has just lately attained focus in the energy and environmental fields despite being there since the early 20th century.

The MFC is unique as it can generate electricity directly from biomass. MFCs are used to generate electricity from microorganisms used as biocatalysts in an organic medium or biomass (Ogugbue et al., 2015). It is an environment-friendly and renewable energy source. The chemical energy has been deposited in the organic medium is degraded into electrical energy by microorganisms (G. G. Kumar et al., 2013). The concept of applying microorganisms to generate electricity was first described by Michael Potter in 1910 (Kaur et al., 2020).

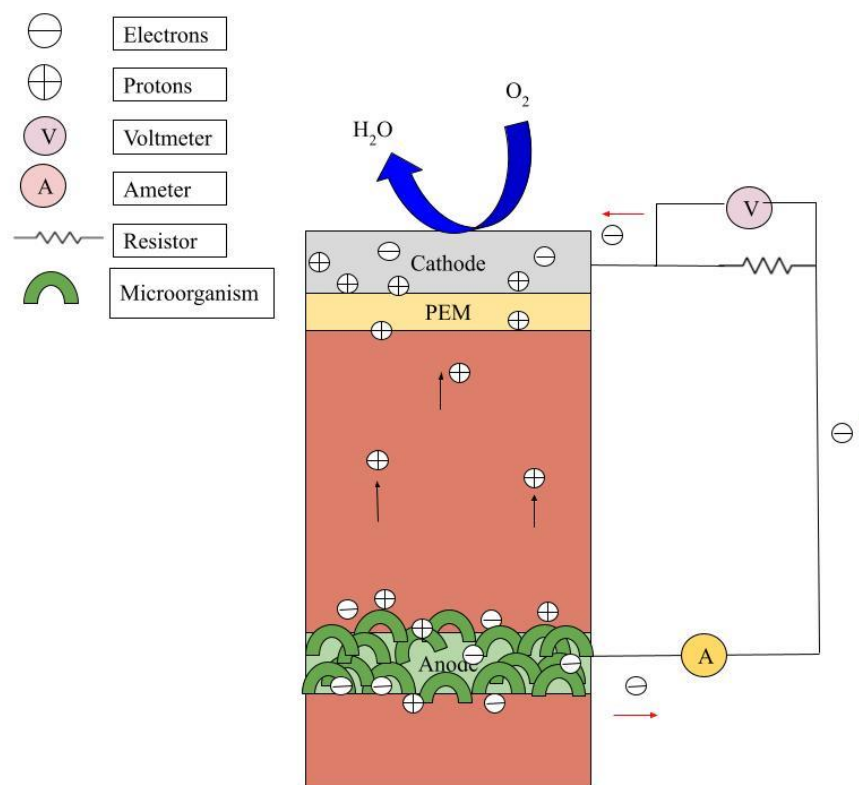
However, conventional biomass energy generates heat by burning the biomass and then use to create electricity. Biomass is broken down into CO<sub>2</sub> and water when exposed to oxygen. This process releases energy and can be facilitated by combustion or by bacteria. The complete breakdown of biomass into CO<sub>2</sub> and water is not possible in the absence of oxygen. Without oxygen, bacteria may still partially decompose biomass. Anaerobic bacteria are the name given to these kinds of bacteria. Certain anaerobic bacteria are electrogenic, meaning they can break down biomass and release electrons, CO<sub>2</sub>, and hydrogen ions (H<sup>+</sup>). (J. Y. Chen et al., 2019). In MFC it is possible to use these electrons to generate power. In order to produce a current, the H<sup>+</sup> and electrons combine with O<sub>2</sub> in a separate chamber called a cathodic chamber to form water (Mohamed et al., 2018).



There are two categories of MFC, which are single chamber and dual chamber MFC. The single-chamber MFC contains anode and cathode in the same chamber. Sometimes a proton exchange membrane (PEM) is applied to separate the anode and cathode (Kamali et al., 2022). In this type of MFC the cathode chamber is directly open to the air, as shown in Figure 2.1

**Figure 2.1**

*Single Chamber MFC*

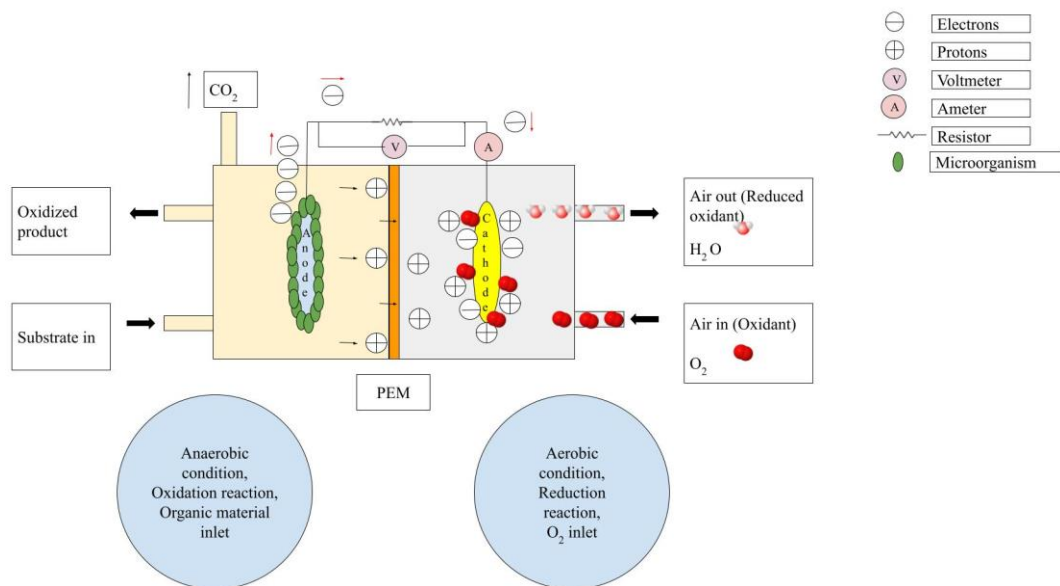


The main components of the dual chamber MFC are two half cells immersed in electrolyte and both are disconnected by a PEM, as shown in Figure 2.2. The anodic half-cell of the dual chamber MFC contains bacteria that feed on biomass, often called the substrate, and produce H<sup>+</sup> and electrons. The bacteria live on the surface of the electrode and this electrode is called the anode because electrons flow out of it. The cathodic half-cell, containing a negatively charged electrode, is called the cathode electrons flow into it. The cathodic half-cell is filled with electrolyte solution and oxygen is supplied continuously into it (Mohamed et al., 2018). Both compartments are separated by a PEM, which allows the transfer of protons from the anode compartment

to the cathode and blocks the transfer oxygen from the cathode to the anode (Abd-Elrahman et al., 2022). O<sub>2</sub> must be kept separated from the bacteria region so that it cannot harm the bacteria or combine with the H<sup>+</sup> and electrons without them entering the circuit. Because of the PEM, electrons cannot migrate directly to the cathode chamber and enter into it through a wire connecting the anode and cathode with an electric load such as a light bulb, thus producing electricity that can be stored (Hu et al., 2019). In the cathodic half-cell, electrons reduce the O<sub>2</sub> to O<sub>2</sub><sup>-</sup> which combines with the H<sup>+</sup> to produce water. The anode chamber works under neutral pH to maintain the growth and metabolic activities of the electrochemically active biocatalyst. The pH in the cathode chamber is maintained in slightly alkaline conditions (Chandrasekhar, 2018).

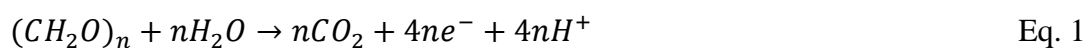
**Figure 2.2**

*Components of the Dual Chamber MFC*



The electrical energy generation in the MFC happens through a series of redox reactions, as described below, involving the organic substances (Y. Liu et al., 2020).

Anode reaction:

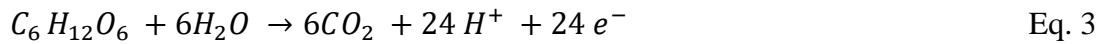


Cathode reaction:



Considering the substrate as glucose dissolved in water, the anodic and cathodic reactions will look like below

The anodic oxidation reaction,



The cathodic reduction reaction.



The overall reaction of the MFC is, therefore, can be expressed as,



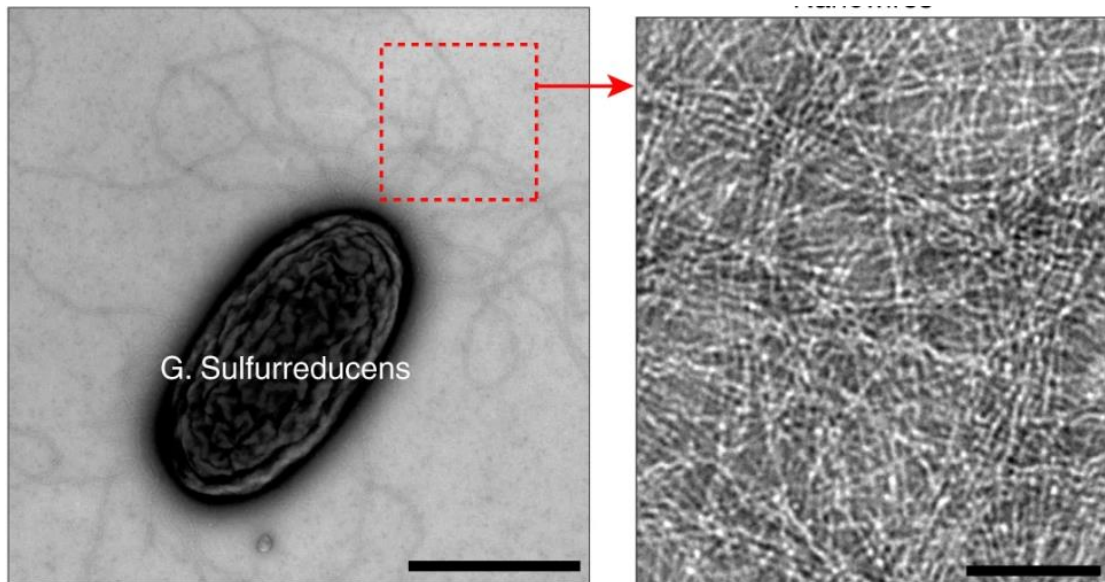
For the purpose of generating energy, the electrodes drive the growth of the potential difference, which works as a net driving force for the transfer of electrons from the anode to the cathode and in doing so results in reducing equivalents like electrons in the form of redox carriers (Silva-Palacios et al., 2023). Electroactive microorganisms have the capacity to either contribute or take electrons from a substrate (electrogenic or electrotrophic, respectively). Electrogenic bacteria release electrons onto the anode surface, which are measurable and represented as a positive electric current. Electrotrophic microorganisms are responsible for recapturing these electrons onto the cathode surface (Silva-Palacios et al., 2023). Extracellular electron transfer occurs through two mechanisms, namely direct transfer and indirect transfer.

During the direct transfer, the microorganisms involved transport electrons through their cell membrane, which helps the cytoplasm move electrons to the outside membrane of the cell and then form biofilms on the anode surface (Rabaey & Verstraete, 2005). As an example, *Shewanella putrefaciens*, *Geobacteraceae sulfurreducens* (Park & Zeikus, 2002) and *Rhodospirillum rubrum* (Bond & Lovley, 2003) microorganisms can directly transfer the electron to the anode which are capable of extending nanowires from cell outside to transfer the electron from cell surface to

anode surface (Min & Logan, 2004). In nature, *Geobacteraceae sulfurreducens* consumes acetate or hydrogen and reduces metals and sulfur. Thereby transferring electrons to the reductant (Butti et al., 2016).

### Figure 2.3

TEM Images of a *G. sulfurreducens* (left) and Purified Protein Nanowires (right) Scale Bars, 1  $\mu\text{m}$  (left) and 100 nm (right) (Fu et al., 2020)



It is difficult to transfer electrons directly to the anode because the outer layer of some microorganisms is made up of non-conductive lipid membranes, peptidoglycans, and lipopolysaccharides which are unable to directly transfer electrons to the anode (Davis & Higson, 2007). Therefore, electron carriers and electron mediators are introduced (Yamasaki et al., 2018). The second method is known as an indirect or mediated transfer of electrons, in which the microorganism receives an electron from within the cell membrane before reducing and sending it to the anode. These mediators fall into two categories: extracellular enzymes released by other microorganisms that produce diffusible chemical compounds and mediators by redox shuttles (Butti et al., 2016). Electron mediators can capture the electrons from the cell membrane, move across the cell membrane, and then move to the anode (Lovley, 2008). Electron mediators should be non-biodegradable and non-toxic for microorganisms (Ieropoulos et al., 2005). Some synthetic mediators are methylene blue, thionine, and natural red (Park & Zeikus, 2002).

The performance and efficiency of the MFC depend on the bacteria (microorganisms), organic materials, properties of the electrode material, the membrane, the internal resistance of the MFC, and the concentration of ions of the MFC (Abd-Elrahman et al., 2022). The electrode properties of surface area and porosity, electrical conductivity, stability, durability, cost, and accessibility play a major role in the efficiency of the MFC (Kaur et al., 2020).

## 2.2 Components of the Microbial Fuel Cell

### 2.2.1 Cathode

In the MFC, the cathode is largely responsible for the electron transport. The cathode initiates the fundamental potential difference for the electron transport (Kamali et al., 2022). The electrons generated at the anode compartment transfer through the external circuit and gather around the cathode. The electrons in the medium dissociate oxygen associating with hydrogen ions, resulting in the formation of water molecules (Lim et al., 2010). The ORR in two pathways (Abd-Elrahman et al., 2022).

4-electron path (W. Yang, Peng, et al., 2019)



2-electron path (peroxide path) (Liew et al., 2015)



In the 4-electron path, oxygen is directly reduced to water. This is mostly seen in noble metal electrodes used as the catalyst materials. The 2-electron path produces hydrogen peroxides which is mostly seen in the carbon materials (Abd-Elrahman et al., 2022).. Higher ORR potential occurs at the cathode by the 4-electron path which causes higher power density in the MFC (W. Yang, Peng, et al., 2019). The 4-electron path is more preferred than the 2-electron path.

Different cathode materials are carbon paper, graphite, carbon cloth, graphite felt, Platinum black, Platinum and Reticulated vitreous carbon (RVC) (Z. Du et al., 2007) Figure 2.4. The cathode material in most cases is carbon black (CB) because of its intrinsic characteristics, which include high stability, strong electron conductivity, and large surface area. It is an economically feasible material as well.

## Figure 2.4

*Different Cathode Materials Used in the MFC, a) Graphite, b) Graphite Felt, c) Carbon Paper, d) Carbon Cloth, e) Reticulated Vitreous Carbon and f) Platinum*



Different functional groups have been introduced to the CB to enhance the ORR. In an air-cathode MFC, a polypyrrole/carbon black (Ppy/C) composite was used as an electrocatalyst for the oxygen reduction process (ORR). In comparison to the carbon black electrode, the peak potential of the ORR at the Pp/C electrode changes towards positive potential by approximately 260 mV, confirming the electrocatalytic activity of Ppy toward ORR. The greatest power density produced from the MFC with a Ppy/C cathode is  $401.8 \text{ mW}/\text{m}^2$ , which is greater than the  $90.9 \text{ mW}/\text{m}^2$  obtained with a carbon black cathode and the  $336.6 \text{ mW}/\text{m}^2$  obtained with a non-pyrolyzed iron phthalocyanine cathode (FePc)/C (Y. Yuan et al., 2010).

Graphite fiber brush, graphite brush and graphite granules have various qualities in terms of electrical conductivity, biocompatibility, catalytic sites, and surface areas (Freguia et al., 2007). A non-catalyzed cathode consisting of granular graphite can deliver substantial steady currents. Power outputs of up to  $21 \text{ W}/\text{m}^3$  (cathode total volume) or  $50 \text{ W}/\text{m}^3$  (cathode liquid volume) were achieved in an acetate-fed continuous MFC. Granular graphite with nanoscale pores has a large surface area for oxygen reduction. The cathode is made by covering a graphite fiber brush current collector with a self-supporting nitrogen and phosphorous co-doped carbon (GB/NPC) ORR catalyst layer. The performance is measured under rotating conditions which causes to increase in the availability of catalytic sites for the ORR. The high performance was observed at 20 rpm,  $879 \text{ mW}/\text{m}^2$  (S. Chen et al., 2018).

Carbon cloth is loaded by hydrothermally synthesized MnO<sub>2</sub> (HSM) due to their distinct features and prospective applications as cathode catalysts in MFCs. The HSM increased the ORR through the 4-electron path and achieved a maximum power density of 119.07mW/m<sup>2</sup> which was 64.68% higher than that with the naturally synthesized MnO<sub>2</sub> (Haoran et al., 2014). In Table 2.1 the cathode materials used in the MFC and the performances are described.

### **2.2.2 Anode**

The anode is important to collect the electrons generated by microorganisms and transfer them through the external circuit. Carbon and its composite-based electrodes and nanocomposite-based electrodes are used as anode materials (Kaur et al., 2020). Carbon nanotubes, graphite felt and graphite rod have been developed with other materials to increase the performance of the MFC. Carbon cloth or carbon paper is a conductive material with a high surface area. The microorganisms utilized in MFC may block the anode's surface due to the small pore size of the 2-dimensional material (R. Kumar et al., 2018). Therefore 3-dimensional materials, reticulated vitreous carbon, carbon fiber nonwovens and graphite fiber brush are applied. Bacteria can attach to the electrode surface more successfully in three-dimensional anode designs because they have a larger surface area than two-dimensional anodes. (Jing Liu et al., 2012). To provide a large surface area, interfacial transport, and a friendly interface for microorganisms, carbon-based nanoparticles such as graphene and carbon nanotubes are deposited onto three-dimensional anode materials to make further improvements (Kaur et al., 2020).

The stainless-steel fiber felts (SSFFs), which have an open, solid, and macroporous structure, were coated with carbon nanoparticles (graphene, carbon nanotubes, or activated carbon) to create the three-dimensional (3D) macroporous anodes. The high reactivity, biocompatible surface, and low overpotential are achieved by the carbon nanoparticles-modified electrodes, giving the maximum power density of 2142 mW/m<sup>2</sup> at a current density of 6.1 A/m<sup>2</sup> in MFC (Hou et al., 2014). Graphene-modified SSM (GMS) has shown better electrochemical performance delivering a maximum power density of 2668mW/m<sup>2</sup> (Y. Zhang et al., 2011). The direct electron transfer process is increased by the Chitosan/Vacuum-Stripped Graphene scaffolds with hierarchically porous structures (He et al., 2012). Better conductivity, excellent biocompatibility,

good hydrophilicity, and superior electrocatalytic activity were achieved by a novel carboxylate multiwalled carbon nanotube/carbon nanofibers (CNTs/CNFs) composite electrode. This enhanced microbial adhesion and proliferation as well as extracellular electron transfer between bacteria cells and the anode(Cai et al., 2019).

Compared to the unmodified carbon paper electrode, the multiwall carbon nanotube/polyelectrolyte polyethyleneimine on carbon paper (MWCNT/PEI onto CP) self-assembled electrode demonstrated superior electrochemical performance. The maximum power density of 480 mW/m<sup>2</sup> was achieved by the self-assembled MWCNT/PEI onto CP, which was 48% higher than that of the plain CP anode (Roh, 2013). Different anode materials used in MFC and the performances are described in the Table 2.2.

### Figure 2.5

#### *Anode Electrode Modifications*

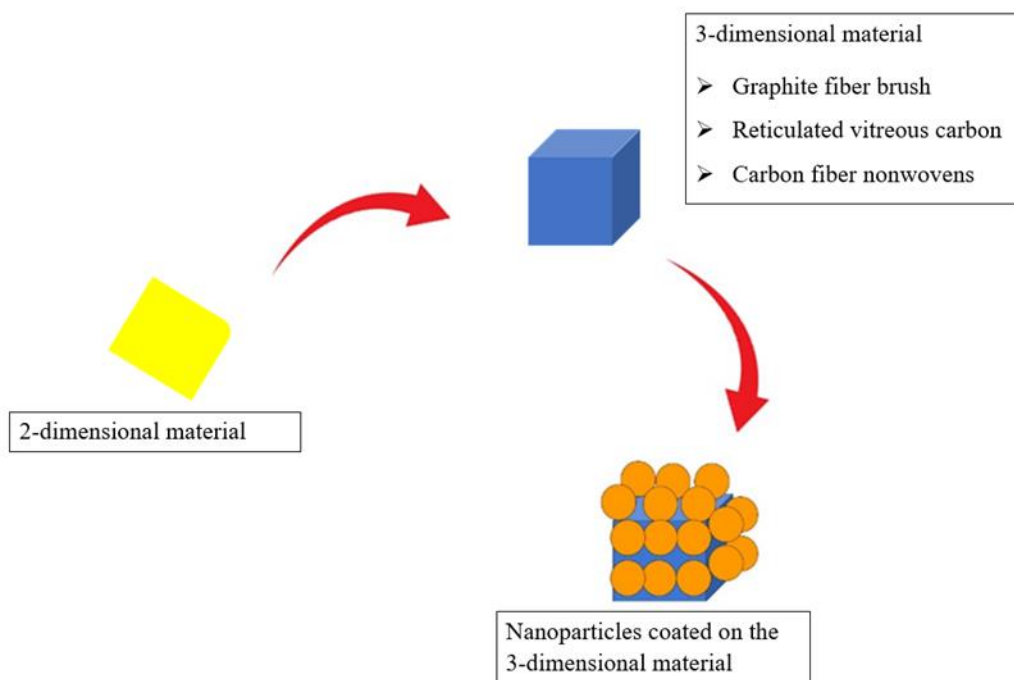




**Table 2.1**  
*Different Cathode Materials Used in MFC and the Performances*

MFC type	Cathode material	Material characteristics	Catalyst	Power density	Performances	Drawbacks	Reference
Single chamber	Carbon black	High surface area, good electron conductivity, high stability	Polypyrrole	401.8 mW/ m <sup>2</sup>	Power increases due to its catalytic activity to ORR. Polypyrrole's mode of action involves weakening the oxygen O-O bond and lowering the activation energy required for reduction. Polypyrrole has a function in the production of electricity and oxygen catalytic reduction.	A higher amount of Polypyrrole resulted in a lower power density	(Y. Yuan et al., 2010)
Dual chamber	Granular graphite	Electrical conductivity, biocompatibility, catalytic sites, and surface area	None	21W/m <sup>3</sup> (Power to cathode total volume)	Nanoscale pores on granular graphite provide a high surface area for oxygen reduction	The cathodic pH continuously increases	(Freguia et al., 2007)

MFC type	Cathode material	Material characteristics	Catalyst	Power density	Performances	Drawbacks	Reference
Dual chamber	Graphite fiber brush	3-dimensional, stability, strength,	N and P co-doped	$879 \pm 16 \text{mW/ m}^2$	The ORR's catalytic sites were more readily available due to the spinning circumstances, which also enhanced OH-transport and oxygen diffusion at or inside the air cathode.	Rotating the air cathodes diminishes the net energy production and increases the initial cost.	(S. Chen et al., 2018)
Single chamber	Carbon cloth	High electrical conductivity, stability	$\text{MnO}_2$	$119.07 \text{mW/ m}^2$	$\text{MnO}_2$ is structured by nanorods of high aspect ratio and multivalve nanoflowers. 4- electron pathway ORR.	Poor electrical conductivity , poor mechanical stability	(Haoran et al., 2014)

**Table 2.2***Different Anode Materials Used in MFC and the Performances*

MFC type	Anode material	Material characteristics	Power density (mW/m <sup>2</sup> )	Performances	References
Dual chamber	Stainless steel fiber felt	Large surface area, good biocompatibility, high strength, and resistance to corrosion	2142	The altered electrodes offered a significant response surface, interfacial transport, and biocompatible interface that were open to substrate transfer and bacterial colonization.	(Hou et al., 2014)
Dual chamber	Graphene-modified stainless-steel mesh	Electrically conductive better porosity	2668	High power generation as a result of the anode's large surface area and an increase in the number of bacteria attached to it	(Y. Zhang et al., 2011)
Dual chamber	Vacuum-Stripped Graphene (VSG)	High surface area	1530	Anode interior for bacterial colonization and improve the affinity contact between biocompatible VSG and multilayered bacteria, so enhancing process of direct electron transfer	(He et al., 2012)

MFC type	Anode material	Material characteristics	Power density (mW/m <sup>2</sup> )	Performances	References
Dual chamber	Carbon nanofibers/ Carboxylated multiwalled carbon nanotubes/ (CNFs /CNTs) compound	Good conductivity, biocompatibility, electrocatalytic activity	362 ± 20	Improved extracellular electron transport between the anode and bacterial cells	(Cai et al., 2019)
Dual chamber	Multiwall carbon nanotube/polyelectrolyte polyethyleneimine on carbon paper (MWCNT/PEI onto CP)	Highly conductive electrode, high specific surface area	480	Three-dimensional interlaced nanotubes allowed anodic bacteria to attach to MFCs with a more focused surface area	(Roh, 2013)

### ***2.2.3 Proton Exchange Membrane***

The ions moving membrane are classified into different way according to the working mechanism and the construction material. Depending on the working behavior of the membrane, the classification will be as follows,

1. Cation exchange membrane (Proton exchange membrane)
2. Anion exchange membrane
3. Amphoteric ion exchange membrane
4. Bipolar membrane
5. Mosaic ion exchange membrane

The membrane made out of static anions are suitable to separate cations, known as cation exchange membrane. The membrane made out of static cations are suitable to separate anions, known as anion exchange membrane. When the membrane made out both anions and cations it is known as the amphoteric ion exchange membranes. In the bipolar membranes both cation- and an anion-exchange membrane woven together and in the mosaic ion-exchange membranes which are constructed of macroscopic regions of polymers with negatively set ions and those with positively fixed ions irregularly distributed in a neutral polymer matrix (Riza et al., 2001).

The performance of the proton exchange membrane is very important to the MFC. It can selectively move protons from the anode to the cathode while inhibiting oxygen crossover from the cathode to the anode and the transfer of substrate from the anode to the cathode (Abd-Elrahman et al., 2022). This is crucial for keeping O<sub>2</sub> out of the anode half-cell while allowing H<sup>+</sup> to migrate to the cathode half-cell. Not all MFCs need membrane but there always has to be a way to keep O<sub>2</sub> away from the microbes and also away from the electrons before they reach the cathode half-cell. Nafion and Ultrex are the most common PEMs used in the MFC.

## **2.3 Properties of the Electrode Materials**

### ***2.3.1 Electrical Conductivity***

High electrical conductivity electrode material causes to fast electrons passage via an electrical circuit from an anode to a cathode (Sonawane et al., 2017).

### ***2.3.2 Surface Area and Porosity***

The electrodes surface has a significant impact on the power generated by MFCs. Enhancing the ratio of surface area to volume enhances the efficiency of fuel cells.

The number of reaction sites and the movement of electrons are correlated with surface area(Kaur et al., 2020). However greater porosity results in reduced electrical conductivity(Kultayeva et al., 2020).

### ***2.3.3 Stability and Durability***

Corrosion and degradation are caused by the anode and cathode during the oxidation-reduction cycle that takes place in the MFC. As a result, the electrode material needs to be strong and robust in both acidic and alkaline environments(Tao & Irvine, 2003).

### ***2.3.4 Cost and Accessibility***

The price of the electrode substrates are pivotal when developing the MFC. The material needs to be easily available for the development of the MFC.

## **2.4 The Catalyst for the Oxygen Reduction Reaction**

The ORR is an electrochemical reaction that happens in the MFC. By taking electrons from the anode and interacting with a hydrogen ion and oxygen in the cathode chamber, oxygen is reduced and produces water. The ORR is two pathways, mentioned in equations 6 and 7 in section 2.2.1. The ORR has a slow reaction kinetics due to the little presence of protons and hydroxyl/ hydroxide ions, which leads to high overpotential. Therefore the catalyst was applied to the cathode to overcome this limitation and speed up the ORR (Chandrasekhar, 2018).

Pt and gold (Au) are the best catalyst materials showing a 4-electron pathway (Liew et al., 2015). These two materials are high cost. Therefore, a significant area of research now focuses on creating effective, reliable, and non-precious metal cathode catalysts to reduce oxygen in MFCs. When researching noble cathode catalysts for MFCs, price, stability, activity, and manufacture should be given top consideration (Chandrasekhar, 2018).

Because the cathode is constantly exposed to water, composite organic matter, and biocatalysts, its stability is thought to be a major challenge. When alcohol, nitrides, sulfides, or chlorides are present in the electrolyte or substrate, the catalyst shouldn't react with them. The microorganisms in the anode chamber form bio-film which may

obstruct the catalyst performance. Power generation of the MFC depends on the durability and activity of the cathode catalyst, which is significant to encourage the sluggish kinetics of the ORR (Y. Du et al., 2019).

Various research has been conducted on low-cost cathode catalysts and different non-noble metal catalysts were proposed to the Pt catalyst. Manganese dioxide, lead oxide, cobalt oxide, graphene oxide and nickel powder are investigated as Pt/C alternative inexpensive cathode catalysts. The non-metal catalyst shows more stability and is inexpensive than the metal catalyst. Nitrogen-doped (N-doped) carbon materials have high ORR catalytic activity. As an example, carbon nanotubes (CNT), CNT cups, and carbon nano capsules are a few examples of N-doped carbon materials that are created using chemical vapor deposition.

Copper (Cu) has high electrical conductivity which is able to improve the charge transfer between the active sites and reactants (Xie et al., 2019). Cu – carbon-based catalyst under the potassium hydroxide electrolyte showed better catalytic activity towards the ORR with four electron pathway (L. P. Yang et al., 2019). Zehua Yang et al have developed the catalyst that demonstrated the highest ORR in both acidic and alkaline media was nitrogen-doped porous carbon anchored by individual Cu atoms and Cu clusters. The reason was that active sites are dominated by nitrogen-coordinated Cu atoms and, electron density is increased by a closed Cu cluster that causes to weakened oxygen double bond, finally boosting the ORR (Z. Yang et al., 2022).

Considering the polarization curve and cathode potential, which reveal the MFC's overall internal resistance. The long-term assessment of MFC offers details on the electrode and catalyst stability as well as biofouling and catalyst poisoning brought on by wastewater (Chandrasekhar, 2018).

The majority of materials employed as catalysts are carbonaceous because graphitized nanostructures are more conductive, extremely stable, and have a larger surface area. Better biocompatibility, proper conductivity, resourcefulness, high porosity, low price, non-corrosive nature, and, versatility are the most important characteristics that carbon-based electrodes differ from other electrodes (Jaswal et al., 2023). Activated carbon has good electrical conductivity and it can be further increased by incorporating carbon black into the cathode electrode during the preparation process. Mainly catalyst

materials can be classified into, metal-carbon hybrids, metal-based catalysts, carbon-based catalysts and M-N-C (metal-nitrogen-carbon) composite, photocatalyst and biocatalyst. Table 2.3 summarizes different types of catalyst materials applied in MFC.

Metal oxides have been applied as cathode catalyst material. Titanium dioxide has been applied as a cathode catalyst as it has a fair price, proper activity, earth abundance, proper stability, and chemical inertness, (Yahia et al., 2016). Recent studies have looked into how metal oxide's ORR rate and antibacterial qualities can lengthen cathode lifetimes (Jaswal et al., 2023). A restricted amount of silver ions can be released by the antibacterial substance Ti, into a liquid environment, where sulfhydryl group enzymes are involved in aerobic bacterial respiration(A. Kumar et al., 2023).

Applying carbon-based nanocomposites to MFC will cause biofilms to grow on the cathode surface, which will increase the carbon nanomaterials' high biocompatibility(W. Yang, Chata, et al., 2019). A physical barrier against the mass transfer of ions and oxygen will be formed on the cathode surface, generating an increase of concentration overpotential (W. Yang, Chata, et al., 2019). It will cause to increase the pH and reduce the power generation (W. Yang, Chata, et al., 2019). Additionally, ZnO exhibits antibacterial qualities against both gram-positive and gram-negative bacteria (Junli Liu et al., 2018).



**Table 2.3***Different Catalyst Materials are Applied in MFC*

Anodic electrode	Cathodic material	Cathode catalyst	Cathode surface area (cm <sup>2</sup> )	Cathodic chamber volume (mL)	Maximum power density $\mu\text{W}/\text{cm}^2$ ( $\mu\text{W}/\text{cm}^3$ )	External resistance $\Omega$	Reference
Carbon brush	Gas diffusion layer (GDL)	Co/NSC	14.3	250 (200 working volume)	18		(Ashmath et al., 2022)
Carbon brush	A pellet based on activated carbon, carbon black, polytetrafluoroethylene (PTFE)	Fe-N-C	2.8		195 $\pm$ 7		(Santoro et al., 2016)
Carbon paper	Carbon paper	MnO <sub>2</sub> /f-CNT	24		52	1 k	(Liew et al., 2015)
Carbon felt	Carbon black	CuZn	100	150	7.51 $\pm$ 0.71 (0.0075 $\pm$ 0.00071)	100	(Das et al., 2020)
Carbon paper	Carbon paper coated with 0.5 mg/cm <sup>2</sup> Pt	Vanadium oxide/ polyaniline composite	12	423	7.926		(Sarkar & Bhattacharyya, 2012)
Carbon electrode	Indium tin oxide (ITO)	Cobaltic oxide and nitrogen-doped graphene (Co <sub>3</sub> O <sub>4</sub> /N-G)	4	250	134 $\pm$ 1		(Su et al., 2013)

Anodic electrode	Cathodic material	Cathode catalyst	Cathode surface area (cm <sup>2</sup> )	Cathodic chamber volume (mL)	Maximum power density $\mu\text{W}/\text{cm}^2$ ( $\mu\text{W}/\text{cm}^3$ )	External resistance $\Omega$	Reference
Carbon cloth	Gas diffusion electrode	SSM-supported cobalt oxide (Co <sub>3</sub> O <sub>4</sub> )	7		N/A (17.8)	50 - 10 k	(Gong et al., 2014)
Carbon paper	Carbon paper	Activated electrospun carbon nanofiber (ACNF)	12	423	6.128		(Ghasemi et al., 2011)
Carbon cloth	Carbon cloth	Cobalt/cobalt phosphide and cobalt/cobalt sulfide nanoparticles embedded in N-doped carbon nanofiber	4		Co/CoP/ Co <sub>2</sub> P@N- CNF = 37.516 and Co/CoS <sub>2</sub> @N- CNF = 40.006	70 - 9999	(Guo et al., 2023)
Carbon brush		Fe-AAPyr and Fe-MBZ	4	130	Differ with pH value (61–68 at pH 6, 68–80 at pH 11)	1 k	(Santoro et al., 2015)
Carbon papers	Glass carbon electrode	Iron tetrasulfophthalocyanine functionalized graphene (FeTsPc-graphene)		115	81.7	0–10 k	(Y. Zhang et al., 2012)

Anodic electrode	Cathodic material	Cathode catalyst	Cathode surface area (cm <sup>2</sup> )	Cathodic chamber volume (mL)	Maximum power density $\mu\text{W}/\text{cm}^2$ ( $\mu\text{W}/\text{cm}^3$ )	External resistance $\Omega$	Reference
Carbon-cloth	Titanium sheet	PbO <sub>2</sub> /Ti (butanol) and PbO <sub>2</sub> /Ti (Nafion) cathodes	16	450	PbO <sub>2</sub> /Ti (butanol) = 7.7 $\mu\text{W}/\text{cm}^2$ PbO <sub>2</sub> /Ti (Nafion) = 7.8 $\mu\text{W}/\text{cm}^2$	50 - 50,000	(Morris et al., 2007)
Carbon cloth	Carbon cloth	RuCoSe		250	0.75	1 k	(Rozenfeld et al., 2017)
Graphite plate	Graphite electrode	NiTiO <sub>3</sub> and CuNiTiO <sub>3</sub>	24.5	251	CuNiTiO <sub>3</sub> = 6.218	500	(Rezaei et al., 2022)
Carbon felt	Stainless steel wire mesh	Cu-Sn alloy/ acetylene black (AB) composite	6.25	30	47	100	(Noori et al., 2018)
Carbon cloth	Teflonized carbon cloth	Graphene oxide/ Zinc/ Cobalt		28	77.3	1000	(W. Yang, Chata, et al., 2019)
Graphite	Titanium	Palladium deposited on TiO <sub>2</sub> nanotubes	15	125	20	2M - 10	(Hosseini & Ahadzadeh, 2012)
Carbon felt	Carbon felt	TiO <sub>2</sub> , Bismuth-TiO <sub>2</sub>		80	22.4	100	(Bhowmick et al., 2018)
Carbon cloth	Carbon cloth	TiO <sub>2</sub>	42	500	16.25	5- 5k	(Jaswal et al., 2023)

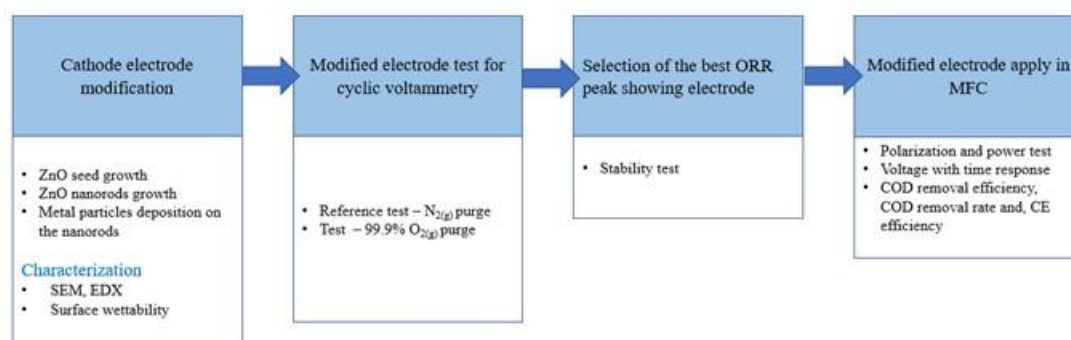
## CHAPTER 3

### METHODOLOGY

The overall process of developing a nanostructured cathode for the enhanced cathodic oxygen reduction reaction in MFC can be mainly classified into four sections as mentioned in Figure 3.1. In brief, the cathode electrode surface was modified with ZnO nanorods by microwave-assisted hydrothermal method and decorated with metal nanoparticles. The modified electrodes were then studied for their morphology under SEM, the elemental analysis of the metal particles on the cathode surface was conducted using EDX, and the surface wettability was studied measuring water contact angle. Then modified electrodes were tested for their ORR ability using three electrodes electrochemical cell. The 99.9%  $N_{2(g)}$  was purged through the cell before starting the test as the reference, and ORR potential was studied using 99.9%  $O_{2(g)}$ . The electrode showing the highest ORR capability was selected and further tested for the stability test using 1000 cycles in cyclic voltammetry test. All the cyclic voltammetry tests were conducted in phosphate buffer solution (pH 6.8) at a scan rate of 20 mV/s at the potential range of -0.6 V to 0.8 V using an Ag/AgCl reference electrode. After doing the stability test, the electrodes were applied in the MFC. The MFC was characterized for its maximum power density, internal resistance, and coulombic efficiency using the modified cathode electrodes. The detailed methodology used in this research study is described below.

**Figure 3.1**

*The Overall Methodology of the Research*

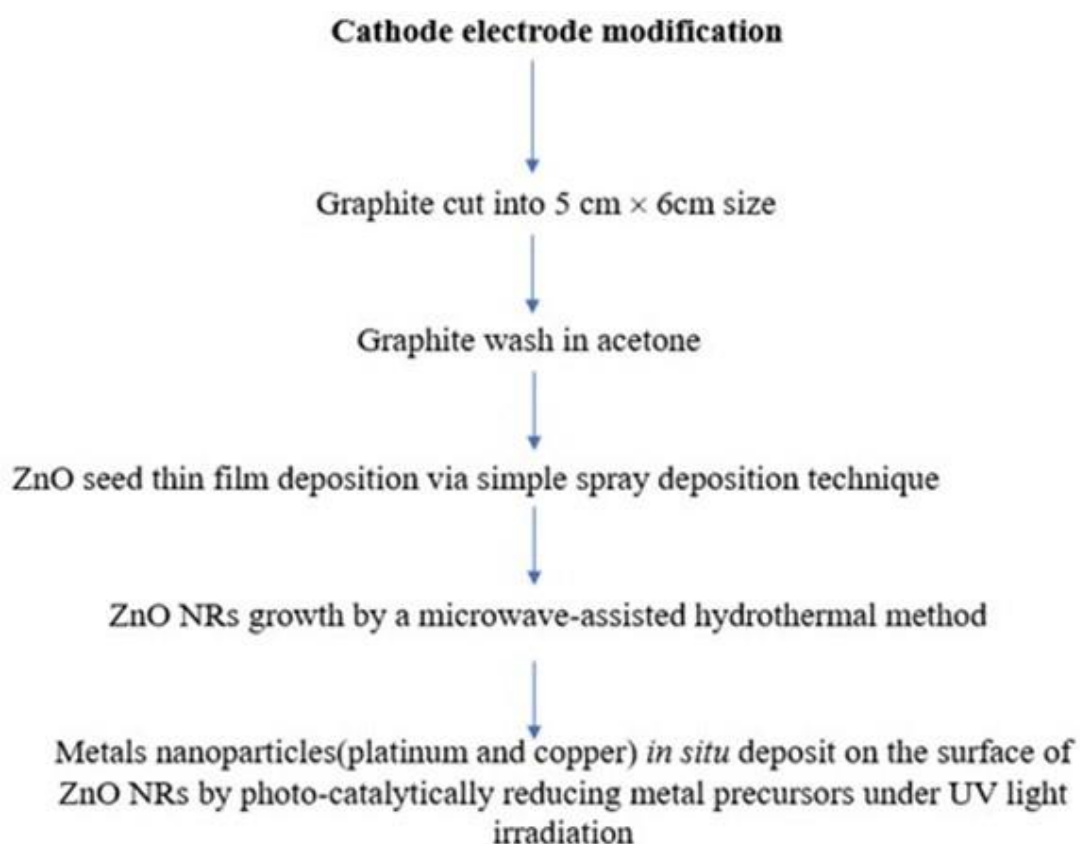


### 3.1 Cathode Electrode Modification

Graphite was used as the cathode electrode and it was modified using ZnO NRs as a surface modifier and metal nanoparticles (Cu NPs and Pt NPs) were deposited on the ZnO NRs to improve ORR in a two-chamber MFC. Briefly, the graphite was cut into 5 cm × 6 cm size and washed in acetone and DI water followed by drying in the oven at 100°C for 1 hour. ZnO seed thin film was deposited on the surface of the graphite via a simple spray deposition technique. Then ZnO NRs were grown on a graphite substrate by a microwave-assisted hydrothermal method. Finally, metal NPs were deposited *in situ* on the surface of the prepared ZnO NRs by photo-catalytically reducing metal precursors (Bora et al., 2016).

**Figure 3.2**

*Cathode Electrode Modification Steps*



### 3.1.1 Chemicals

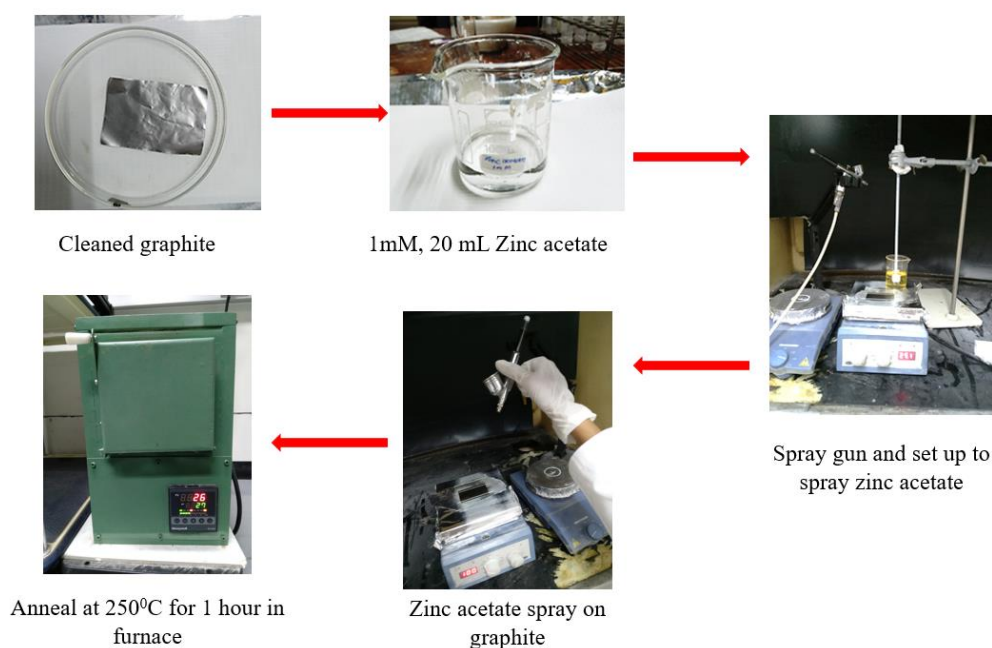
Zinc acetate dihydrate  $[(\text{CH}_3\text{COO})_2\text{Zn} \cdot 2\text{H}_2\text{O}]$ , MW= 219.49 g/mol, Merck], Zinc nitrate hexahydrate  $[\text{Zn}(\text{NO}_3)_2 \cdot 6\text{H}_2\text{O}]$ , MW= 297.47 g/mol CARLO ERBA Regents], Hexamethylenetetramine  $[\text{C}_6\text{H}_{12}\text{N}_4]$ , MW= 140.19 g/mol, HIMEDIA], Ethyl alcohol  $[\text{C}_2\text{H}_5\text{OH}]$ , Duksan Pure Chemicals], Copper (II) nitrate  $[\text{Cu}(\text{NO}_3)_2 \cdot 2.5\text{H}_2\text{O}]$ , MW = 232.59 g/mol, Ajax Finechem], Hexachloroplatinic (IV) acid hexahydrate  $[\text{H}_2(\text{PtCl}_6) \cdot 6\text{H}_2\text{O}]$ , MW= 517.90 g/mol, Sigma Aldrich] and DI water.

### 3.1.2 ZnO Seed Growth on the Graphite

The ZnO seed thin film layer was deposited on the graphite substrate by a spray deposition process. Before depositing the ZnO, the graphite substrate was cut into 5 cm  $\times$  6 cm dimensions and was used as substrates in the preparation of ZnO nanostructure, hence known as graphite substrates. Next, the graphite substrate was cleaned by immersing it in acetone for 12 hours and washed with DI water to remove the surface impurities before use. A solution was prepared using zinc acetate dihydrate as a precursor and DI water as a solvent. The solution of 1mM zinc acetate 20 mL was mixed in the ultrasonic bath at room temperature for 10 min to make the solution precursor for a seed layer before using it in the spray deposition process.

**Figure 3.3**

*Preparation of ZnO Seed Thin Film Layer on Graphite Surface*



The surface of a hot plate was covered with aluminum foil. The hot plate was heated to the temperature of 90°C. Next, the solution was sprayed onto the graphite substrates using the spray gun at a deposition pressure of 1 bar. The distance between the graphite and the spray gun was fixed at 25 cm. The solution volume for a 1-time spray was 1 mL, and this solution was sprayed over the graphite surface by rotating the substrate at the right angle in between to make sure uniform spray on the graphite surface. Therefore, a total of 4 mL solution was sprayed on one side of the graphite substrate. During the spraying process, the temperature of the heating surface was maintained at 90°C. Finally, the graphite substrates with deposited seed layer were annealed at 250°C for 1hr in the furnace and then allowed to cool down naturally to form a ZnO seed uniform layer on the graphite substrate.

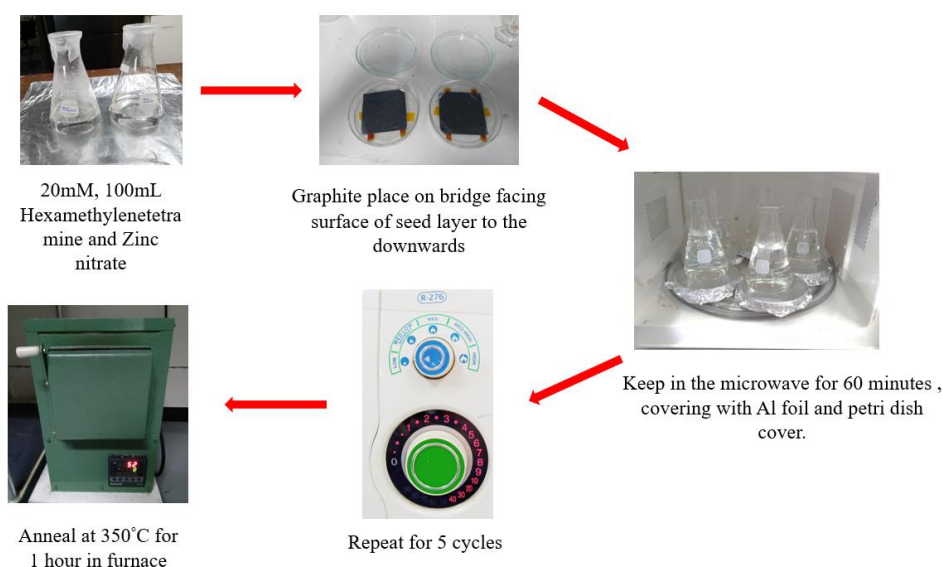
### ***3.1.3 ZnO Nanorods Growth on the ZnO Seeds***

After uniformly coating the graphite substrates with the ZnO seed layer, ZnO nanorod arrays were grown from the seed layer via a hydrothermal method using microwave radiation. The solution for growing the ZnO nanorods was prepared by dissolving the equimolar of hexamethylenetetramine (HMT) and zinc nitrate with 20 mM concentration. 20 mM of hexamethylenetetramine and 20 mM of Zinc nitrate dissolve in DI water in separate beakers. The solutions were mixed using an ultrasonic bath for 10 minutes without heating. The two solutions were then mixed into a beaker to obtain the ZnO NR growth solution. Next, the ZnO seed substrates (5×6 cm<sup>2</sup>) were placed on the glass bridge in a petri dish, with the seed layer facing downwards, and filled with the prepared zinc nitrate + HMT aqueous solution.

The samples were then irradiated with microwave radiation at 90 °C (Sharp, R-276, power output of 800Watt) for 60 min, followed by 20 min cooldown per cycle. Thus, a total of 5 cycles were repeated to grow the ZnO NRs, and during each cycle, the growth solution was replenished with fresh solution. After the hydrothermal reaction, the ZnO nanorod film samples were taken out and washed with DI water several times to remove residual chemicals. Lastly, the ZnO nanorods coated samples were annealed at 350°C for 1h in a furnace.

**Figure 3.4**

*ZnO NRs Growth on the Seed Layer*



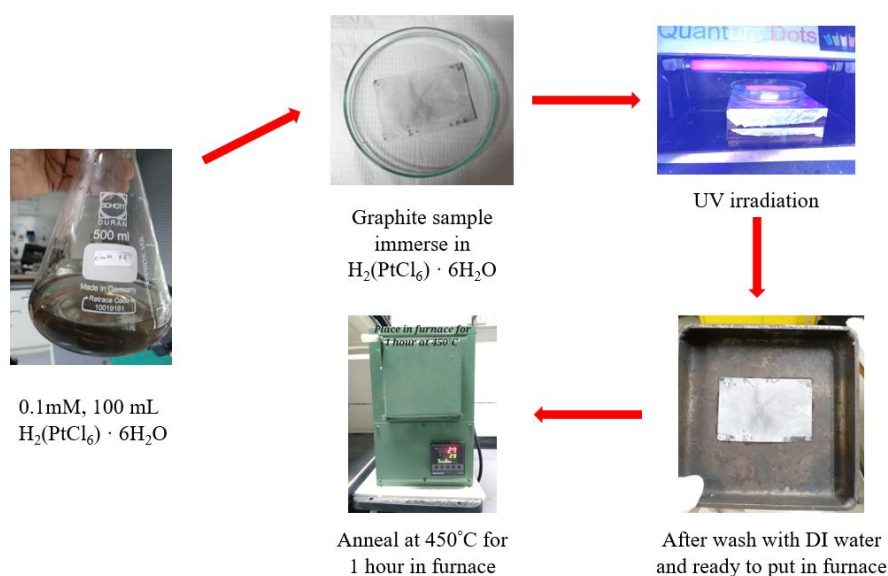
**3.1.4 Metal Nanoparticles Deposition on the ZnO Nanorods**

A photocatalytic reduction process was used to deposit the metal NPs onto the ZnO nanorods. Firstly, the ZnO nanorods substrate was immersed into a solution of metal precursor with 0.1 mM in concentrations mixed with a 1:1 ratio of DI water and ethanol. Then, the mixture was kept under irradiation with UV for 10 minutes. The distance between the light source and the samples was fixed at 5 cm. The UV light was provided by a UV lamp (Philips, TUV 6W). In some cases, several deposition cycles of metal particles were carried out in a similar way to vary the metal concentration by repeating the UV irradiation cycles from 1 to 10 times. After the irradiation, the as-synthesized samples were thoroughly cleaned with DI water. Then the samples were soft baked in a dry oven for one hour. Finally, all samples were annealed at 450 °C for 1 h in the furnace. This completes the preparation of the Graphite/ ZnO NRs/ metal NPs cathode process, and the samples were then stored in a dry place at room temperature for further use.



### Figure 3.5

#### *Metal NPs Deposition on ZnO NRs*



#### **3.1.5 Sample Characterization**

##### SEM

The morphology of the GZ, GZC, and GZP catalysts was studied by a Field Emission Scanning Electron Microscope (FE-SEM SU8230, Hitachi, Tokyo, Japan). The catalyst material was electrically conducting. Therefore, the modified GZ, GZC, and, GZP electrodes were directly attached to the SEM sample holder through carbon tape. The samples were tested under 50000× and 100000× magnification at the acceleration of 15 kV. The EDX was done on GZC and GZP to determine the elemental composition of the catalyst.

##### Surface Wettability

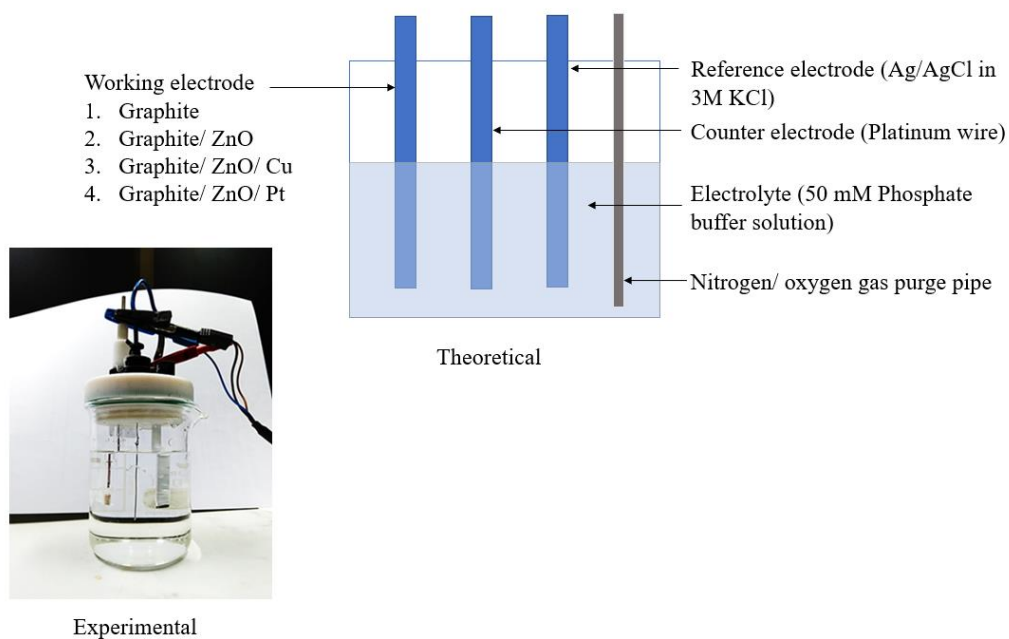
The surface wettability was measured by using the Ossila Contact Angle Goniometer. The modified electrode was placed on the stage of the instrument and 0.01 mL water drop was put on the top of the electrode surface perpendicularly using a syringe. Three replicas from each electrode type were tested to measure the WCA. The water contact angle was measured using the ImageJ software.

### 3.1.6 Electrode Performances Testing

The ORR activity of the graphite, graphite/ ZnO NRs, and graphite/ ZnO NRs with different metal NPs were evaluated using the cyclic voltammetry technique with a standard 3-electrodes systems [Ossila Potentiostat with Cell (T2006B1)]. During the measurements graphite and other modified metallic cathode electrodes were used as the working electrode, Pt wire as the counter electrode, and Ag/AgCl in 3M KCl was used as the reference electrode. The electrolyte was 50 mM phosphate buffer at 6.8 pH containing  $\text{NaH}_2\text{PO}_4$  (2.76 g/L) and  $\text{Na}_2\text{HPO}_4$  (4.26 g/L)(Liew et al., 2015). The scanning potential was varied from -0.6 V to +0.8 V at a scan rate of 20 mV/s. Before ORR tests, background tests were conducted by purging 99.9% pure  $\text{N}_2$  gas for 30 minutes. ORR tests were then conducted by purging 99.9% pure  $\text{O}_2$  gas for 30 minutes prior to the start of the test. The CV was taken at ambient temperature and repeated for 3 cycles until a consistent scan was achieved (Liew et al., 2015). The test results were compared with the graphite and the modified graphite cathode electrode area of the ORR peak at the reduction curve. The area under the ORR peak was evaluated by using the MATLAB 2022b software.

**Figure 3.6**

*Electrochemical Cell Using Three Electrodes System*



### ***3.1.7 Stability Test of the Modified Cathode Electrode***

The stability test was only conducted for the modified graphite electrodes which had more ORR peak. During the stability test, the atmospheric air was filtered through a filter and pass-through air control valve which released one air bubble per 10 seconds. The stability of the modified cathode electrode was achieved by potential cycling of the working electrode by recording cyclic voltammograms for 1000 cycles at the scan rate of 20 mV/s (Ashmath et al., 2022). The area of ORR peak at the reduction curve of the 1 cycle and 1,000 cycles were compared with each other (Das et al., 2020).

## **3.2 MFC Fabrication**

### ***3.2.1 MFC Design***

The design of the MFC was developed using solid works software. A two-chamber MFC was designed using acrylic sheets of 5 mm and 20 mm thickness, as shown in Figure 3.7. A 5 mm thickness acrylic sheet was used for the outer frame of the MFC and a 20 mm thickness acrylic sheet was used to make the chamber for the MFC(Kuppurangam et al., 2019).

### ***3.2.2 MFC Configuration and Assembly***

The inner volume of each chamber of the MFC was 120 mL and the working volume was 116 mL. A cation exchange membrane (PEM) (CMI – 7000; Membranes International Inc) was placed between the anode and cathode chambers as the separator. Silicon rubber seals were used to prevent the leakage. The area of the membrane which was opened to anolyte/catholyte in a chamber was 56 cm<sup>2</sup>. Graphite was used for the cathode and carbon fiber fabric (3K, plain weave at 200 gsm, thickness is 0.2 mm) was used as an anode electrode as it is rough and has a high surface area to grow biofilm. The electrodes were placed 2.3 cm from the membrane and were fixed to the outer frame of the MFC to minimize the movement of the electrodes and to maintain the same distance to have uniform electric field distribution between the electrodes. The surface area of the electrode was 24.75 cm<sup>2</sup>. The acrylic sheets, PEM, and silicon rubber seals were finally connected through 5M threaded studs, washers, and nuts. The MFC components and their configuration order are shown in Figure 3.8.

**Figure 3.7**

*MFC Drawing From the Solid Works*

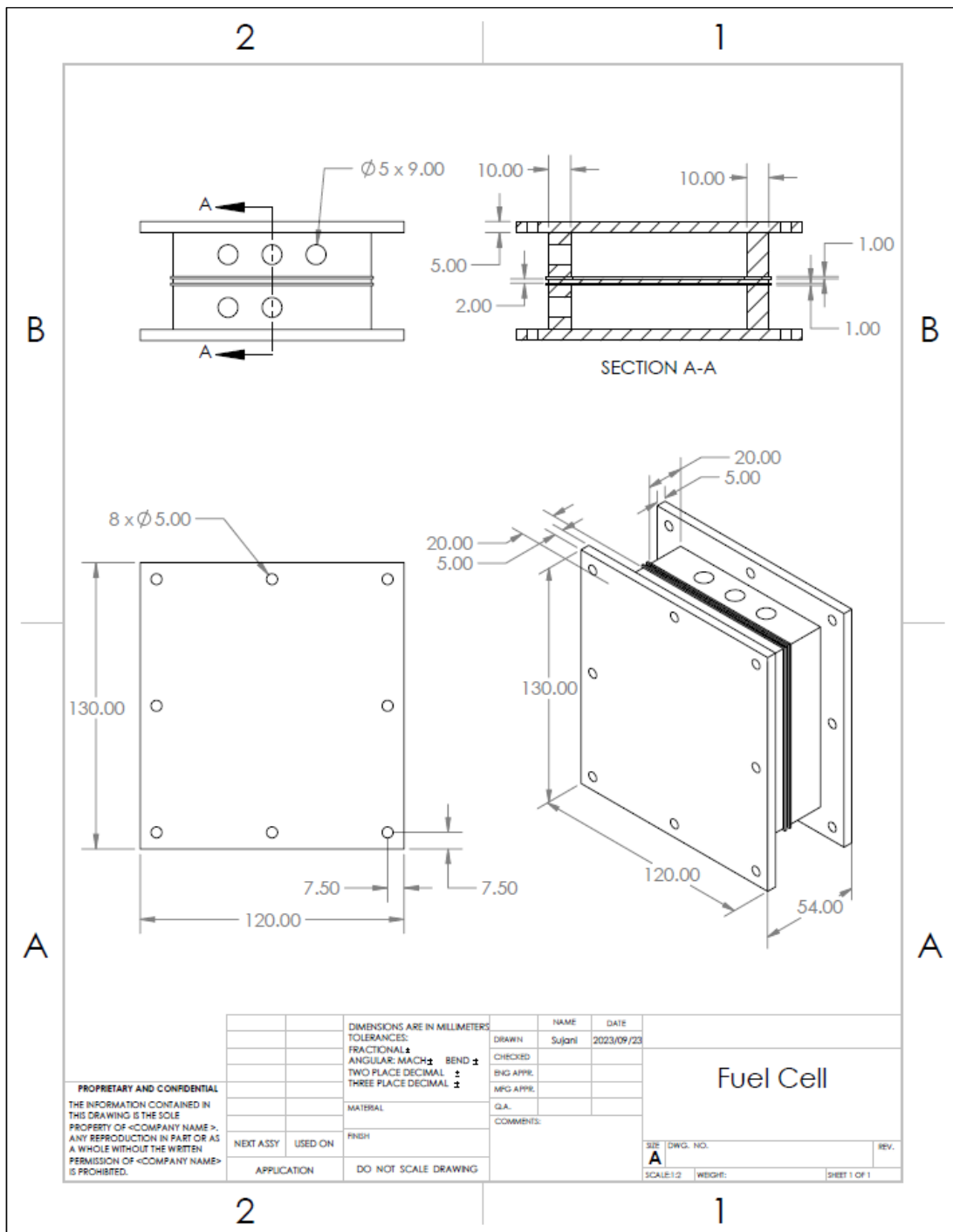
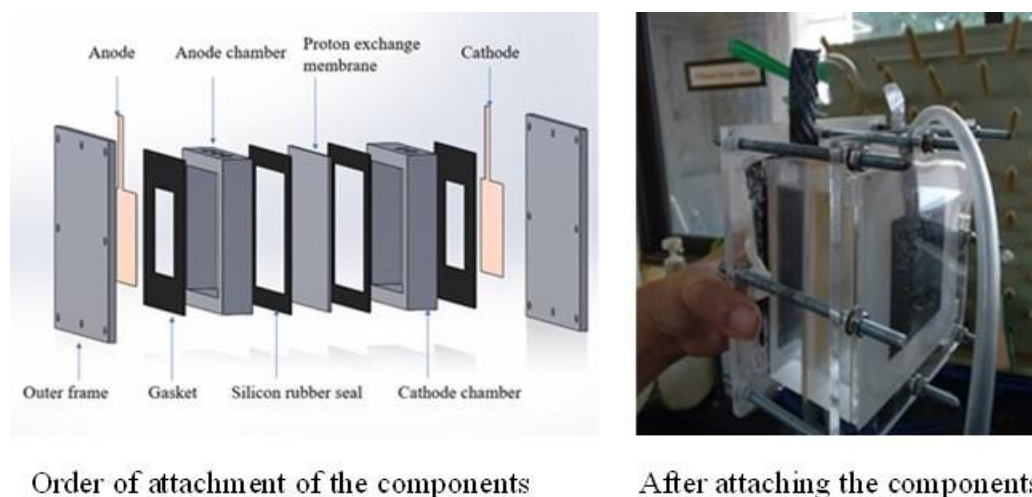


**Figure 3.8**

*Microbial Fuel Cell - Order of the Component Attachment*



### **3.2.3 The Anode Electrode Acclimatization**

The anode electrode was acclimatized to obtain an electrochemically active bacteria biofilm. The anaerobic sludge sample was collected from the biological sludge from Ranhill water technologies (Thai)LTD, RWTT 1.5 MLD wastewater treatment plant. Sludge was mixed with synthetic medium at a ratio of 1:1. Synthetic medium contains 50 mM PBS buffer solution (2.76 g/L of  $\text{Na}_2\text{HPO}_4$ , 4.26 g/L of  $\text{NaH}_2\text{PO}_4$ , 0.31 g/L of  $\text{NH}_4\text{Cl}$ , 0.13 g/L of  $\text{KCl}$  and DI water) and trace minerals. The sodium acetate was used as the organic carbon to the level of 3 g/L (Liew et al., 2015). The anode chamber was sealed with  $\text{N}_2$  gas to maintain anaerobic conditions. The anode chamber was replenished with fresh medium every time the MFC voltage decreased below 50 mV.

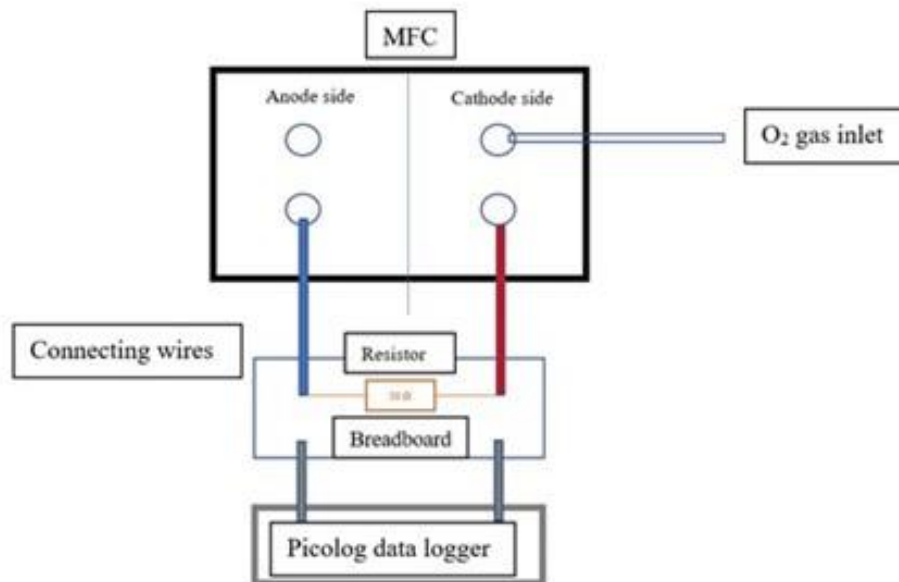
### **3.2.4 MFC Operation**

The anode chamber was filled with synthetic medium and 3g/L of COD. The anode chamber was purged with  $\text{N}_2$  gas to remove the  $\text{O}_2$  and sealed with a silicon rubber stopper. The cathode chamber was inserted with the graphite and other modified cathode electrodes, filled with 50 mM PBS buffer solution (2.76 g/L of  $\text{Na}_2\text{HPO}_4$ , 4.26 g/L of  $\text{NaH}_2\text{PO}_4$ , 0.31 g/L of  $\text{NH}_4\text{Cl}$ , 0.13 g/L of  $\text{KCl}$ ), and purged continuously with  $\text{O}_2$  gas using a stone head diffuser to control the air pressure. Conducting wires were used to connect the electrodes, and an external resistor of 1 k $\Omega$  was connected to the circuit (Guo et al., 2023). A voltage data logger (Picolog 1012, 10 bits, 12 channels) was

used to measure and record the voltage of the cell. The MFC was operated at room temperature conditions (Figure 3.9).

**Figure 3.9**

*The External Hardware Attachment Diagram to the MFC*



### 3.3 Data Acquisition and Chemical Analysis

#### 3.3.1 Voltage and Polarization Curve

The cell voltage across the external circuit of the MFC was recorded using the PicoLog 1012 data logger and the polarization curve was obtained by giving various external loads ranging from 50  $\Omega$  to 30 k $\Omega$  within 15 min (Noori et al., 2018). First, the MFC was put into the open circuit voltage condition and waited until it was stabilized. Then the voltage was recorded. Afterward, 30 k $\Omega$  was applied and wait for the stabilization and recorded the voltage reading. This step was continued until the 50  $\Omega$  resistor.

#### 3.3.2 Electrical Characterization of the MFC

Current Density

The current of the MFC was determined using the simple equation of  $V= IR$  and the current density was calculated from the current divided by the surface area of the electrode which was immersed in the catholyte.

$$I_d = \frac{V}{R \times A} \quad \text{Eq. 9}$$

Where,  $I_d$  = current density,  $V$ = voltage,  $R$  = resistance, and  $A$  = surface area of the electrode

#### Power Density

The power density was obtained by dividing the power by the surface area of the electrode.

$$P_d = \frac{V \times I}{A} \quad \text{Eq. 10}$$

Where,  $P_d$ = power density,  $V$ = voltage,  $I$  = current, and  $A$  = area of the electrode.

The internal resistance emerged by each electrode, interconnections to proton and electron transport process, and substrate was measured from the slope of the polarization curve plotted for all external resistance (30 k $\Omega$  – 50  $\Omega$ ) for each electrode. The polarization graph was plotted as the voltage obtained for each resistance value at the corresponding current density which was considered the immersed surface area of the cathode in the electrolyte. Internal resistance should be minimized to obtain better performance of the MFC.

The maximum power density of each electrode was obtained from the power curve that has been plotted, power density vs current density which was considered the cathode surface area immersed in the electrolyte. The highest value of the bell-shaped power curve refers as maximum power density.

#### ***3.3.3 Chemical Oxygen Demand and Coulombic Efficiency Calculations***

The reduction of chemical oxygen demand (COD) over time indicates the efficiency of the system in treating organic pollutants and generating electricity. In order to estimate the COD, the samples were collected before being inserted into the MFC anode chamber is the initial COD sample (which is known as influent). Samples collected after the operation of MFC on the third day are known as the final COD sample (which is known as effluent). The COD was determined by the closed reflux method described in the “Manual distribution record” paper(Yusri, 2020).

The experimental methods were followed as 10 mL volume from the sample was inserted into the 25×150 mm size digestion vessel. Then 0.200 g of mercury sulphate

(HgSO<sub>4</sub>) was added into the vessel. Afterward, 98% concentrated sulfuric acid (H<sub>2</sub>SO<sub>4</sub>) 1 mL was added and mixed well until all mercury sulphate dissolved in the solution. Then standard potassium dichromate solution 5 mL (0.250 N, K<sub>2</sub>Cr<sub>2</sub>O<sub>7</sub>) was added to the vessel. Finally, 12 mL of sulfuric acid reagent was added to the solution and mixed well the solutions. The digestion vessels with the caps were kept in the reflux oven at 150°C for 2 hours.

After being kept in the oven, the vessels were allowed to reach room temperature. The solution inside the digestion vessel was transferred to an Erlenmeyer flask and washed the vessel 3 or 4 times with distilled water and topped up to 60 mL. Then two drops of ferroin indicator were added to the Erlenmeyer flask and titrated with 0.25 N ferrous ammonium sulfate (Fe(NH<sub>4</sub>)<sub>2</sub>(SO<sub>4</sub>)<sub>2</sub>) to the end point. The color change of the solution was observed as the blue-green to reddish-brown. The COD value was calculated according to the equation as follows,

$$COD\left(\frac{mg}{L}\right) = \frac{(A-B)N \times 8000}{S} \quad \text{Eq. 11}$$

Where *A* is milliliters of Fe(NH<sub>4</sub>)<sub>2</sub>(SO<sub>4</sub>)<sub>2</sub> solution required for titration of the blank, *B* is milliliters of Fe(NH<sub>4</sub>)<sub>2</sub>(SO<sub>4</sub>)<sub>2</sub> solution required for titration of the sample, *N* = normality of the Fe(NH<sub>4</sub>)<sub>2</sub>(SO<sub>4</sub>)<sub>2</sub> solution and, *S* is milliliters of sample used for the test.

Coulombic efficiency (CE) gives the measure of the number of coulombs recovered as electrical current and was determined by integrating the current measured over time (*t*), and calculated as per the equation,

$$CE = \frac{M_o \int_0^t I dt}{F V_A n \Delta COD} 100 \quad \text{Eq. 12}$$

Where, *I* is the current produced (A), *t* is the period of the experiment (s), *M<sub>o</sub>* is the molecular weight of oxygen (32 g/mol), *F* is the Faradays constant (96,485.3 C/mol - electrons), *V<sub>A</sub>* is the volume of the anode chamber (L), *n* is the stoichiometry number of moles of electrons exchanged per mole of oxygen (4 mole/ e mol O<sub>2</sub>) and Δ COD is the change in the COD over time (*t*) (g/L)(López Zavala & Cámara Gutiérrez, 2023).



## CHAPTER 4

### RESULTS AND DISCUSSION

In this chapter, the modified electrodes characterization and their MFC performances were discussed compared to the bare graphite electrode applied in the cathode chamber. Table 4.1 below shows the various types of electrodes used in this study and their respective abbreviations which are used throughout this chapter,

**Table 4.1**

*Names and Abbreviations of the Various Cathodic Electrodes Used in This Study*

Electrode name	Abbreviation
Graphite	G
Graphite/ZnO	GZ
Graphite/ZnO/Cu 1 time deposition layer	GZC(1)
Graphite/ZnO/Cu 3 times deposition layer	GZC(3)
Graphite/ZnO/Cu 10 times deposition layer	GZC(10)
Graphite/ZnO/Pt 1 time deposition layer	GZP(1)
Graphite/ZnO/Pt 3 times deposition layer	GZP(3)
Graphite/ZnO/Pt 10 times deposition layer	GZP(10)

#### 4.1 Electrode's Morphological & Elemental Analysis

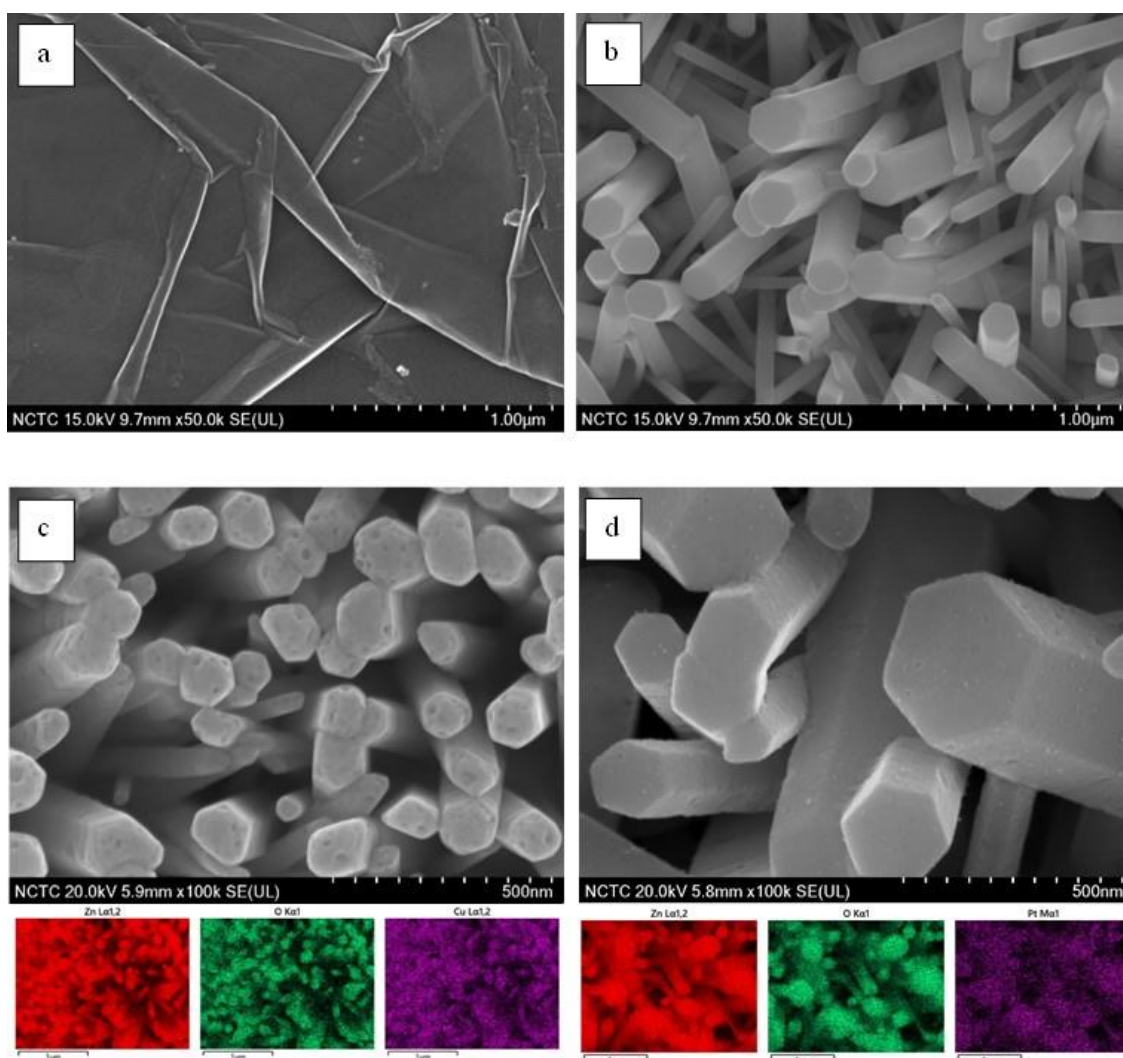
The electrode morphological studies performed by using FESEM (Hitachi SU8230) and the micrographs are shown in Figure 4.1. The samples were tested at 50000× magnification and also, and further analysis of the tiny metal particles was done at 100000× at 20kV of electron acceleration. The plain graphite substrate G relatively exhibited a flat surface where graphitic layers were observed (Figure 4.1.a). Upon the growth of the ZnO nanorods, the GZ sample showed the presence of the characteristic hexagonal and vertically standing ZnO nanorods on the graphite surface (Figure 4.1.b).. The ZnO nanorods were found to have difference diameters ranging from ~50 nm to ~230 nm. The surface of this rods shows clear and smooth surfaces. After the metal

deposition on the surface of the ZnO nanorods, it shows surface roughness and presence of extremely small metal nanoparticles on the surface of the nanorods. The Figure 4.1.c(up) and Figure 4.1.d(up) represent the SEM micrographs of Cu and Pt catalyst on ZnO NRs, respectively.

In order to find out the elemental distribution of the metal catalyst on the ZnO surface, we then conducted EDX analysis. Figure 4.1.c(bottom) and figure 4.1.d(bottom) represent the EDX mapping of the GZC & GZP surfaces, where the uniform distribution of Cu & Pt is clearly visible indicating the presence and successful incorporation to the electrodes, respectively.

**Figure 4.1**

*FESEM Micrographs of the (a) G, (b) GZ, (c) GZC(up), EDX (bottom), (d) GZP(up), EDX (bottom)*



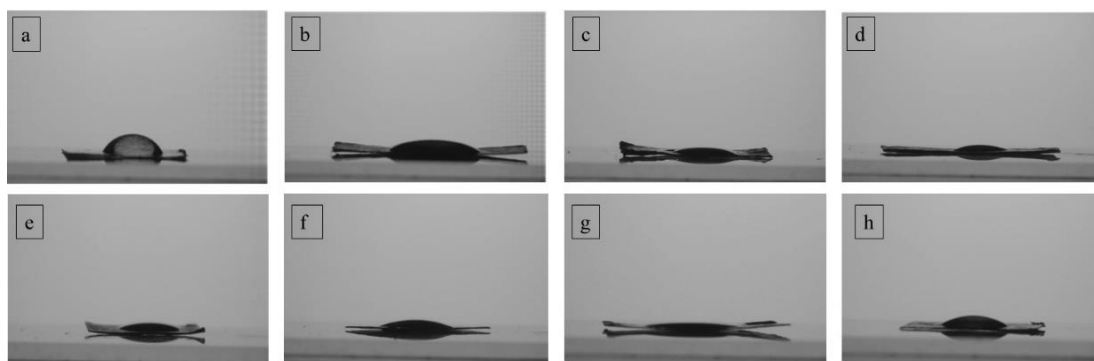
For the GZC sample, the weight percentage Zn, O and Cu were found to be 73.37%, 15.73%, and 0.30%. For the GZP sample the weight percentage of Zn, O, and Pt were 73.01%, 16.78%, and 0.73% respectively. This indicated that compared to ZnO, the amount of metal particles is relatively very low and remain within 1%.

## 4.2 Surface Wettability of the Electrodes

The water contact angle results of bare graphite and modified electrode are shown in Figure 4.2 and the summary of the water contact angle (WCA) is given in Figure 4.3. The uncoated bare graphite showed higher WCA(61°) when compared with the modified graphite electrode with ZnO and metal nanoparticles (<30°). According to these results we can say that all electrodes have hydrophilic nature, while the hydrophilicity is increased upon the growth of the ZnO nanorods on the graphite surface and subsequent deposition of metal particles.

**Figure 4.2**

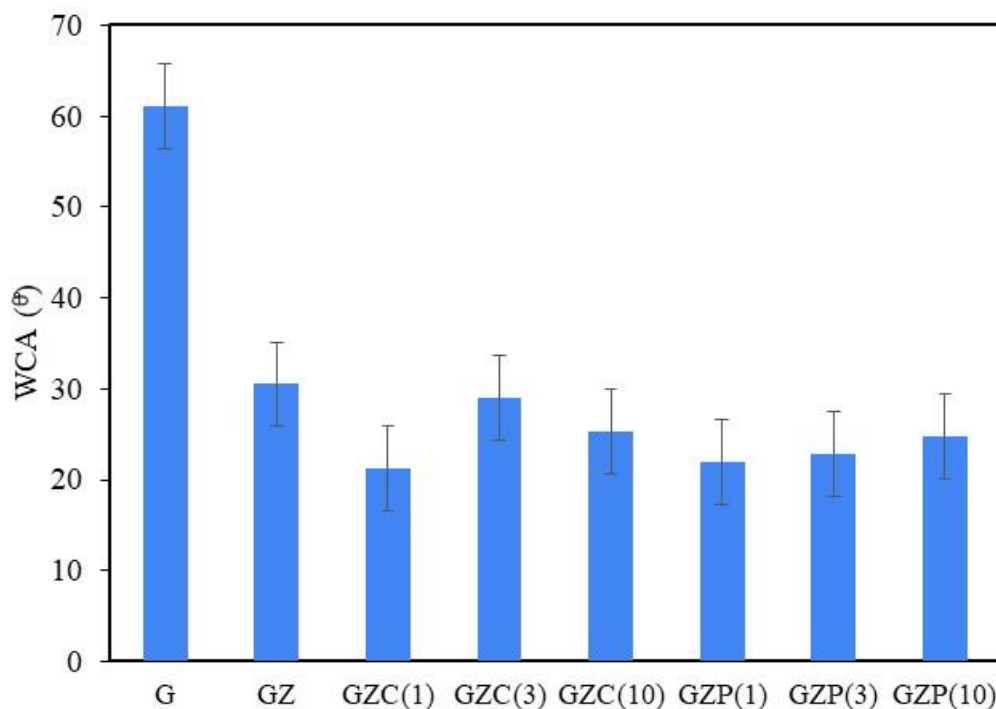
*Images Showing Water Droplet Interaction with the Electrode Surface, (a) G, (b) GZ, (c) GZC(1), (d) GZC(3), (e) GZC(10), (f) GZP(1), (g) GZP(3) and, (h) GZP(10)*



All-modified electrodes show nearly 50% reduction in the WCA compared to the bare graphite surface. Naturally, ZnO shows hydrophilic behavior due to the existence of the hydroxyl groups on the surface (Ennaceri et al., 2016). When ZnO NRs coated with metal nanoparticles there was not much significance change of WCA. When metal nanoparticle concentration was increased the WCA found to vary marginally suggesting that the small amount of metal nanoparticles on the surface of the ZnO nanorods do not affect the surface wetting behavior of the electrodes. (Figure 4.3).

**Figure 4.3**

*Summary of the WCA From Various Electrode Surface*



### **4.3 Electrochemical Analysis for ORR Evaluation**

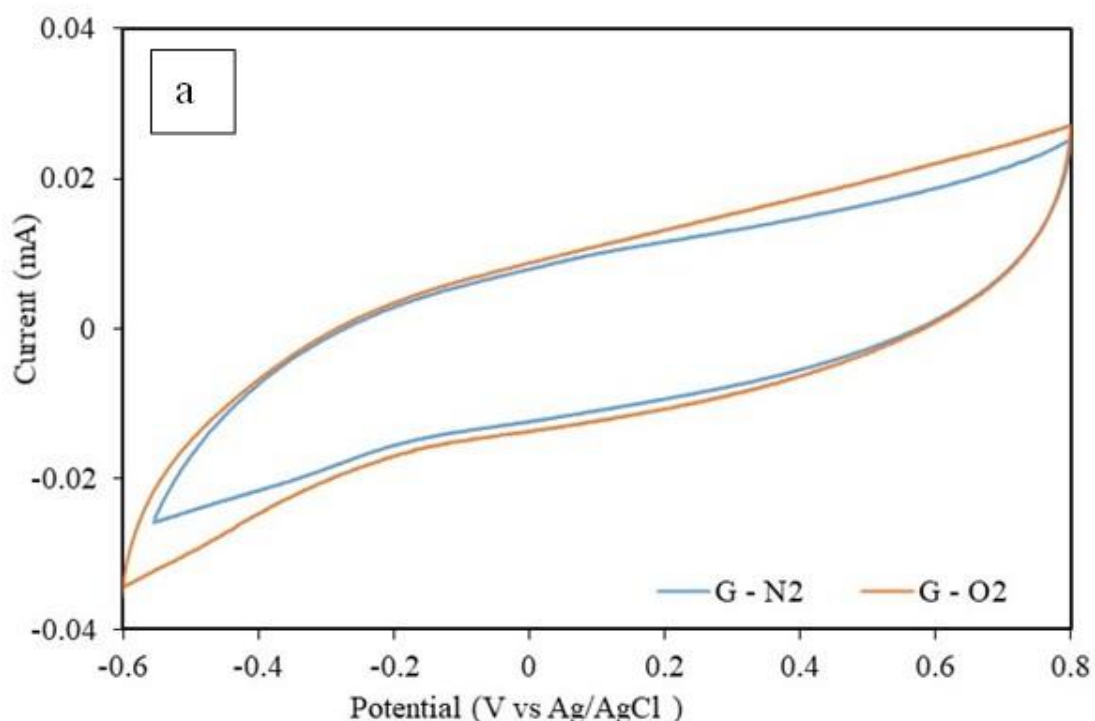
The ORR electrocatalytic performances of the prepared catalyst were evaluated by CV measurements under an oxygen-saturated condition at room temperature with PBS buffer (pH 6.8) using scan rate of 20 mV/s. Prior to that, nitrogen-saturated tests were conducted as the background test to observe the performance of the catalyst without oxygen. As shown in Figure 4.4, the reduction peak current of the synthesized catalyst under oxygen-saturated conditions were found to move to a more negative current than in the nitrogen-saturated condition. In the graphite electrode, no significant peak was visible due to the unavailability of a catalyst on the surface of the electrode (Figure 4.4a).

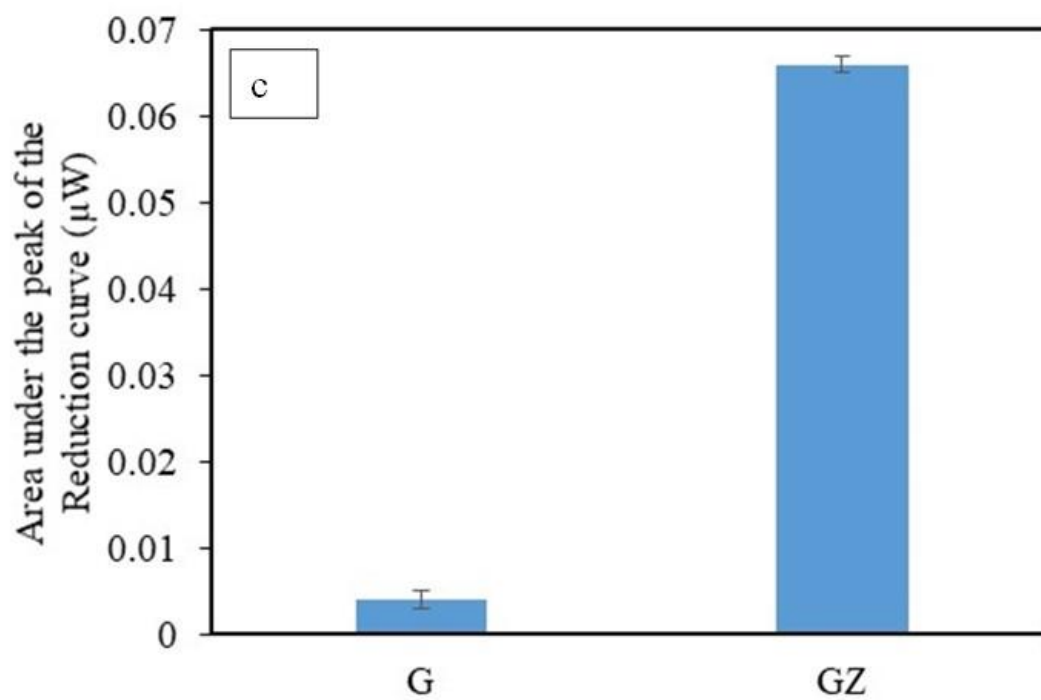
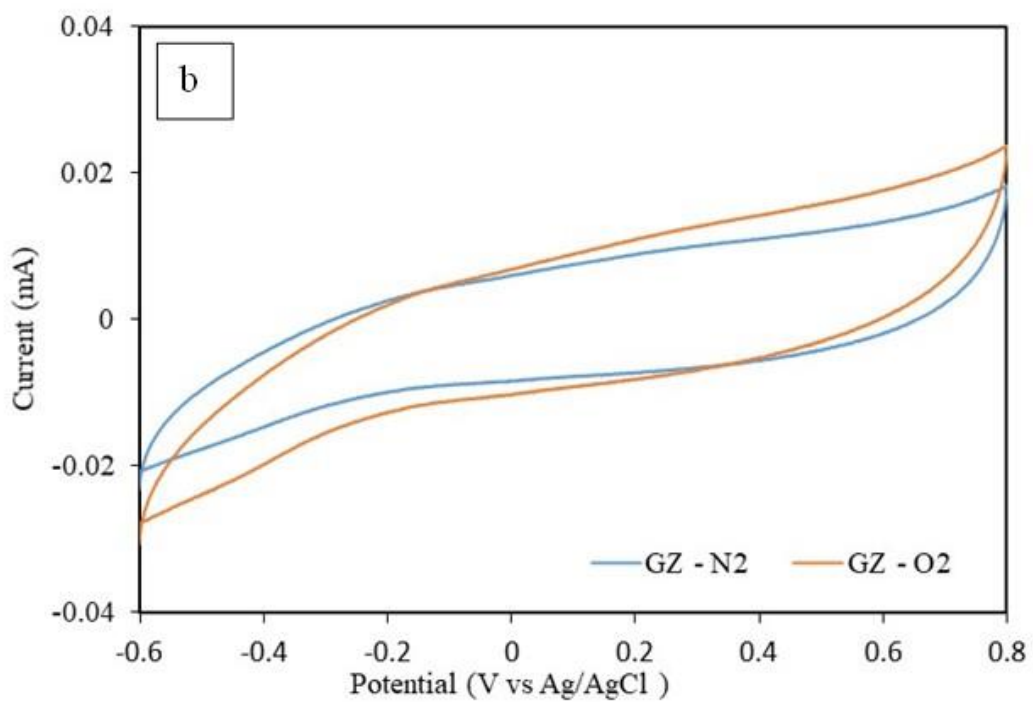
In contrast, the GZ electrode showed a very small reduction peak at the half-wave potential of -0.3241 V to -0.5087 V. Figure 4.4c shows the area under the reduction peak of both G and GZ. After the ZnO NRs deposition on the graphite surface, it has shown almost 16.5 times larger area under the reduction peak indicating a small improvement in the ORR process.

The main reason for this is the improvement in the active surface area of the GZ electrode due to the presence of ZnO nanorods and its improved hydrophilicity which allows more oxygen to interact with the surfaces. Additionally, ZnO nanorods can offer enhance charge transfer at the electrode surface, lowering the charge transfer resistance at the surface, and thus lowers the activation losses(Pushkar et al., 2019). At electrode surface, low activation loss means improved kinetics for the electron transport. Similar observations were earlier reported for cerium oxide, where the capacitance of the electrode was increased by the nano cerium oxide coating, which also increased the electrodes' surface area, porosity, and roughness(Heimböckel et al., 2018).

**Figure 4.4**

*Cyclic Voltammetry of the Electrodes at 20 mV/s in Oxygen-Saturated 50 mM PBS Solution, a) G, b) GZ, and, c) Area Under the Reduction Peak in  $\mu W$*





After the catalyst metal coating on the ZnO NRs, there were clearly visible reductive peak current with respect to potential could be observed.

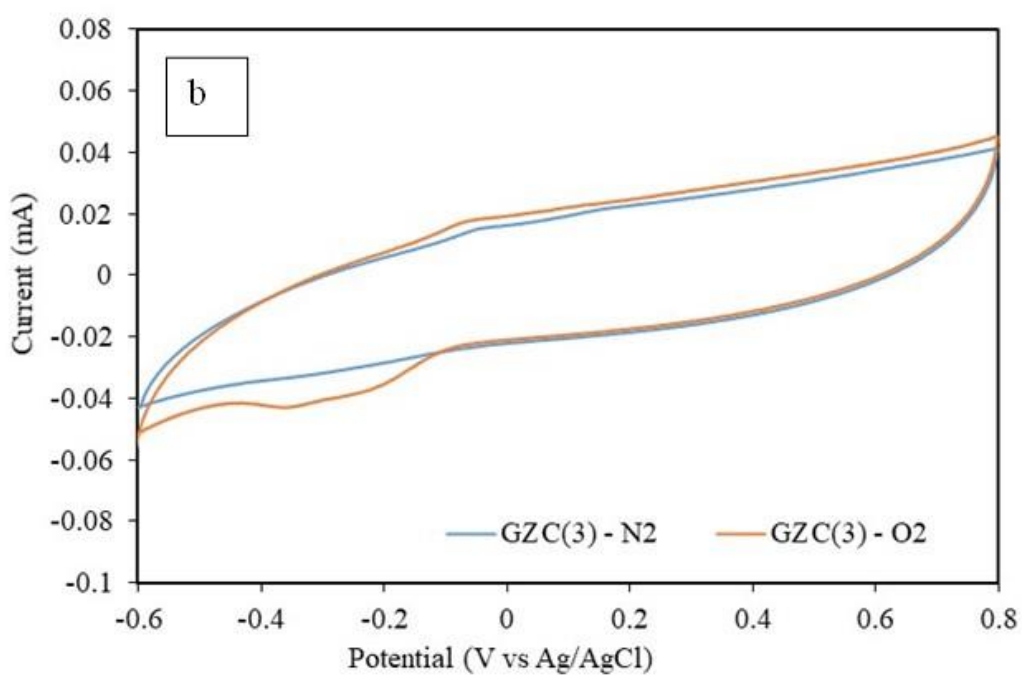
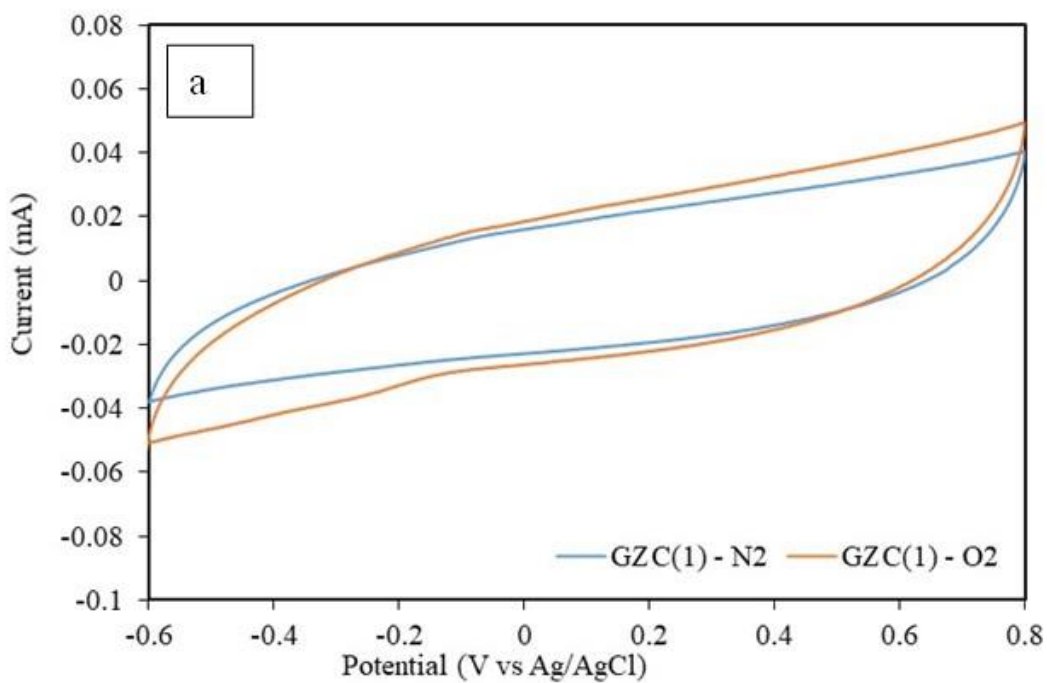
Both the Cu and Pt metal coating showed a distinct oxygen reduction peak, while in some cases a small oxidative peak was observed, as shown in Figure 4.5. The GZC(1) electrode showed the reduction peak starting at the potential of -0.1467 V to -0.3471V. GZC(3) electrode similarly showed an oxygen reduction peak starting at the potential of -0.10362V to -0.41566V, resulting highest area under the peak. GZC(10) electrode, on the other hand, demonstrated lower reduction peak at -0.12788 V to -0.3813V. GZC(3) electrode showed the highest area under the reduction peak indicating maximum ORR when compared to the other Cu metal coated electrodes. The GZC(3) electrode was therefore chosen to construct the MFC for further studies.

To evaluate the electrocatalytic activity of a modified electrode the onset potential is very important. The onset potential is where the ORR peak starts which means the high voltage transfer through the working electrode and counter electrode. High voltage indicates high current. In our experiment, the onset potential of all GZC electrodes was at around -0.1 V which is the same reported by other studies conducted on Cu/ reduced graphene oxide for ORR catalyst (onset potential -0.140 V) and CuO on nitrogen-doped graphene oxide as an electrochemical catalytic activity (Ania et al., 2015) (Paquin et al., 2015).

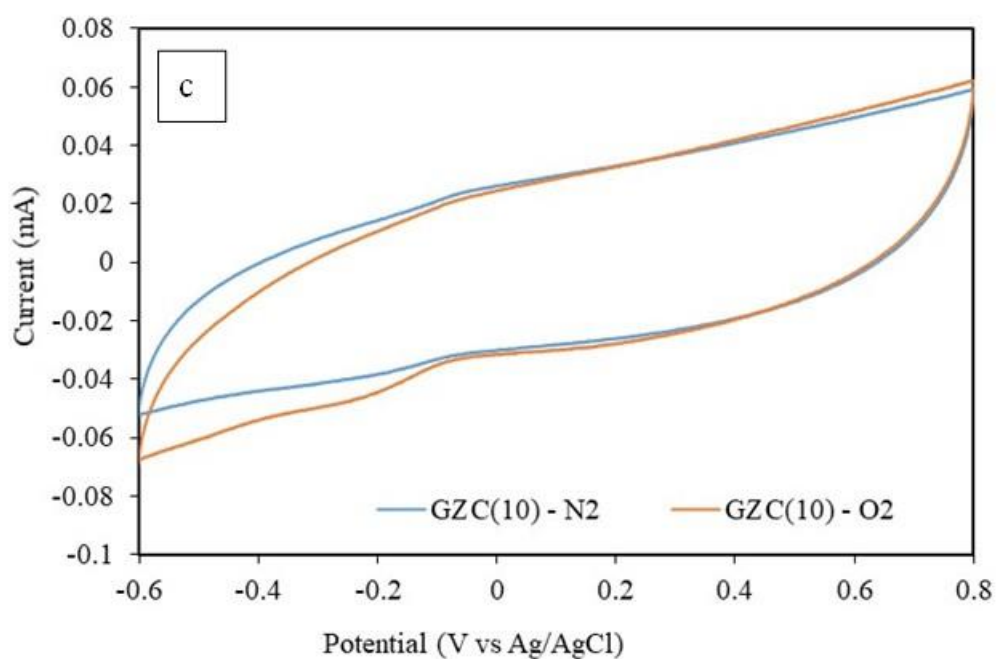
In the case of the Pt catalyst, GZP(1) electrode showed a reduction peak starting at a potential of 0.002 V(at -0.04 mA) and rapidly going into negative current until -0.06 mA then continued to the edge of the CV curve(Figure 4.6). The GZP(3) electrode also showed very broad and low reduction current. A sharp and clear reduction peak was observed from the GZP(10) electrode starting at 0.096975 V. Among all the GZP electrodes, GZP(10) electrode exhibited the highest reduction current asserting its ORR capability, and used in MFC for further studies.

**Figure 4.5**

*Cyclic Voltammetry of the Electrodes of GZC at 20 mV/s in Oxygen-Saturated 50 mM PBS Solution, CV Plot of a) GZC(1), b) GZC(3), and c)GZC(10)*

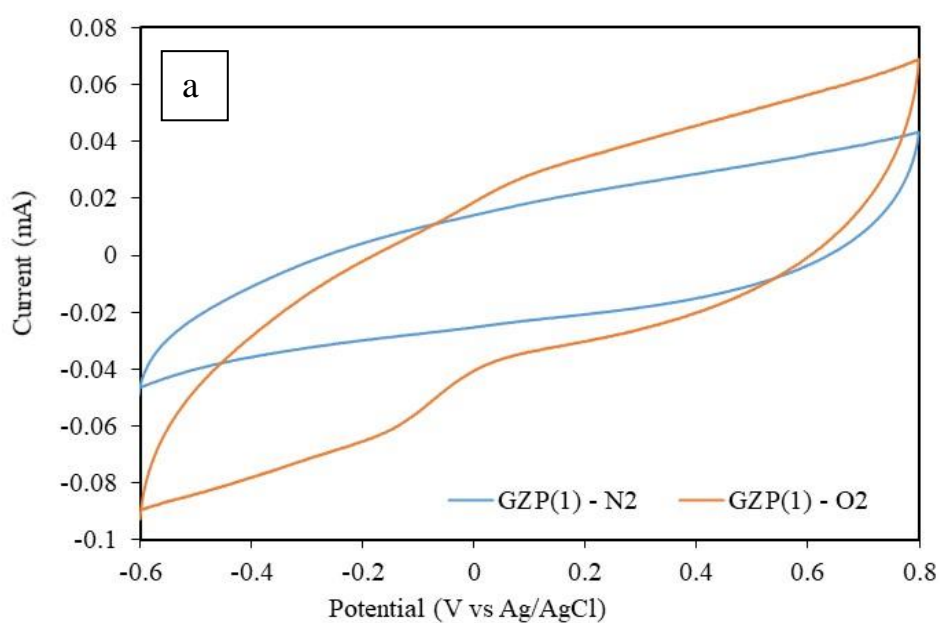






**Figure 4.6**

*Cyclic Voltammetry of the Electrodes of GZP at 20 mV/s in Oxygen-Saturated 50 mM PBS Solution, CV Plot of a) GZP(1), b) GZP(3), and c) GZP(10)*



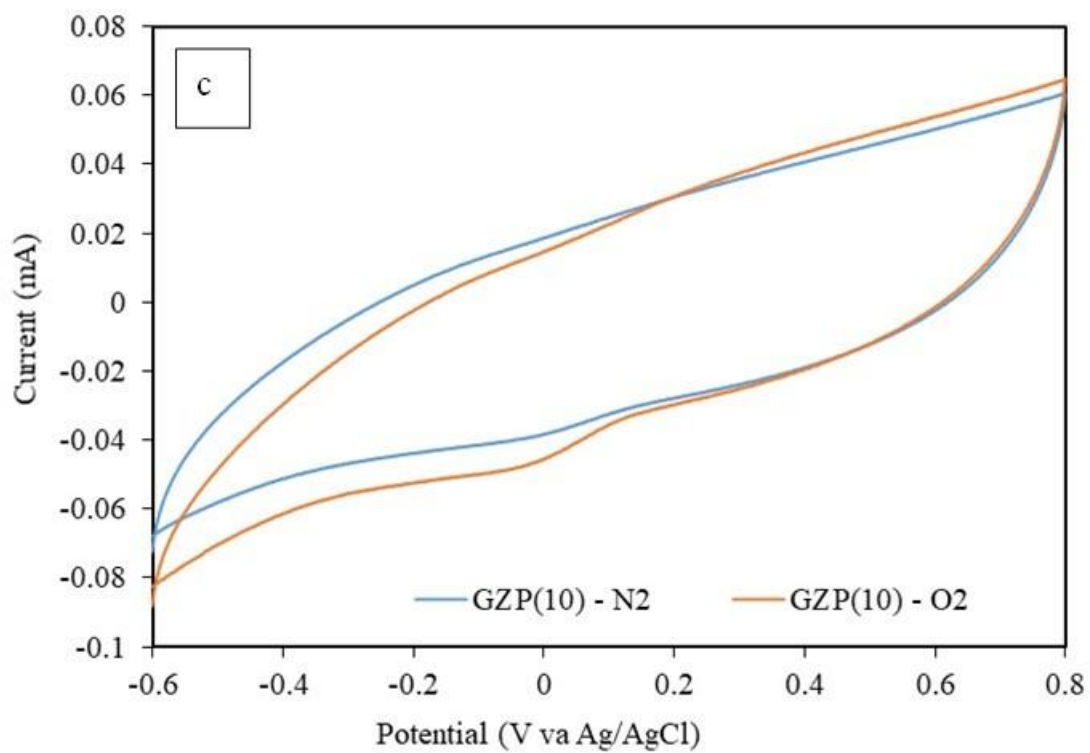
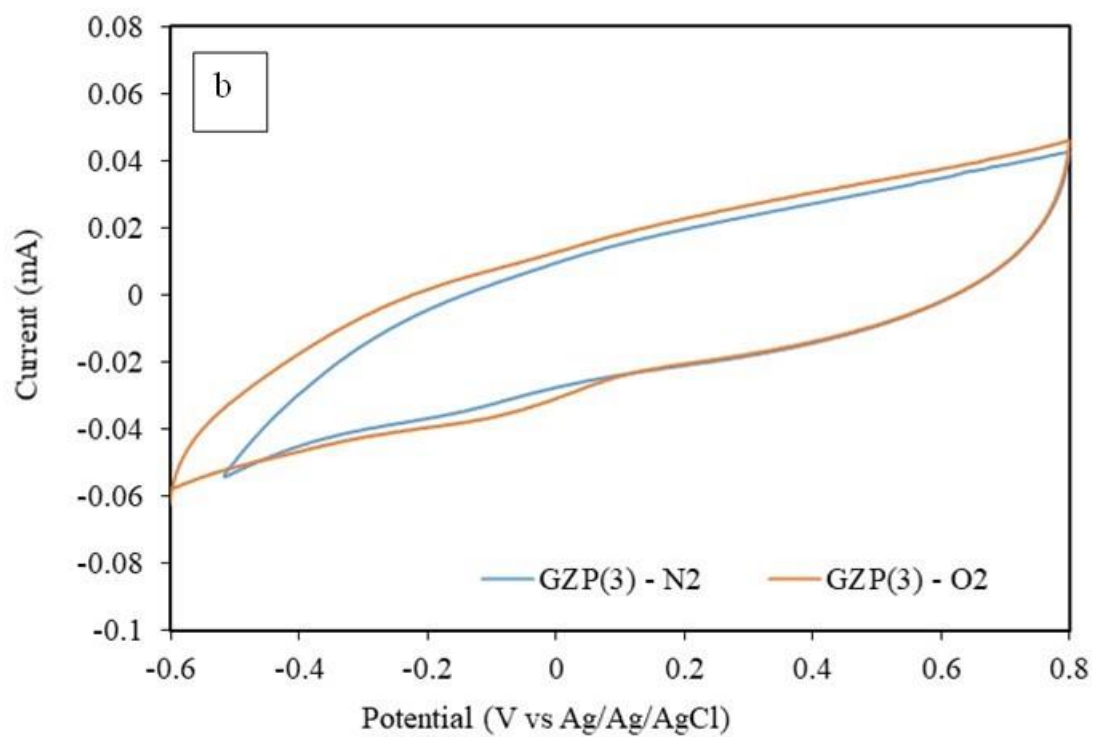
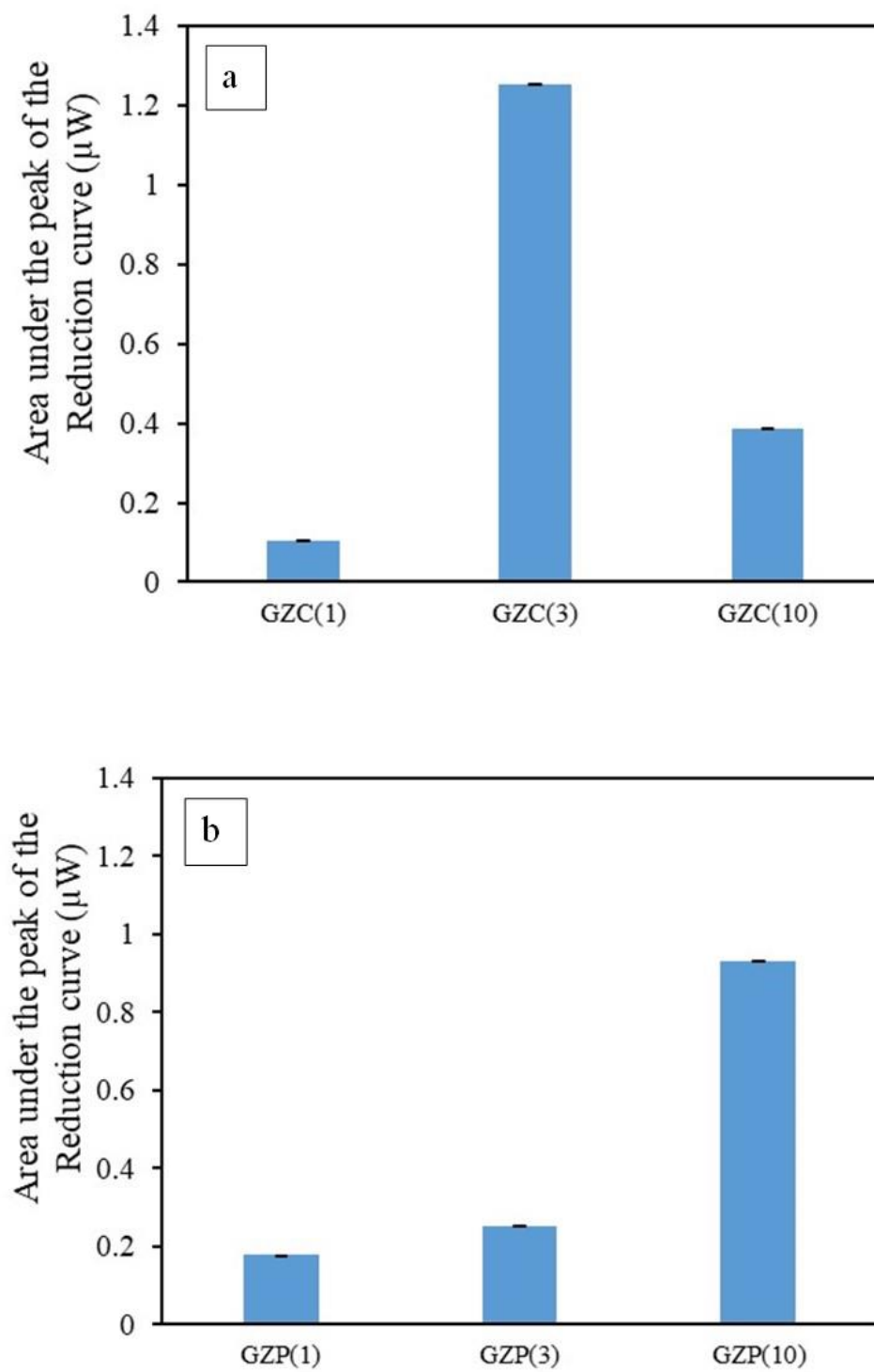


**Figure 4.7**

*Area Under the Reduction Peak in  $\mu\text{W}$  of the Electrodes. a) GZC(3) and b)GZP(10)*



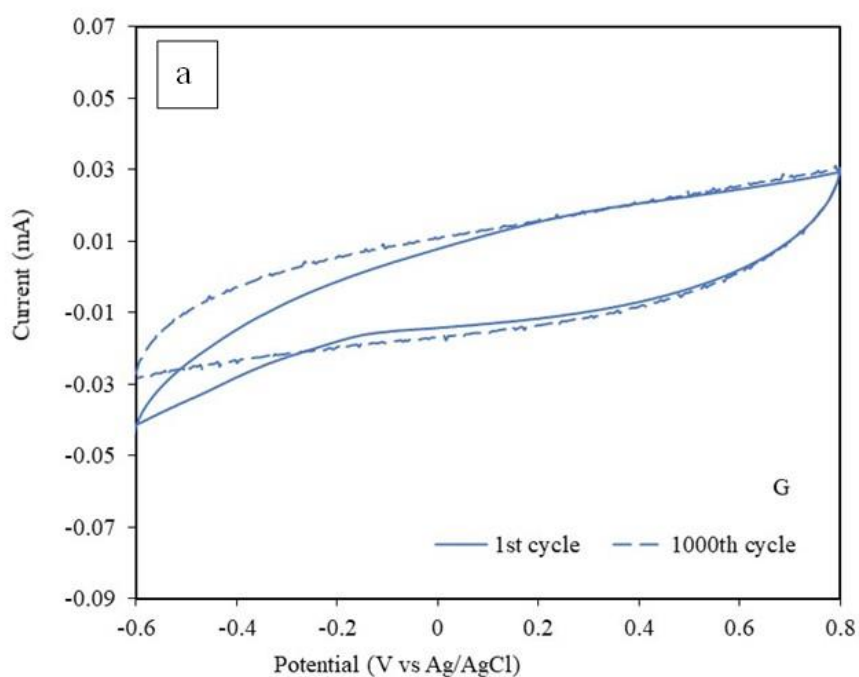
#### 4.4 Electrode Electrochemical Stability

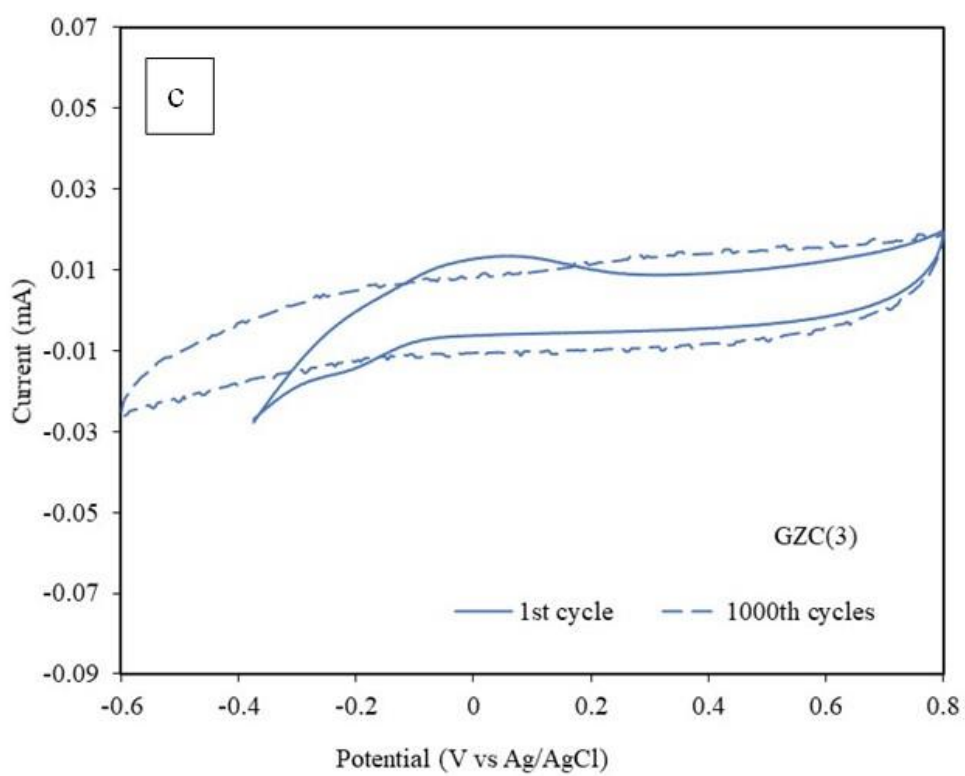
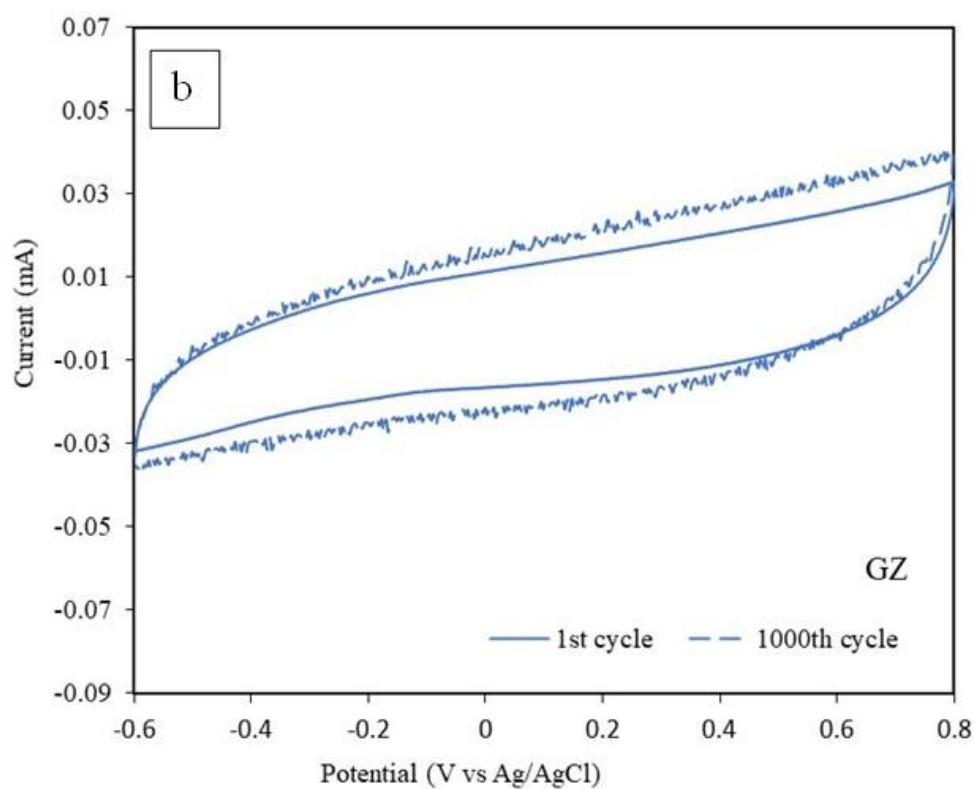
The CV test was repeated for G, GZ, GZC(3), and GZP(10) electrodes up to 1000 cycles to determine the electrochemical stability of the modified electrodes as shown in Figure 4.8. The GZC(3), and GZP(10) electrodes were selected from the modified electrodes due to the high reduction peak observed during the ORR. The stability of the G electrode was found very low as it demonstrated negligible reduction peak at the 1000<sup>th</sup> cycle of the CV curve (Figure 4.8a).

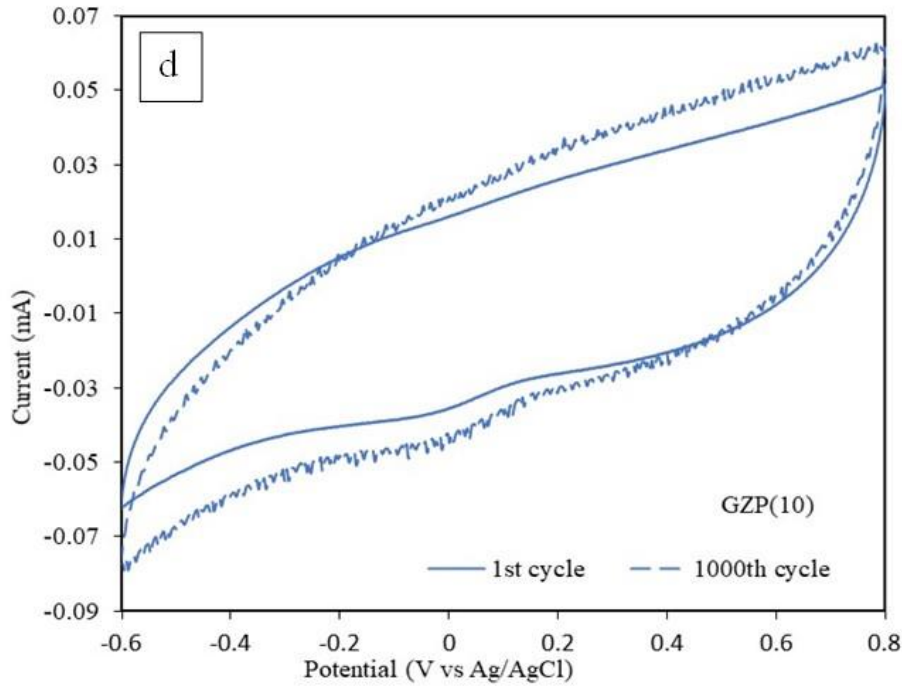
For the GZ electrode at 1000<sup>th</sup> cycle, the reduction curve was shifted by 0.005 mA to more negative current without showing any significant peak in the reduction curve. The GZC(3) electrode, on the other hand, exhibited reduction peak at 1<sup>st</sup> cycle but at the 1000<sup>th</sup> cycle, the reduction peak was not visible indicating their relatively low stability. The GZP(10) electrode, however, showed better stability having the reduction peak at same potential at the initial cycle to the 1000<sup>th</sup> cycle (Figure 4.8d).

**Figure 4.8**

*Cyclic Voltammetry Test of the Electrodes at 1<sup>st</sup> Cycle and 1000<sup>th</sup> Cycle. a) G, b) GZ, c) GZC(3), and GZP(10)*







After conducting the electrochemical experiments, the GZC(3) and GZP(10) electrodes were selected to apply in the MFC to evaluate the performances compared with G and GZ electrode performances. The MFC was operated for three days under applying each electrode to distinguish the performance of the MFC considering the maximum power density (MPD), maximum current density (MCD) observed at MPD, internal resistance ( $R_{in}$ ), chemical oxygen demand removal efficiency (COD removal efficiency %) and coulombic efficiency (CE%).

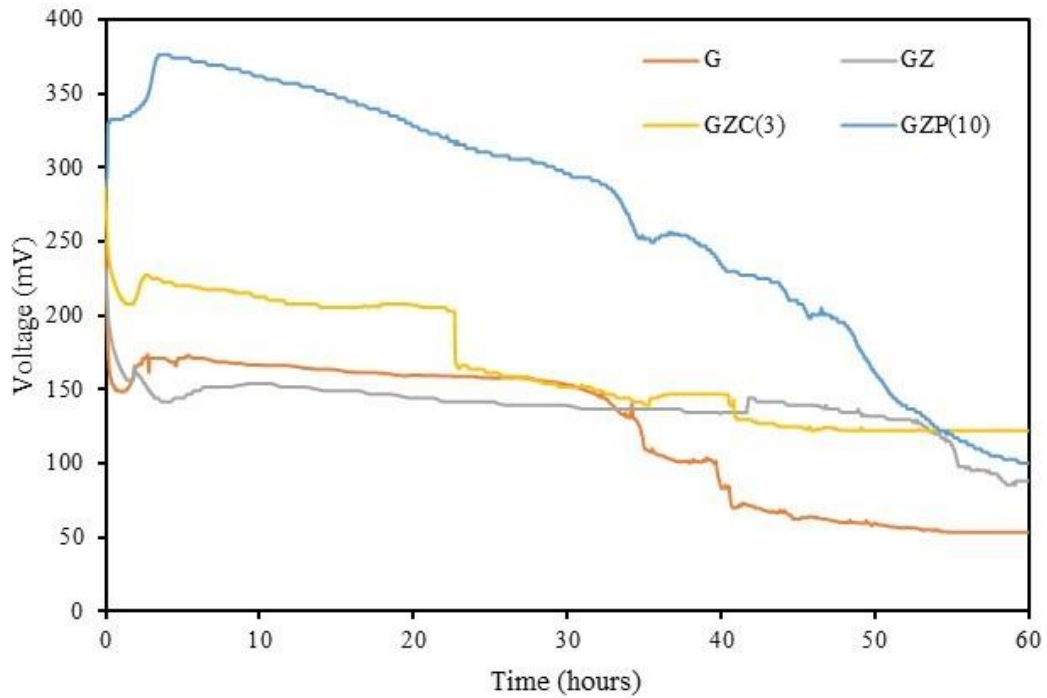
#### 4.5 Electrode Performances When Applied in the MFC

##### 4.5.1 Voltage vs Time Response of the Electrode During 72hrs

The MFC voltage response was recorded up to 72 hours (Figure 4.9). The graphite electrode showed stable voltage output of 175 mV until about 48 hours, but then it was dropped to 50 mV at 72 hours. In the case of the GZ electrode, a continuous and stable voltage output of 150 mV was observed throughout the operation hours of the MFC. This is due to the graphite surface modification with the ZnO nanorods. The increased surface roughness of the GZ electrode increases the active sites for adsorption of oxygen molecules and thus increases the electrochemical reaction as described in the CV.

**Figure 4.9**

*Voltage vs Time Response of the MFC Under Different Electrode*



When compare, both of GZC and GZP electrodes demonstrated increased voltage output. For the Pt coated electrode, the voltage output was found to reduce gradually over the operation time. Initially when electrode was set to the MFC it showed the highest voltage response of about 330 mV. The voltage was then increased up to 375 mV until the first 5 hours and started to gradually decrease. The Cu coated GZC(3) electrode demonstrated 225 mV voltage output during the operation of first day, and then reduced sharply by 50 mV and stabilized at 150 mV. The sharp drop in the output voltage is most probably due to some circuit glitch, and not due to the electrode characteristics. However, further investigation is necessary to understand this.

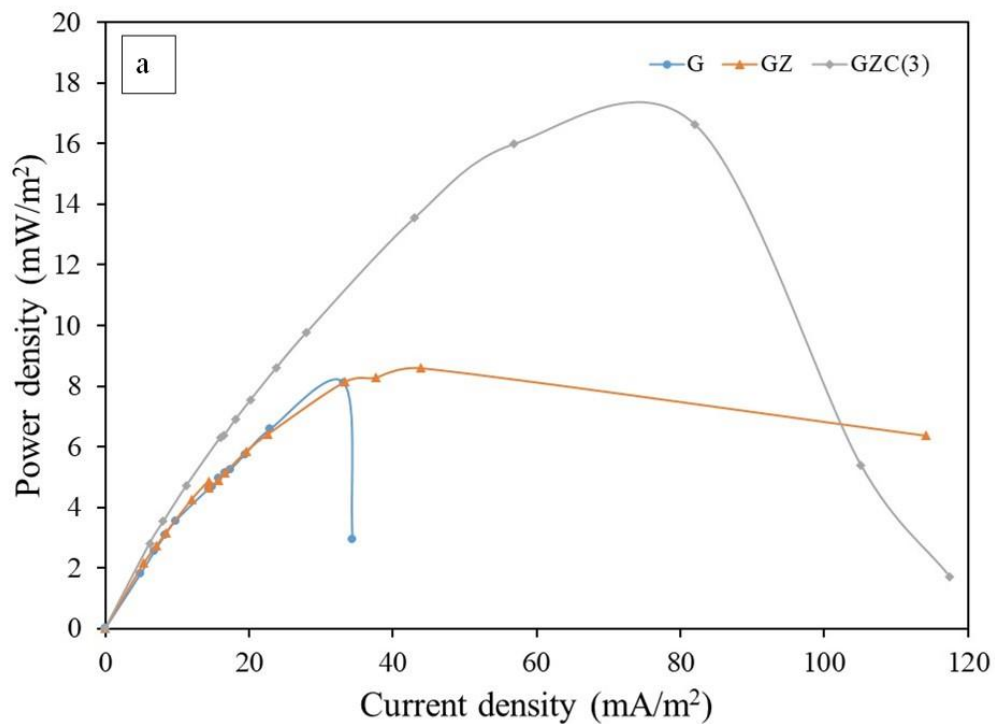
#### **4.5.2 Power Curves of MFC**

The power recovery of the MFC with different modified electrodes were calculated at 24, 48 and, 72 hours to study the behavior of the MFC. From the power curves, the maximum power density (MPD) was estimated, as shown in (Figure 4.10). The current density of each electrode was calculated according to equation 9 mentioned in section 3.3.2 per unit area of the cathode immersed in the catholyte under different variable resistor values ranging from 30 k $\Omega$  to 50 $\Omega$  resistors. The power density is also calculated by using the same unit area of the cathode according to equation 10 in the same section. Then afterwards power density versus current density graph was drawn.

According to the Figure 4.10 (a), at the end of the first day of operation of MFC GZC(3) has shown the highest MPD of 16.636 mW/m<sup>2</sup>. The generated MPD values are almost similar around 8.2 mW/m<sup>2</sup> for G and GZ electrodes. It can be observed that the MPD of GZC(3) is twice the value of G and GZ. The observed MCD values for G and GZ are 33 mA/m<sup>2</sup> and 44 mA/m<sup>2</sup> while that MPD value becomes 82 mA/m<sup>2</sup> for GZC(3). The reason for this increase in both MPD and MCD values is the availability of Cu particle coating on GZC(3).

**Figure 4.10**

*Power Curves of the Electrode Operated in MFC at a) 24 hrs, b) 48 hrs, and c) 72 hrs*

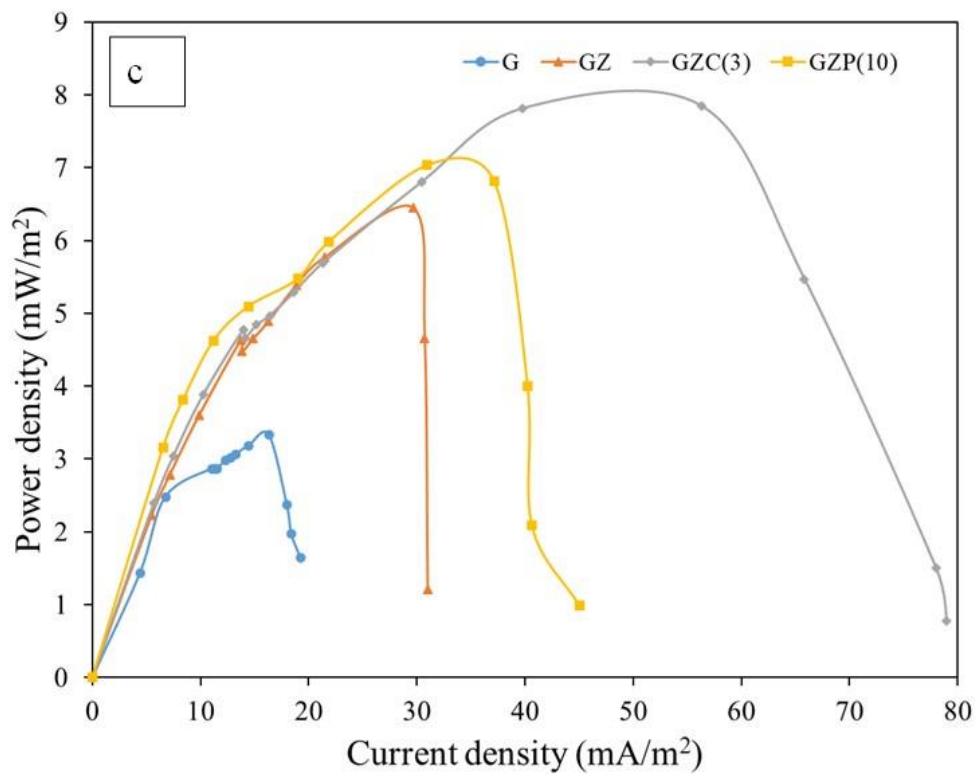
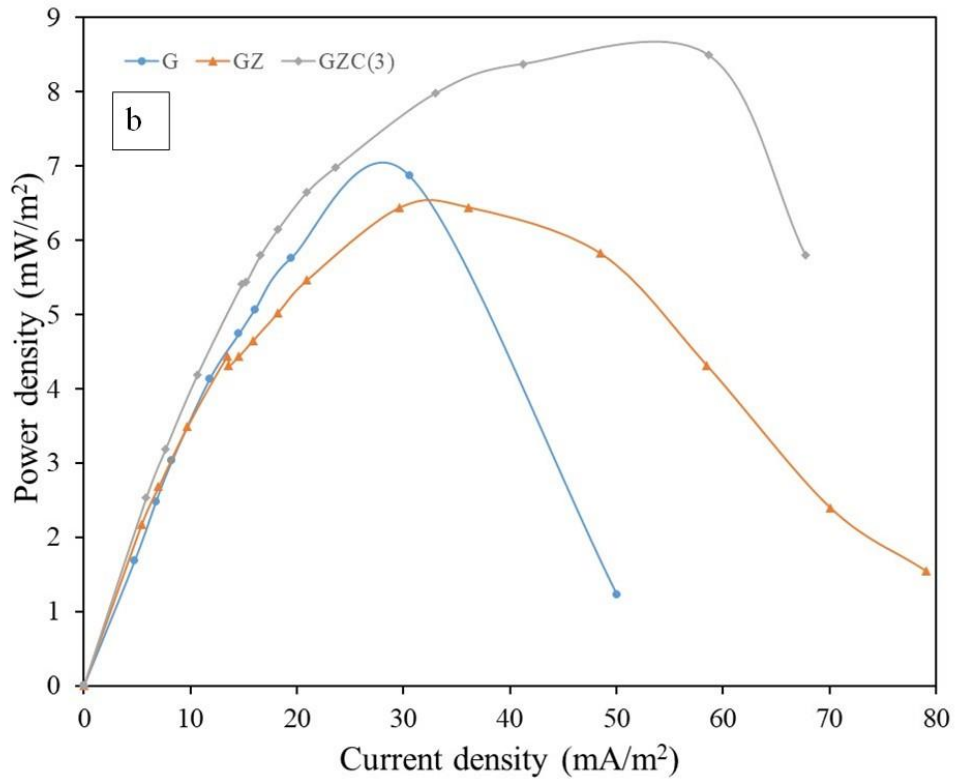


When comparing the values for 48 hours (Figure 4.10 (b)), the same trend can be observed even though the increase in GZC(3) values are not wide like it was in 24 hours comparison.

Although the Figure 4.10 (c) graph has the plot of GZP(10), its' readings were not included in the Figure 4.10 (a) and Figure 4.10 (b) graphs as the GZP(10) did not have a stable continuous voltage in the voltage vs time response graph (**Figure 4.9**).



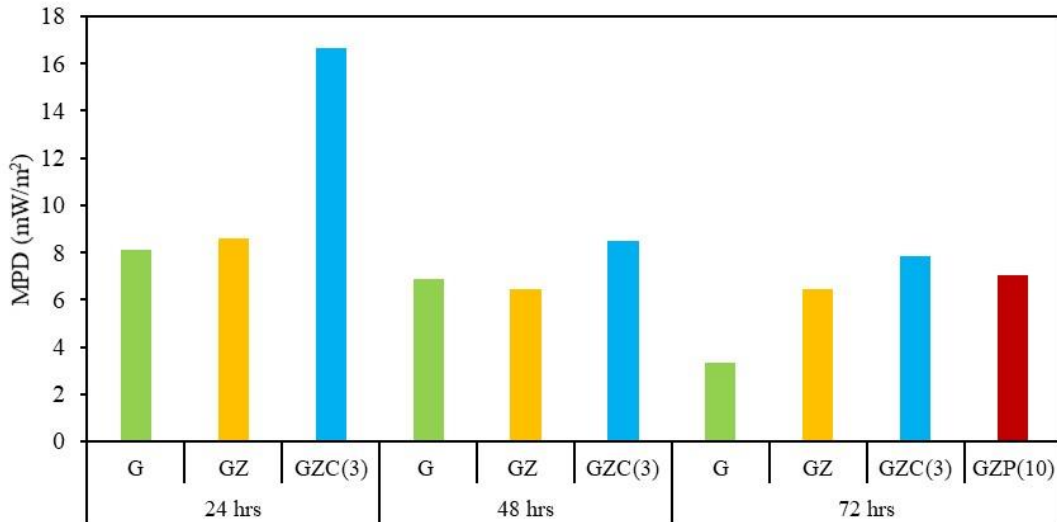
According to Figure 4.10 (c), the MPD and MCD readings of GZP(10) are higher than that of G and GZ, but GZC(3) has the highest MPD and MCD values.



Averagely GZC(3) shows the higher MPD at the end of each operation day of the MFC . But the MPD is reduced over operation time as shown below Figure 4.11.

**Figure 4.11**

*MPD of the MFC with Modified Electrodes at the Operation Time of 24, 48 and, 72 hours*



The reason can be the more active sites adsorbed the O<sub>2</sub> molecules and performed more ORR kinetics. The ORR through the 4-electron pathway which is known as the dissociative mechanism described by Md. T. Noori et al (Noori et al., 2018). The suggested ORR has 3 steps, as follows, (\*, is represents the reaction site on the Cu metal)

Step 1 is adsorption of O<sub>2</sub> on the surface of Cu,



Step 2 is hydrogenation (protonation) of adsorbed oxygen



Step 3 is hydrogenation (protonation) of HO\*

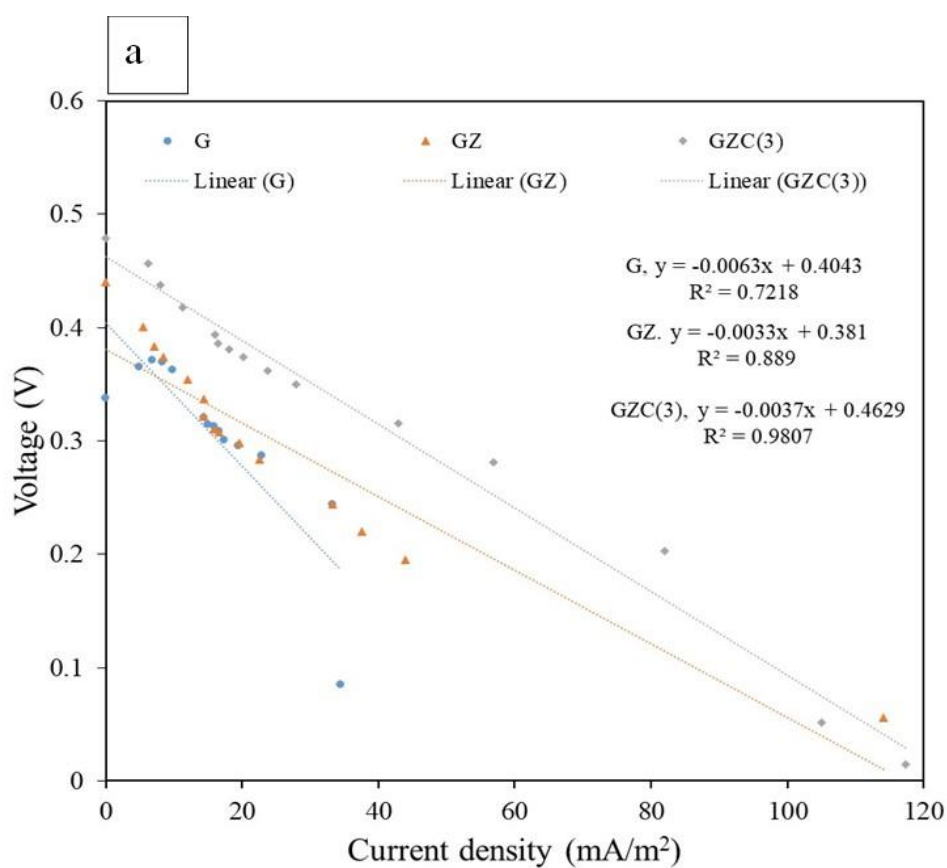


### 4.5.3 Polarization Curves of MFC

The voltage response of each electrode was recorded using the Picolog data logger at different variable resistors starting from 30 k $\Omega$  to 50  $\Omega$ . The polarization curve was plotted, voltage versus current density as shown in Figure 4.12. The slope of the linear range of the polarization curve indicates the internal resistance of the MFC. The calculated internal resistance of each electrode is presented in the Figure 4.13.

**Figure 4.12**

*Polarization Curves of the Electrode Operated in MFC at ,a) 24 hrs, b) 48 hrs, and c)72 hrs*



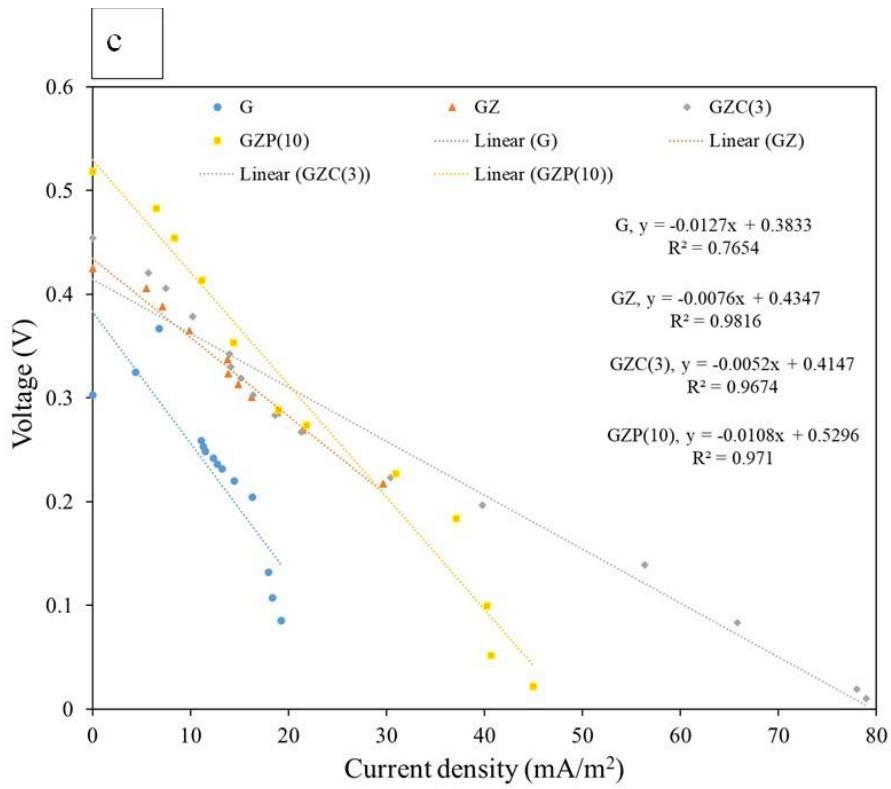
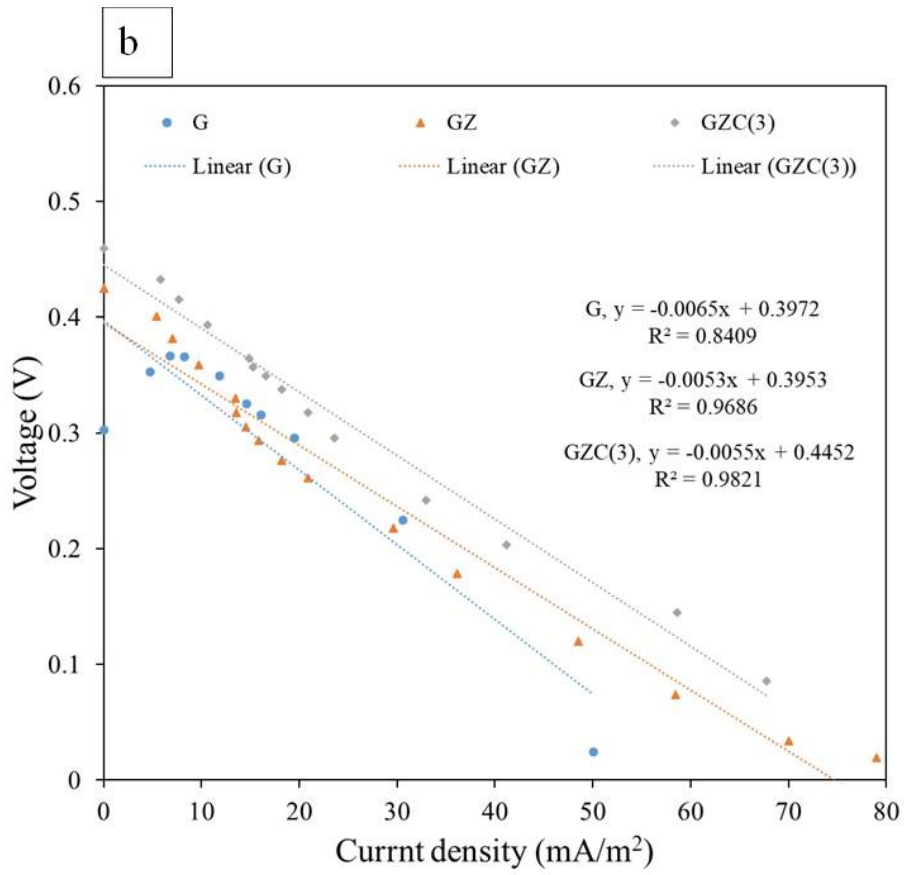
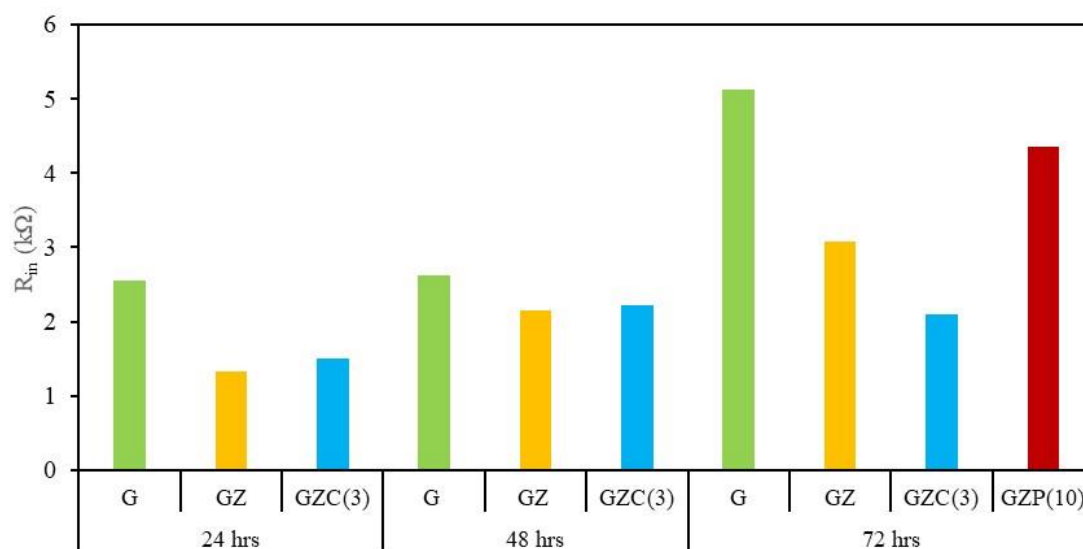


**Figure 4.13**

*R<sub>in</sub> of the MFC Under Modified Electrodes at the Operation Time of 24, 48 and, 72 hrs*



The internal resistance value was minimum in the GZ electrode at the first day of the MFC with 1.333 k $\Omega$ . The highest internal resistance was achieved in the G electrode that was 2.545 k $\Omega$ . GZC(3) showed slightly higher value resistance of 1.495 k $\Omega$  than the GZ electrode but less than G electrode. The same internal resistance was observed in the second day of the G, CZ and GZC(3) electrodes at the MFC operation.

At the last day of the operation of MFC showed different internal resistance under each electrode. As usual G electrode applied MFC had high internal resistance of the 5.313 k $\Omega$ . It was doubled the  $R_{in}$  from the first day operation. The GZC(3) electrode applied MFC showed the less internal resistance at 2.101 k $\Omega$  while GZ electrode applied MFC electrode has been increased to 3.071 k $\Omega$ . The CZP(10) electrode has the high  $R_{in}$  next to the G electrode. Overall, the bare G and GZC electrodes indicates an increment in the  $R_{in}$  during the operation of the MFC. When compared to the each electrode GZC(3) electrode showed the less  $R_{in}$  at 2.101 k $\Omega$ .

The internal resistance is a crucial factor in having the maximum operation of the MFC. (Helder et al., 2012) The lowest  $R_{in}$  was depicted in the GZC(3) electrode(Figure 4.13). Table 4.2 summarizes all the data of the MFC. GZC electrode has the highest MPD which is 2.3 times higher than the bare graphite electrode at 72 hrs operation of MFC. Also, it was higher than the GZP electrode which has an MPD of 7.039 mW/m<sup>2</sup>. The GZC has a high current density of 56.33 mA/m<sup>2</sup> which is 1.8 times higher than the GZP

electrode. The high current was drawn due to the low internal resistance of the MFC. The GZC electrode showed  $R_{in}$  less than twice the GZP electrode with having MPD of  $7.846 \text{ mW/m}^2$ , MCD of  $56.328 \text{ mA/m}^2$  and  $R_{in}$  of  $2.101 \text{ k}\Omega$ .

**Table 4.2**

*MPD, MCD at MPD, and  $R_{in}$  Changes Over the Electrodes at an Operation Time of 24, 48, and 72hrs.*

Electrode and operation time in the MFC	MPD ( $\text{mW/m}^2$ )	MCD at MPD ( $\text{mA/m}^2$ )	$R_{in}$ ( $\text{k}\Omega$ )
G - 24hrs	8.108	33.240	2.545
G - 48hrs	6.868	30.592	2.626
G - 72hrs	3.333	16.315	5.131
GZ - 24hrs	8.595	43.966	1.333
GZ - 48hrs	6.447	36.140	2.141
GZ - 72hrs	6.447	29.640	3.071
GZC(3) - 24hrs	16.636	82.017	1.495
GZC(3) - 48hrs	8.501	58.629	2.222
GZC(3) - 72hrs	7.846	56.328	2.101
GZP(10) - 72hrs	7.039	30.971	4.364

#### ***4.5.4 COD Concentration, COD Removal Efficiency, and CE of the Electrodes at an Operation Time of 72hrs***

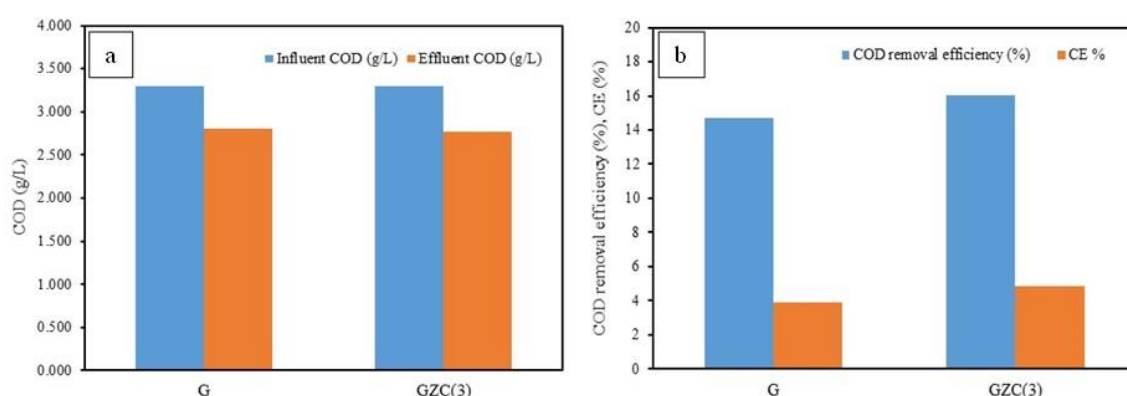
The anodic organic substrate degradation and conversion to generate electricity can be observed through the COD test and CE calculation. After three days of operating the MFC, the organic substrates were utilized by the microorganism for the oxidation process. Due to the increased oxidation of organic materials, the production of protons and electrons were concurrently increased. The COD concentration of the influent was to be around  $3.300 \text{ g/L}$ . The COD removal efficiency of the GZC electrode is  $16.0\%$

higher than the bare graphite electrode which has a COD removal efficiency of 14.7%. (Figure 4.14 a).

The ratio of the electrical output (current) produced during the electrochemical process to the chemical energy of the substrate utilized in microbial fuel cells (MFCs) is known as the coulombic efficiency. The CE of 4.9% was achieved in the Cu metal coating electrode and 3.9 % CE was observed in the G electrode. These results clearly prove that Cu metal has the ORR ability to be used in the electrode modification and applied in the MFC replacing the Pt metal at a low cost.

**Figure 4.14**

*(a) COD Concentration (Influent, Effluent) and, (b) COD Removal Efficiency and CE of the G and GZC Electrodes at an Operation Time of 72hrs*



## 4.6 Discussion

In this section the results were presented in according to the SEM, surface wettability of the electrodes, the ORR ability of the electrons under the CV test, and further application in the MFC in the operation time of continuous 3 days were tested as the following results, voltage versus time response, power curve, polarization curve, chemical oxygen demand, and coulombic efficiency.

The surface wettability shows a hydrophilic effect when the metal particles are attached to the surface of the electrode. The Cu metal-coated electrode shows higher ORR with wide and high surface area when compared to the Pt metal nanoparticles. The voltage versus time response over the time of the Pt metal-coated electrode was not stabilized. Some reasons can affect the instability of the voltage response over time due to electrode degradation, pH change, electrode fouling, temperature variations, the

substrate in the cathode and anode, and microbial activity (Z. Du et al., 2007). Voltage instability can result from electrode degradation brought on by corrosion or fouling, which can lower the electrodes' conductivity and electron transfer efficiency over time. Voltage variations can result from microbial activity altering the pH of the electrolyte solution, which can impact the electrochemical reactions occurring at the electrodes. Voltage fluctuations and decreased MFC efficiency might result from biofilm growth or byproduct accumulation on the electrodes interfering with electron transport. Temperature variations can affect the rate of microbiological activity and the effectiveness of electrochemical reactions, which can cause variations in voltage output (Solomon et al., 2022). Variations in the availability of organic substrates for the microorganisms to digest can cause variations in the activity of the microbes and, as a result, in the voltage output. Variations in the MFC's microbial community can cause variations in metabolic activity and electron transfer rates. The voltage output may be impacted by this.

However, a variety of losses can be identified to lower the MFC voltage. Based on a variety of procedures, MFC performance can be evaluated in terms of internal losses and OCV or in terms of both overpotentials and ohmic losses. Both the resistance to ions passing through the proton exchange membrane and the anodic and cathodic electrolytes, as well as the resistance to electrons flowing through the electrodes and connections, are examples of ohmic losses in a MFC. Ohmic losses can be decreased by using a membrane with low resistivity, reducing the electrode spacing, checking all connections, and raising solution conductivity to the highest level that the bacteria can withstand.

Bacteria move electrons from a substrate at a low potential via the electron transport chain to the final electron acceptor (oxygen) at a higher potential to regenerate metabolic energy. The anode in an MFC is the last electron acceptor, and the bacteria's energy gain depends on its potential. The maximum attainable MFC voltage decreases as the difference between the substrate's redox potential and the anode potential increases, hence increasing the potential metabolic energy gain for the bacteria. Therefore, the anode's potential needs to be maintained as low (negative) as feasible to optimize the MFC voltage. However, electron transport will be impeded and substrate fermentation may occur if the anode potential drops too low.



Activation losses happen when electrons move from or to a molecule reacting at the electrode surface because of the activation energy required for an oxidation/reduction process. Activation losses frequently exhibit a sharp rise at low currents and a gradual rise with increasing current density. Increasing the electrode surface area, enhancing electrode catalysis, raising the operating temperature, and allowing an enriched biofilm to form on the electrode(s) are some methods for achieving low activation losses.

Concentration losses happen when current output is constrained by a species' mass transport rate to/from the electrode. Concentration losses are mostly caused by limited mass transport of chemical species to the electrode surface through diffusion at high current densities. Losses at the anode concentration are brought on by a restricted flow of reduced species toward the electrode or a limited discharge of oxidized species from the electrode surface.

This can lead to an increase in the electrode potential by increasing the ratio of reduced to oxidized species at the electrode surface. The opposite could happen at the cathode side, resulting in a decrease in cathode potential. Diffusional gradients may also appear in the bulk liquid of poorly mixed systems. Another kind of concentration loss is the limiting of substrate flow to the biofilm due to mass transport constraints in the bulk fluid (Bruce E. Logan, Bert Hamelers, René Rozendal, Uwe Shroder, Jurg Keller, Stefano Freguia, Peter Aelterman, 2006).

The COD removal efficiency of this research was low when compared to the other research. The efficiency of COD removal efficiency in microbial fuel cells (MFCs) can be affected by a variety of factors. The amount of organic matter (COD) in the wastewater has a significant effect on the MFC's work. In general, increasing COD from low to moderate levels improves power generation. However, further increases in COD may eventually lead to a decline in efficiency. Furthermore, MFCs should not be exposed to very low COD concentrations

Appropriate pH and temperature ranges promote microbial activity and boost COD removal efficiency. On several days during the experimental investigations, the outside weather was altered from hot to cold and cold to hot. The kind of microbes used in the MFC has an impact on COD removal. Some bacteria are better suited for specific substrates. We employed anaerobic biofilm formation in the investigation with a 3 g/L

COD sodium acetate solution in a 50 mM phosphate buffer solution. However, section 2.1 contains two distinct anaerobic bacteria: *Shewanella putrefaciens* and *Geobacteraceae sulfurreducens* are most suitable (Malekmohammadi & Mirbagheri, 2021).

A low coulombic efficiency indicates that a large amount of substrate energy is either wasted or inefficiently transformed into electrical power. The following factors may have an impact on MFCs' coulombic efficiency. Oxygen diffusion and mass transfer, electron donor and acceptor, microbial diversity and activity, electrolyte composition, and pH and temperature are some of them. Microbial activity requires an effective oxygen supply to the cathode. Performance can be hampered by poor oxygen diffusion. The MFC's performance is influenced by the kind of microorganisms it contains. A lower electro-catalytic activity in certain microbes can result in a poorer coulombic efficiency (Jalili et al., 2024).

## CHAPTER 5

### CONCLUSION

#### 5.1 Conclusion

The main aim of this research was to develop a catalyst material with high ORR to apply in MFC. The FESEM was proved that the development of the ZnO NRS on the graphite substrate clearly in the shape of hexagonal NRs (at a magnification of 50000×). The coated metal particles were clearly seen under the higher magnifications (1000000×) and the elemental composition of the catalysts was done using the EDX. The metal particles were increased the active sites of the surface area of the substrate to adsorb more O<sub>2</sub> molecules. The surface wettability of the all-modified electrodes was showed hydrophilic behavior (WCA is < 30 °).

The developed GZC catalyst was proved that it has better ORR under oxygen-saturated conditions when compared with the G (bare graphite) and GZP (Pt metal applied electrode). GZC all electrodes had the same onset potential of -0.1 V which indicates less ORR activation energy barrier that is able to catalyze the rate-determining step. Compared to the GZP(10) electrode. GZC(3) has the best ORR peak intensity among all the electrodes.

GZC has 2.3 times higher power recovery than the bare graphite and also higher than the GZP electrode. The maximum power density of the GZC was 7.846 mW/m<sup>2</sup> which is slightly higher than the GZP, which had 7.039 mW/m<sup>2</sup>. The internal resistance of the GZC electrode was 2.101 Ω which was less than twice to the internal resistance of the GZP. Due to the low internal resistance inside the MFC, high electron charge transformation happens which leads to more ORR kinetics. The high COD removal efficiency and CE was occurred at the GZC electrode at 16.0% and 4.9% compared with the bare graphite electrode has COD removal efficiency and CE of 14.7%, and 3.9% respectively.

## 5.2 Future Recommendations

After completing the development of the MFC following recommendations can be given which will further enhance the properties of the MFC,

1. The cathode electrode can be a double-sided coat (flat electrode) or full surface area coating can be introduced with the catalyst material.
2. Understanding the effect of active surface area by introducing multiwall carbon nanotubes on the electrode surface area.
3. Observing the effect of inter-electrode distance between the anode and cathode on the functionality of the MFC.
4. Examining the effect of the operating environmental temperature of the MFC.
5. The anaerobic sludge wants to be pretreated before use in the MFC applications.
6. The  $N_{2(g)}$  content in the anodic chamber and the dissolved oxygen content should be considered in the experimental calculations during the MFC performance.

## REFERENCES

- Abd-Elrahman, N. K., Al-Harbi, N., Basfer, N. M., Al-Hadeethi, Y., Umar, A., & Akbar, S. (2022). Applications of Nanomaterials in Microbial Fuel Cells: A Review. *Molecules*, *27*(21), 1–28. <https://doi.org/10.3390/molecules27217483>
- Ania, C. O., Seredych, M., Rodriguez-Castellon, E., & Bandosz, T. J. (2015). New copper/GO based material as an efficient oxygen reduction catalyst in an alkaline medium: The role of unique Cu/rGO architecture. *Applied Catalysis B: Environmental*, *163*, 424–435. <https://doi.org/10.1016/j.apcatb.2014.08.022>
- Ashmath, S., Kwon, H. J., Peera, S. G., & Lee, T. G. (2022). Solid-State Synthesis of Cobalt/NCS Electrocatalyst for Oxygen Reduction Reaction in Dual Chamber Microbial Fuel Cells. *Nanomaterials*, *12*(24). <https://doi.org/10.3390/nano12244369>
- Ben Liew, K., Daud, W. R. W., Ghasemi, M., Leong, J. X., Su Lim, S., & Ismail, M. (2014). Non-Pt catalyst as oxygen reduction reaction in microbial fuel cells: A review. *International Journal of Hydrogen Energy*, *39*(10), 4870–4883. <https://doi.org/10.1016/j.ijhydene.2014.01.062>
- Bhowmick, G. D., Noori, M. T., Das, I., Neethu, B., Ghangrekar, M. M., & Mitra, A. (2018). Bismuth doped TiO<sub>2</sub> as an excellent photocathode catalyst to enhance the performance of microbial fuel cell. *International Journal of Hydrogen Energy*, *43*(15), 7501–7510. <https://doi.org/10.1016/j.ijhydene.2018.02.188>
- Bond, D. R., & Lovley, D. R. (2003). Electricity production by *Geobacter sulfurreducens* attached to electrodes. *Applied and Environmental Microbiology*, *69*(3), 1548–1555. <https://doi.org/10.1128/AEM.69.3.1548-1555.2003>
- Bora, T., Zoepfl, D., & Dutta, J. (2016). Importance of Plasmonic Heating on Visible Light Driven Photocatalysis of Gold Nanoparticle Decorated Zinc Oxide Nanorods. *Scientific Reports*, *6*(March), 1–10. <https://doi.org/10.1038/srep26913>
- Bruce E. Logan, Bert Hamelers, René Rozendal, Uwe Shroder, Jurg Keller, Stefano Freguia, Peter Aelterman, W. V. and K. R. (2006). Critical Review Microbial Fuel Cells: Methodology and Technology. *Environmental Science & Technology*, *40*(17), 5181–5192.

<http://pubs.acs.org/doi/abs/10.1021/es0605016>

- Butti, S. K., Velvizhi, G., Sulonen, M. L. K., Haavisto, J. M., Oguz Koroglu, E., Yusuf Cetinkaya, A., Singh, S., Arya, D., Annie Modestra, J., Vamsi Krishna, K., Verma, A., Ozkaya, B., Lakaniemi, A. M., Puhakka, J. A., & Venkata Mohan, S. (2016). Microbial electrochemical technologies with the perspective of harnessing bioenergy: Maneuvering towards upscaling. *Renewable and Sustainable Energy Reviews*, *53*, 462–476. <https://doi.org/10.1016/j.rser.2015.08.058>
- Cai, T., Huang, M., Huang, Y., & Zheng, W. (2019). Enhanced performance of microbial fuel cells by electrospinning carbon nanofibers hybrid carbon nanotubes composite anode. *International Journal of Hydrogen Energy*, *44*(5), 3088–3098. <https://doi.org/10.1016/j.ijhydene.2018.11.205>
- Celik, C., Boyaci San, F. G., & Sarac, H. I. (2010). Improving the direct borohydride fuel cell performance with thiourea as the additive in the sodium borohydride solution. *International Journal of Hydrogen Energy*, *35*(16), 8678–8682. <https://doi.org/10.1016/j.ijhydene.2010.04.150>
- Chandrasekhar, K. (2018). Effective and nonprecious cathode catalysts for oxygen reduction reaction in microbial fuel cells. In *Biomass, Biofuels, Biochemicals: Microbial Electrochemical Technology: Sustainable Platform for Fuels, Chemicals and Remediation*. Elsevier B.V. <https://doi.org/10.1016/B978-0-444-64052-9.00019-4>
- Chen, J. Y., Xie, P., & Zhang, Z. P. (2019). Reduced graphene oxide/polyacrylamide composite hydrogel scaffold as biocompatible anode for microbial fuel cell. *Chemical Engineering Journal*, *361*(December 2018), 615–624. <https://doi.org/10.1016/j.cej.2018.12.116>
- Chen, S., Patil, S. A., & Schröder, U. (2018). A high-performance rotating graphite fiber brush air-cathode for microbial fuel cells. *Applied Energy*, *211*(November 2017), 1089–1094. <https://doi.org/10.1016/j.apenergy.2017.12.013>
- Das, I., Das, S., & Ghangrekar, M. M. (2020). Application of bimetallic low-cost CuZn as oxygen reduction cathode catalyst in lab-scale and field-scale microbial fuel cell. *Chemical Physics Letters*, *751*(March), 137536. <https://doi.org/10.1016/j.cplett.2020.137536>
- Davis, F., & Higson, S. P. J. (2007). Biofuel cells-Recent advances and applications. *Biosensors and Bioelectronics*, *22*(7), 1224–1235.

<https://doi.org/10.1016/j.bios.2006.04.029>

- Du, Y., Ma, F. X., Xu, C. Y., Yu, J., Li, D., Feng, Y., & Zhen, L. (2019). Nitrogen-doped carbon nanotubes/reduced graphene oxide nanosheet hybrids towards enhanced cathodic oxygen reduction and power generation of microbial fuel cells. *Nano Energy*, *61*(March), 533–539. <https://doi.org/10.1016/j.nanoen.2019.05.001>
- Du, Z., Li, H., & Gu, T. (2007). A state of the art review on microbial fuel cells: A promising technology for wastewater treatment and bioenergy. *Biotechnology Advances*, *25*(5), 464–482. <https://doi.org/10.1016/j.biotechadv.2007.05.004>
- Ennaceri, H., Wang, L., Erfurt, D., Riedel, W., Mangalgi, G., Khaldoun, A., El Kenz, A., Benyoussef, A., & Ennaoui, A. (2016). Water-resistant surfaces using zinc oxide structured nanorod arrays with switchable wetting property. *Surface and Coatings Technology*, *299*, 169–176. <https://doi.org/10.1016/j.surfcoat.2016.04.056>
- Freguia, S., Rabaey, K., Yuan, Z., & Keller, J. (2007). Non-catalyzed cathodic oxygen reduction at graphite granules in microbial fuel cells. *Electrochimica Acta*, *53*(2), 598–603. <https://doi.org/10.1016/j.electacta.2007.07.037>
- Fu, T., Liu, X., Gao, H., Ward, J. E., Liu, X., Yin, B., Wang, Z., Zhuo, Y., Walker, D. J. F., Joshua Yang, J., Chen, J., Lovley, D. R., & Yao, J. (2020). Bioinspired bio-voltage memristors. *Nature Communications*, *11*(1), 1–10. <https://doi.org/10.1038/s41467-020-15759-y>
- Ghasemi, M., Shahgaldi, S., Ismail, M., Kim, B. H., Yaakob, Z., & Wan Daud, W. R. (2011). Activated carbon nanofibers as an alternative cathode catalyst to platinum in a two-chamber microbial fuel cell. *International Journal of Hydrogen Energy*, *36*(21), 13746–13752. <https://doi.org/10.1016/j.ijhydene.2011.07.118>
- Gong, X. B., You, S. J., Wang, X. H., Zhang, J. N., Gan, Y., & Ren, N. Q. (2014). A novel stainless steel mesh/cobalt oxide hybrid electrode for efficient catalysis of oxygen reduction in a microbial fuel cell. *Biosensors and Bioelectronics*, *55*, 237–241. <https://doi.org/10.1016/j.bios.2013.12.015>
- Guo, S., Liu, Y., Sun, Y., & Li, C. (2023). Heterostructure-induced enhanced oxygen catalysis behavior based on metal cobalt coupled with compound anchored on N-doped carbon nanofiber for microbial fuel cell. *Journal of Colloid and Interface Science*, *636*, 305–316. <https://doi.org/10.1016/j.jcis.2023.01.013>

- Gwak, G., Lee, K., Ferekh, S., Lee, S., & Ju, H. (2015). Analyzing the effects of fluctuating methanol feed concentration in active-type direct methanol fuel cell (DMFC) systems. *International Journal of Hydrogen Energy*, *40*(15), 5396–5407. <https://doi.org/10.1016/j.ijhydene.2015.01.062>
- Haoran, Y., Lifang, D., Tao, L., & Yong, C. (2014). Hydrothermal synthesis of nanostructured manganese oxide as cathodic catalyst in a microbial fuel cell fed with leachate. *The Scientific World Journal*, *2014*. <https://doi.org/10.1155/2014/791672>
- He, Z., Liu, J., Qiao, Y., Li, C. M., Thatt, T., & Tan, Y. (2012). *Nano Lett.* *2012\_12\_4738\_4.pdf*. 10–13.
- Heimböckel, R., Kraas, S., Hoffmann, F., & Fröba, M. (2018). Increase of porosity by combining semi-carbonization and KOH activation of formaldehyde resins to prepare high surface area carbons for supercapacitor applications. *Applied Surface Science*, *427*, 1055–1064. <https://doi.org/10.1016/j.apsusc.2017.08.095>
- Helder, M., Strik, D. P., Hamelers, H. V., & Buisman, C. J. (2012). The flat-plate plant-microbial fuel cell: The effect of a new design on internal resistances. *Biotechnology for Biofuels*, *5*. <https://doi.org/10.1186/1754-6834-5-70>
- Hosseini, M. G., & Ahadzadeh, I. (2012). A dual-chambered microbial fuel cell with Ti/nano-TiO<sub>2</sub>/Pd nano-structure cathode. *Journal of Power Sources*, *220*, 292–297. <https://doi.org/10.1016/j.jpowsour.2012.07.096>
- Hou, J., Liu, Z., Yang, S., & Zhou, Y. (2014). Three-dimensional macroporous anodes based on stainless steel fiber felt for high-performance microbial fuel cells. *Journal of Power Sources*, *258*, 204–209. <https://doi.org/10.1016/j.jpowsour.2014.02.035>
- Hu, M., Li, X., Xiong, J., Zeng, L., Huang, Y., Wu, Y., Cao, G., & Li, W. (2019). Nano-Fe<sub>3</sub>C@PGC as a novel low-cost anode electrocatalyst for superior performance microbial fuel cells. *Biosensors and Bioelectronics*, *142*(July), 111594. <https://doi.org/10.1016/j.bios.2019.111594>
- Ieropoulos, I. A., Greenman, J., Melhuish, C., & Hart, J. (2005). Comparative study of three types of microbial fuel cell. *Enzyme and Microbial Technology*, *37*(2), 238–245. <https://doi.org/10.1016/j.enzmictec.2005.03.006>
- Jalili, P., Ala, A., Nazari, P., Jalili, B., & Ganji, D. D. (2024). A comprehensive review of microbial fuel cells considering materials, methods, structures, and microorganisms. *Heliyon*, *10*(3), e25439.



<https://doi.org/10.1016/j.heliyon.2024.e25439>

- Jaswal, V., J. R. B., & N, Y. K. (2023). Synergistic effect of TiO<sub>2</sub> nanostructured cathode in microbial fuel cell for bioelectricity enhancement. *Chemosphere*, 330(March), 138556. <https://doi.org/10.1016/j.chemosphere.2023.138556>
- Kamali, M., Aminabhavi, T. M., Abbassi, R., Dewil, R., & Appels, L. (2022). Engineered nanomaterials in microbial fuel cells – Recent developments, sustainability aspects, and future outlook. *Fuel*, 310(PB), 122347. <https://doi.org/10.1016/j.fuel.2021.122347>
- Kaur, R., Marwaha, A., Chhabra, V. A., Kim, K. H., & Tripathi, S. K. (2020). Recent developments on functional nanomaterial-based electrodes for microbial fuel cells. *Renewable and Sustainable Energy Reviews*, 119(November 2019), 109551. <https://doi.org/10.1016/j.rser.2019.109551>
- Kultayeva, S., Ha, J. H., Malik, R., Kim, Y. W., & Kim, K. J. (2020). Effects of porosity on electrical and thermal conductivities of porous SiC ceramics. *Journal of the European Ceramic Society*, 40(4), 996–1004. <https://doi.org/10.1016/j.jeurceramsoc.2019.11.045>
- Kumar, A., Siddiqui, T., Pandit, S., Roy, A., Gacem, A., Souwaileh, A. Al, Mathuriya, A. S., Fatma, T., Sharma, P., Rustagi, S., Yadav, K. K., Jeon, B. H., & Park, H. K. (2023). Application of Biogenic TiO<sub>2</sub> Nanoparticles as ORR Catalysts on Cathode for Enhanced Performance of Microbial Fuel Cell. *Catalysts*, 13(6), 1–13. <https://doi.org/10.3390/catal13060937>
- Kumar, G. G., Sarathi, V. G. S., & Nahm, K. S. (2013). Recent advances and challenges in the anode architecture and their modifications for the applications of microbial fuel cells. *Biosensors and Bioelectronics*, 43(1), 461–475. <https://doi.org/10.1016/j.bios.2012.12.048>
- Kumar, R., Singh, L., Zularisam, A. W., & Hai, F. I. (2018). Microbial fuel cell is emerging as a versatile technology: a review on its possible applications, challenges and strategies to improve the performances. *International Journal of Energy Research*, 42(2), 369–394. <https://doi.org/10.1002/er.3780>
- Kuppurangam, G., Selvaraj, G., Ramasamy, T., Venkatasamy, V., & Kamaraj, S.-K. (2019). *An Overview of Current Trends in Emergence of Nanomaterials for Sustainable Microbial Fuel Cells* (Issue January). [https://doi.org/10.1007/978-3-030-04474-9\\_8](https://doi.org/10.1007/978-3-030-04474-9_8)
- Liew, K. Ben, Wan Daud, W. R., Ghasemi, M., Loh, K. S., Ismail, M., Lim, S. S., &

- Leong, J. X. (2015). Manganese oxide/functionalised carbon nanotubes nanocomposite as catalyst for oxygen reduction reaction in microbial fuel cell. *International Journal of Hydrogen Energy*, *40*(35), 11625–11632. <https://doi.org/10.1016/j.ijhydene.2015.04.030>
- Lim, D. H., Lee, W. D., Choi, D. H., & Lee, H. I. (2010). Effect of ceria nanoparticles into the Pt/C catalyst as cathode material on the electrocatalytic activity and durability for low-temperature fuel cell. *Applied Catalysis B: Environmental*, *94*(1–2), 85–96. <https://doi.org/10.1016/j.apcatb.2009.10.024>
- Liu, Jing, Qiao, Y., Guo, C. X., Lim, S., Song, H., & Li, C. M. (2012). Graphene/carbon cloth anode for high-performance mediatorless microbial fuel cells. *Bioresource Technology*, *114*, 275–280. <https://doi.org/10.1016/j.biortech.2012.02.116>
- Liu, Junli, Rojas-Andrade, M. D., Chata, G., Peng, Y., Roseman, G., Lu, J. E., Millhauser, G. L., Saltikov, C., & Chen, S. (2018). Photo-enhanced antibacterial activity of ZnO/graphene quantum dot nanocomposites. *Nanoscale*, *10*(1), 158–166. <https://doi.org/10.1039/c7nr07367d>
- Liu, Y., Zhang, X., Zhang, Q., & Li, C. (2020). Microbial Fuel Cells: Nanomaterials Based on Anode and Their Application. *Energy Technology*, *8*(9). <https://doi.org/10.1002/ente.202000206>
- López Zavala, M. Á., & Cámara Gutiérrez, I. C. (2023). Effects of External Resistance, New Electrode Material, and Catholyte Type on the Energy Generation and Performance of Dual-Chamber Microbial Fuel Cells. *Fermentation*, *9*(4). <https://doi.org/10.3390/fermentation9040344>
- Lovley, D. R. (2008). The microbe electric: conversion of organic matter to electricity. *Current Opinion in Biotechnology*, *19*(6), 564–571. <https://doi.org/10.1016/j.copbio.2008.10.005>
- Majidi, M. R., Shahbazi Farahani, F., Hosseini, M., & Ahadzadeh, I. (2019). Low-cost nanowired  $\alpha$ -MnO<sub>2</sub>/C as an ORR catalyst in air-cathode microbial fuel cell. *Bioelectrochemistry*, *125*, 38–45. <https://doi.org/10.1016/j.bioelechem.2018.09.004>
- Malekmohammadi, S., & Mirbagheri, S. A. (2021). A review of the operating parameters on the microbial fuel cell for wastewater treatment and electricity generation. *Water Science and Technology*, *84*(6), 1309–1323. <https://doi.org/10.2166/wst.2021.333>

- Min, B., & Logan, B. (2004). Continuous Electricity Generation from Domestic Wastewater and Organic Substrates in a Flat Plate Microbial Fuel Cell. *Environ. Sci. Technol.*, 38(21), 5809–5814. <https://pubs.acs.org/doi/10.1021/es0491026>
- Mohamed, H. O., Sayed, E. T., Cho, H., Park, M., Obaid, M., Kim, H. Y., & Barakat, N. A. M. (2018). Effective strategies for anode surface modification for power harvesting and industrial wastewater treatment using microbial fuel cells. *Journal of Environmental Management*, 206, 228–235. <https://doi.org/10.1016/j.jenvman.2017.10.022>
- Morris, J. M., Jin, S., Wang, J., Zhu, C., & Urynowicz, M. A. (2007). Lead dioxide as an alternative catalyst to platinum in microbial fuel cells. *Electrochemistry Communications*, 9(7), 1730–1734. <https://doi.org/10.1016/j.elecom.2007.03.028>
- Murugan, A., & Brown, A. S. (2015). Review of purity analysis methods for performing quality assurance of fuel cell hydrogen. *International Journal of Hydrogen Energy*, 40(11), 4219–4233. <https://doi.org/10.1016/j.ijhydene.2015.01.041>
- Noori, M. T., Bhowmick, G. D., Tiwari, B. R., Ghangrekar, O. M., Ghangrekar, M. M., & Mukherjee, C. K. (2018). Carbon Supported Cu-Sn Bimetallic Alloy as an Excellent Low-Cost Cathode Catalyst for Enhancing Oxygen Reduction Reaction in Microbial Fuel Cell. *Journal of The Electrochemical Society*, 165(9), F621–F628. <https://doi.org/10.1149/2.0271809jes>
- Ogugbue, C. J., Ebode, E. E., & Leera, S. (2015). Electricity generation from swine wastewater using microbial fuel cell. *Journal of Ecological Engineering*, 16(5), 26–33. <https://doi.org/10.12911/22998993/60450>
- Paquin, F., Rivnay, J., Salleo, A., Stingelin, N., & Silva, C. (2015). Multi-phase semicrystalline microstructures drive exciton dissociation in neat plastic semiconductors. *J. Mater. Chem. C*, 3(207890), 10715–10722. <https://doi.org/10.1039/b000000x>
- Park, D., & Zeikus, J. (2002). Impact of electrode composition on electricity generation in a single-compartment fuel cell using *Shewanella putrefaciens*. *Applied Microbiology and Biotechnology*, 59(1), 58–61. <https://doi.org/10.1007/s00253-002-0972-1>
- Pushkar, P., Prakash, O., Imran, M., Mungray, A. A., Kailasa, S. K., & Mungray, A. K. (2019). Effect of cerium oxide nanoparticles coating on the electrodes of benthic

- microbial fuel cell. *Separation Science and Technology (Philadelphia)*, 54(2), 213–223. <https://doi.org/10.1080/01496395.2018.1501393>
- Rabaey, K., & Verstraete, W. (2005). Microbial fuel cells: Novel biotechnology for energy generation. *Trends in Biotechnology*, 23(6), 291–298. <https://doi.org/10.1016/j.tibtech.2005.04.008>
- Rezaei, A., Aber, S., Roberts, D. J., & Javid GA, A. (2022). Synthesis and study of CuNiTiO<sub>3</sub> as an ORR electrocatalyst to enhance microbial fuel cell efficiency. *Chemosphere*, 307(P1), 135709. <https://doi.org/10.1016/j.chemosphere.2022.135709>
- Rismani-Yazdi, H., Carver, S. M., Christy, A. D., & Tuovinen, O. H. (2008). Cathodic limitations in microbial fuel cells: An overview. *Journal of Power Sources*, 180(2), 683–694. <https://doi.org/10.1016/j.jpowsour.2008.02.074>
- Riza, F., Ftikos, C., Tietz, F., & Fischer, W. (2001). Preparation and characterization of. *Journal of the European Ceramic Society*, 21(10–11), 1769–1773. [https://doi.org/10.1016/S0955-2219\(01\)00112-1](https://doi.org/10.1016/S0955-2219(01)00112-1)
- Roh, S. H. (2013). Layer-by-layer self-assembled carbon nanotube electrode for microbial fuel cells application. *Journal of Nanoscience and Nanotechnology*, 13(6), 4158–4161. <https://doi.org/10.1166/jnn.2013.7021>
- Rozenfeld, S., Schechter, M., Teller, H., Cahan, R., & Schechter, A. (2017). Novel RuCoSe as non-platinum catalysts for oxygen reduction reaction in microbial fuel cells. *Journal of Power Sources*, 362, 140–146. <https://doi.org/10.1016/j.jpowsour.2017.07.022>
- Santoro, C., Serov, A., Narvaez Villarrubia, C. W., Stariha, S., Babanova, S., Schuler, A. J., Artyushkova, K., & Atanassov, P. (2015). Double-Chamber Microbial Fuel Cell with a Non-Platinum-Group Metal Fe-N-C Cathode Catalyst. *ChemSusChem*, 8(5), 828–834. <https://doi.org/10.1002/cssc.201402570>
- Santoro, C., Serov, A., Stariha, L., Kodali, M., Gordon, J., Babanova, S., Bretschger, O., Artyushkova, K., & Atanassov, P. (2016). Iron based catalysts from novel low-cost organic precursors for enhanced oxygen reduction reaction in neutral media microbial fuel cells. *Energy and Environmental Science*, 9(7), 2346–2353. <https://doi.org/10.1039/c6ee01145d>
- Santoro, C., Stadlhofer, A., Hacker, V., Squadrito, G., Schröder, U., & Li, B. (2013). Activated carbon nanofibers (ACNF) as cathode for single chamber microbial fuel cells (SCMFCs). *Journal of Power Sources*, 243, 499–507.

<https://doi.org/10.1016/j.jpowsour.2013.06.061>

- Sarkar, J., & Bhattacharyya, S. (2012). Application of graphene and graphene-based materials in clean energy-related devices Minghui. *Archives of Thermodynamics*, 33(4), 23–40. <https://doi.org/10.1002/er>
- Silva-Palacios, F., Salvador-Salinas, A., Quezada-Alvarez, M. A., Rodriguez-Yupanqui, M., Segundo, R. F., Renny, N. N., & Cabanillas-Chirinos, L. (2023). Bioelectricity generation through Microbial Fuel Cells using *Serratia fonticola* bacteria and *Rhodotorula glutinis* yeast. *Energy Reports*, 9(February), 295–301. <https://doi.org/10.1016/j.egy.2023.05.255>
- Solomon, J., Kugarajah, V., Ganesan, P., & Dharmalingam, S. (2022). Enhancing power generation by maintaining operating temperature using Phase Change Material for Microbial Fuel Cell application. *Journal of Environmental Chemical Engineering*, 10(1), 107057. <https://doi.org/10.1016/j.jece.2021.107057>
- Sonawane, J. M., Yadav, A., Ghosh, P. C., & Adeloju, S. B. (2017). Recent advances in the development and utilization of modern anode materials for high performance microbial fuel cells. *Biosensors and Bioelectronics*, 90, 558–576. <https://doi.org/10.1016/j.bios.2016.10.014>
- Su, Y., Zhu, Y., Yang, X., Shen, J., Lu, J., Zhang, X., Chen, J., & Li, C. (2013). A highly efficient catalyst toward oxygen reduction reaction in neutral media for microbial fuel cells. *Industrial and Engineering Chemistry Research*, 52(18), 6076–6082. <https://doi.org/10.1021/ie4003766>
- Svardal, K., & Kroiss, H. (2011). Energy requirements for waste water treatment. *Water Science and Technology*, 64(6), 1355–1361. <https://doi.org/10.2166/wst.2011.221>
- Tao, S., & Irvine, J. T. S. (2003). A redox-stable efficient anode for solid-oxide fuel cells. *Nature Materials*, 2(5), 320–323. <https://doi.org/10.1038/nmat871>
- Xie, Y., Zhang, C., He, X., Su, J. W., Parker, T., White, T., Griep, M., & Lin, J. (2019). Copper-promoted nitrogen-doped carbon derived from zeolitic imidazole frameworks for oxygen reduction reaction. *Applied Surface Science*, 464(August 2018), 344–350. <https://doi.org/10.1016/j.apsusc.2018.09.102>
- Yahia, S. A. A., Hamadou, L., Salar-García, M. J., Kadri, A., Ortiz-Martínez, V. M., Hernández-Fernández, F. J., de los Rios, A. P., & Benbrahim, N. (2016). TiO<sub>2</sub> nanotubes as alternative cathode in microbial fuel cells: Effect of annealing treatment on its performance. *Applied Surface Science*, 387, 1037–1045.

<https://doi.org/10.1016/j.apsusc.2016.07.018>

- Yamasaki, R., Maeda, T., & Wood, T. K. (2018). Electron carriers increase electricity production in methane microbial fuel cells that reverse methanogenesis. *Biotechnology for Biofuels*, *11*(1), 1–10. <https://doi.org/10.1186/s13068-018-1208-7>
- Yang, L. P., Mi, J. L., Liang, J. H., Zu, Z. Y., & Zhang, P. (2019). Copper-Carbon: An Efficient Catalyst for Oxygen Reduction. *ACS Applied Energy Materials*, *2*(9), 6295–6301. <https://doi.org/10.1021/acsaem.9b00867>
- Yang, W., Chata, G., Zhang, Y., Peng, Y., Lu, J. E., Wang, N., Mercado, R., Li, J., & Chen, S. (2019). Graphene oxide-supported zinc cobalt oxides as effective cathode catalysts for microbial fuel cell: High catalytic activity and inhibition of biofilm formation. *Nano Energy*, *57*(November 2018), 811–819. <https://doi.org/10.1016/j.nanoen.2018.12.089>
- Yang, W., Peng, Y., Zhang, Y., Lu, J. E., Li, J., & Chen, S. (2019). Air Cathode Catalysts of Microbial Fuel Cell by Nitrogen-Doped Carbon Aerogels. *ACS Sustainable Chemistry and Engineering*, *7*(4), 3917–3924. <https://doi.org/10.1021/acssuschemeng.8b05000>
- Yang, Z., Jiang, K., Tong, G., Ke, C., Wu, H., Liu, P., Zhang, J., Ji, H., Zhu, J., Lu, C., & Zhuang, X. (2022). Copper-involved highly efficient oxygen reduction reaction in both alkaline and acidic media. *Chemical Engineering Journal*, *437*(P2), 135377. <https://doi.org/10.1016/j.cej.2022.135377>
- Yaqoob, A. A., Ibrahim, M. N. M., Umar, K., Parveen, T., Ahmad, A., Lokhat, D., & Setapar, S. H. M. (2021). A glimpse into the microbial fuel cells for wastewater treatment with energy generation. *Desalination and Water Treatment*, *214*, 379–389. <https://doi.org/10.5004/dwt.2021.26737>
- Yuan, H., Hou, Y., Abu-Reesh, I. M., Chen, J., & He, Z. (2016). Oxygen reduction reaction catalysts used in microbial fuel cells for energy-efficient wastewater treatment: A review. *Materials Horizons*, *3*(5), 382–401. <https://doi.org/10.1039/c6mh00093b>
- Yuan, Y., Zhou, S., & Zhuang, L. (2010). Polypyrrole/carbon black composite as a novel oxygen reduction catalyst for microbial fuel cells. *Journal of Power Sources*, *195*(11), 3490–3493. <https://doi.org/10.1016/j.jpowsour.2009.12.026>
- Yusri, A. Z. dan D. (2020). 濟無No Title No Title No Title. *Jurnal Ilmu Pendidikan*,

7(2), 809–820.

- Zhang, T., Li, Z., Sun, P., Wang, L., Niu, X., & Wang, S. (2020).  $\alpha$ -MnO<sub>2</sub> nanorods supported on three dimensional graphene as high activity and durability cathode electrocatalysts for magnesium-air fuel cells. *Catalysis Today*, 355(April 2019), 304–310. <https://doi.org/10.1016/j.cattod.2019.04.055>
- Zhang, Y., Mo, G., Li, X., & Ye, J. (2012). Iron tetrasulfophthalocyanine functionalized graphene as a platinum-free cathodic catalyst for efficient oxygen reduction in microbial fuel cells. *Journal of Power Sources*, 197, 93–96. <https://doi.org/10.1016/j.jpowsour.2011.06.105>
- Zhang, Y., Mo, G., Li, X., Zhang, W., Zhang, J., Ye, J., Huang, X., & Yu, C. (2011). A graphene modified anode to improve the performance of microbial fuel cells. *Journal of Power Sources*, 196(13), 5402–5407. <https://doi.org/10.1016/j.jpowsour.2011.02.067>